UC Berkeley
UC Berkeley Electronic Theses and Dissertations

Title

Probing the Mechanism of Quinone Biogenesis in Copper Amine Oxidase Using Unnatural Amino Acids

Permalink

https://escholarship.org/uc/item/6sq3r8w0

Author

Lang, Albert

Publication Date

2012

Peer reviewed|Thesis/dissertation

Probing the Mechanism of Quinone Biogenesis in Copper Amine
Oxidase Using Unnatural Amino Acids

By

Albert Lang

A dissertation submitted in partial satisfaction of the

requirements for the degree of

Doctor of Philosophy

in

Molecular and Cell Biology

in the

Graduate Division

of the

University of California, Berkeley

Committee in charge:

Professor Judith P. Klinman, Chair
Assistant Professor Michelle C.Y. Chang
Assistant Professor Ming C. Hammond
Associate Professor Matthew B. Francis

Fall 2012

Abstract

Probing the Mechanism of Quinone Biogenesis in Copper Amine

Oxidase Using Unnatural Amino Acids

by

Albert Lang

Doctor of Philosophy in Molecular and Cell Biology

University of California, Berkeley

Professor Judith P. Klinman, Chair

Copper amine oxidases (CAOs) catalyze the oxidative deamination of primary amines to their corresponding aldehydes. They are members of a select group of enzymes that contain cofactors derived from the post-translational modification of specific active site residues. In CAOs, that cofactor is 2,4,5-trihydroxyphenylalanine quinone (TPQ), derived from a precursor active site tyrosine (Y405 in the CAO from *H. polymorpha*, HPAO). Replacing the precursor tyrosine with unnatural amino acids provides a subtle method to perturb and probe the biogenesis pathway. *Para*-aminophenylalanine (pAF) was incorporated into position 405 of HPAO using the *in vivo* stop codon suppression method developed by Peter Schultz (Scripps). By incorporating pAF, we can test the importance of pK_a vs. redox potential for the formation of a charge transfer complex that is essential for TPQ biogenesis. The purified protein (Y405pAF) runs as a single band on SDS-PAGE and is metal-free. Incorporation of pAF at position 405 was confirmed by mass spectrometry. When reconstituted aerobically with Cu(II) at pH 9, a peak grows in with a λ_{max} ~450 nm (WT HPAO λ_{max}TPQ = 480 nm). This new species does not react with phenylhydrazine to form a hydrazone, suggesting that it is not a quinone. In addition, reconstituted protein shows no activity towards benzylamine or ethylamine. When the protein is reconstituted with Cu(II) anaerobically, a similar 450-nm peak appears. No further spectral changes are observed after subsequent exposure to air, suggesting that the addition of Cu(II) alone is sufficient for formation of the 450 nm-species.

Further spectroscopic characterization was carried out on Y405pAF using resonance Raman, EPR, and X-ray absorption spectroscopies in order to detect an organic-based, aniline radical or formation of Cu(I) due to electron transfer from aniline to Cu(II). While these results were not definitive in identifying the 450-nm species, x-ray crystallography of Y405pAF revealed that the aniline ring was unmodified upon addition of Cu(II) and that the aniline was liganded to the metal center, in position to undergo inner sphere electron transfer or to form a charge transfer complex. In addition, single crystal UV-Vis spectrophotometry demonstrated that the reconstituted crystals had similar absorbance at 450-nm as was seen in the solution reaction.

pAF has also been incorporated into position 305, a strictly conserved active site tyrosine in WT HPAO that controls runaway oxidation during cofactor biogenesis and ensures proper cofactor formation. Both aerobic and anaerobic reconstitution of the Y305 variant with Cu(II) produce the same peak at λ_{max} ~450 nm, analogous to what was seen with Y405pAF. While the O-4 of Tyr405 is only ~2.5 Å from the metal center in the precursor structure, the O-4 of Y305 is ~4.9 Å away, too far to undergo inner sphere electron transfer with the metal. Thus, the phenomenon we observe with the Y305pAF protein might be instead outer sphere electron transfer from the Cu center to the aniline group, possibly mediated by active site water molecules.

In order to study the effects of second sphere ligands, pAF was incorporated into position 407, a conserved tyrosine that hydrogen bonds with one of the histidine ligands to the Cu. Unlike Y405pAF and Y305pAF, Y407pAF does form TPQ upon reconstitution with Cu(II) and does turn over benzylamine. Based on a preliminary kinetic characterization, Y407pAF is less reactive toward benzylamine than holo-WT-HPAO. These studies pave the way for a more complete kinetic characterization of Y407pAF and demonstrate how unnatural amino acids can be used to tune active site metals as second sphere ligands.

Overall, our work on incorporating unnatural amino acids into HPAO has been very provocative, both for elucidating the mechanism of the CAOs and for introducing a new tool to prove the behavior of the active site metal in copper-dependent enzyme reactions. Future work will continue to address how the CAO active site catalyzes the formation of a single post-translationally modified product and test the plasticity of this active site in tolerating deviations from the natural configuration.

Table of Contents

Acknowledgements

Foremost, thank you to my advisor, Judith Klinman, for her continued patience and support during this long journey. She has stood by me throughout, even during the tough times. I admire her singular focus on seeking out scientific truth, fearlessness, and desire to continue being innovative. Next, I want to recognize my committee members, Matt Francis, Michelle Chang, and Ming Hammond, for being a great sounding board and providing valuable feedback. I came away from each committee meeting with a clearer idea of my objectives as well as many ideas to pursue.

From day one in the lab, both Cindy Chang and Steve Wecksler have looked after me like a little brother. They have been supportive and a never-ending source of encouragement and insightful advice, even after leaving the lab. I would also like to thank many other current and former Klinman Lab members, including Marcus Carr, Sudhir Sharma, Jordan RoseFigura, Erin Imsand, Florence Bonnot, Jianyu Zhang, Hui Zhu, Jerome Cattin, Yinka Oyeyemi, Liviu Mirica, Zac Nagel, Sam Shen, and Kevin McCusker.

During my time in the lab, I had the pleasure of working with two talented undergraduates, Alissa Brandes and Jessica Winger. Alissa started in the lab when the project was just getting off the ground and had many technical challenges to overcome. I want to thank Jessica for her tireless efforts toward moving the project forward and her always-entertaining singing. I also had the great fortune of working with two visiting students, Julian Esselborn and Reinhard Zschoche. It was a lot of fun working side by side with both of them on this project.

I would like to thank my wonderful collaborators, who were essential to this work and very generous with their time. Specifically, Zac Carrico, Emily Weinert, and Ellen Minnihan lent expertise to getting the unnatural amino acid incorporation up and going. Tony Iavarone helped with the mass spectrometry. Rosalie Tran of the Mathies/Marletta groups ran the resonance Raman samples. Junko Yano and Megan Shelby helped with EPR, as did Stefan Stoll and David Britt. Hyeongtaek Lim and Munzarin Qayyum of the Solomon Group ran the XAS samples. And lastly, Val Klema and Carrie Wilmot collaborated with us on the x-ray crystallography.

To Jeff Munos, Robert Osborne, and Corey Meadows, with whom I have shared many a sports viewing experience, thanks for all the good memories both inside and outside of lab. A special thanks also goes to Seemay Chou, Sarah Rodriguez, and Galo Garcia for all their support and the laughs we have shared over the past six years. I know there will be plenty more in the future. To Jen Colby and Katie Thoren, I do not know what I would have done without all the talks we had over coffee. Thank you to Beth Larimore, whose emails always make me laugh, and who has made me thankful for free Verizon mobile to mobile calls. To Lara Collazo, I am sorry to be leaving the lab before you and will miss all of our hilarious discussions in lab. We will just have to continue them online.

Lastly, I would like to thank my parents and sister for their unflinching support, love, and words of encouragement.

Chapter 1

Introduction

1.1 Quinone Cofactors

Enzymes execute a wide range of chemical functions. Most of the standard twenty amino acid side chains, however, are chemically inert; even those most commonly found in enzyme active sites, such as serine, cysteine, histidine, and carboxylic residues, are generally limited to nucleophilic catalysis and acid-base chemistry (*1*). Thus, metal cofactors such as iron or copper, organic cofactors such as pyridoxal phosphate or flavin, and organometallic cofactors such as hemes or cobalamin, expand the catalytic capacity of enzymes by contributing electron transfer, Lewis acidity, radical, and electrophilic capabilities (*2*). Most of these cofactors are bound reversibly to their cognate protein and are derived from structures distinct from the polypeptide chain. Recent work has demonstrated that certain enzymes undergo posttranslational modification of active site amino acids to generate new protein-derived cofactors (*2*). One class of modifications involves proteins that undergo one-electron oxidations to generate radicals on tyrosine, glycine, tryptophan, and cysteine residues (*3*). This theme is taken one step further in enzymes that form even more complex cofactors and then use them in redox processes (*2*).

One such class of protein-derived redox cofactors is quinocofactors. The enzymes that contain quinocofactors play vital biological roles in both prokaryotic and eukaryotic organisms, making them attractive targets for biochemical studies and inhibitor design. In mammals, the TPQ-containing copper amine oxidase are of great interest because of their association with diseases that include congestive heart failure (*4*), diabetes (*5*), and cancer (*6*). Identification of the physiological substrate(s) for these enzymes is an area of active investigation (*7*). Quinones are a class of organic compounds capable of undergoing two reversible, one-electron reductions to their corresponding diphenols. Because of their redox abilities, quinones have been adopted by nature as versatile cofactors in both one- and two-electron processes. Five enzymatic quinocofactors have been characterized to date: pyrroloquinoline quinone (PQQ), topa quinone (TPQ), tryptophan tryptophylquinone (TTQ), lysine tyrosylquinone (LTQ), and cysteine tryptophylquinone **(Scheme 1-1)**.

The quinocofactors may be classified by several structural distinctions. TPQ, TTQ, LTQ, and CTQ are derived from posttranslational modifications of specific amino acids in their corresponding proteins, while PQQ is a noncovalent, peptide-derived, dissociable cofactor. Further, TTQ, LTQ, and CTQ arise via the cross-linking of two amino acids, while TPQ is derived from modification of a single tyrosine. Finally, TTQ and CTQ are restricted to prokaryotes; LTQ is found solely in eukaryotes; and, TPQ is ubiquitous in aerobic organisms. These quinocofactors participate in two general mechanistic classes of enzymes, oxidases and dehydrogenases. In all cases, the two-electron oxidation of substrate amines or alcohols generates the corresponding aldehydes, with the oxidases using molecular oxygen to reoxidize the cofactor during turnover, and the dehydrogenases using associated electron-transfer proteins in bi- or ter-molecular complexes.

1.2 Copper Amine Oxidases

Introduction

Copper amine oxidases (CAOs) catalyze the oxidative deamination of primary amines. This reaction proceeds via a ping-pong mechanism involving a covalently bound redox cofactor, TPQ, and a copper ion, Cu(II) (*8*). CAOs are found in a wide variety of organisms, including bacteria, plants and mammals. In bacteria these enzymes allow amines to be utilized for growth. For plants, a role for the CAOs in wound healing has been postulated (*8*), whereas, in humans, there is increasing evidence for a role of the ectopic CAOs in immune surveillance (*9*) and extracellular peroxide signaling (*7*). These enzymes exist as homodimers, with each subunit containing a copper ion and, in optimal conditions, one equivalent of the mature TPQ cofactor.

To accomplish its catalytic function, CAOs utilize the quinone cofactor TPQ, derived from a precursor tyrosine. The biogenesis of TPQ, formally a monooxygenation, hydroxylation, and two-electron oxidation of tyrosine, occurs without the aid of any auxiliary enzymes or external reducing equivalents (*10*) (**Scheme 1-2**). This autocatalytic processing depends solely on the presence of molecular oxygen and a functional copper center (*11*). Thus, CAOs are able to catalyze both cofactor formation and, subsequently, the oxidation of amines within a single active site. The active site Tyr that leads to TPQ (Y405 in the CAO from *H. polymorpha*, HPAO) is absolutely conserved among CAO family members and is contained within the consensus sequence T-X-X-N-**Y**-D/E (*12*). Other strictly conserved residues include three histidine residues (H456, H458 and H624 in HPAO) that form the three protein ligands of the copper ion and a second Tyr (Y305 in HPAO) that is located at the active site near the O-4 position of the TPQ cofactor (**Figure 1-1**) (*13*).

Catalytic Mechanism

The reaction catalyzed by CAOs proceeds via a ping-pong mechanism involving a covalently bound redox cofactor, TPQ, and a copper ion, Cu(II) (*14*). The catalytic cycle consists of two half-reactions: (i) a reductive half-reaction, in which the substrate is oxidized to an aldehyde product via a Schiff base intermediate and the cofactor is converted to a reduced, aminoquinol form; and (ii) an oxidative half-reaction in which dioxygen is reduced to hydrogen peroxide and the oxidized TPQ is regenerated following release of an ammonium ion (*14*) (**Scheme 1-3**).

Reductive half-reaction

In the reductive half reaction, TPQ initially undergoes a two-electron reduction, serving as a "storage site" for reducing equivalents that are eventually transferred to O_2 to form hydrogen peroxide in the oxidative half reaction. The starting oxidized form of TPQ gives CAOs their characteristic absorbance around 480 nm and distinct pink color (*14*). TPQ exists as an anion state due to the acidity of the 4-hydroxyl group ($pK_a = 4.1$ in model compound) (*14*). Charge is delocalized between oxygens on C-2 and C-4, which decreases the electrophilicity at these sites and directs nucleophilic attack of amine substrates exclusively to the C-5 position. This nucleophilic attack is aided by an active site base that deprotonates the substrate (Asp319 in HPAO) (*14*). Addition of the substrate amine to TPQ leads to the formation of the first stable intermediate, the substrate Schiff base (*14*). This intermediate is proposed to form through a carbinolamine intermediate that has not been observed directly. The next step is the formation of the product Schiff base, proceeding through base-catalyzed proton abstraction at C-1 of the

substrate (*14*). This involves the transfer of two electrons from the substrate amine to the TPQ cofactor and is driven by the gain of aromaticity in the cofactor (*14*). The final step in the reductive half reaction involves hydrolysis of the product Schiff base, releasing aldehyde product and generating the aminoquinol form of the cofactor (*14*).

Oxidative half-reaction
In the oxidative half reaction, molecular oxygen binds to a hydrophobic pocket in the active site. Then, an electron is transferred from the aminoquinol form of TPQ to O_2, generating the semiquinone form of TPQ and superoxide, respectively (**Mechanism II**, **Scheme 1-3**) (*14*). Superoxide then moves onto the Cu(II), allowing for transfer of a second electron and two protons from the semiquinone, resulting in formation of hydrogen peroxide and an iminoquinone form of the cofactor (*14*). Finally, hydrolysis of the iminoquinone results in release of ammonium ion and regeneration of the oxidized form of TPQ, ready for another round of catalysis (*14*). Alternatively, release of ammonium from the iminoquinone can proceed by a transamination reaction with substrate amine to form the substrate Schiff base (**dashed arrow**, **Scheme 1-3**) (*14*). An alternative mechanism has also been proposed for the oxidative half reaction. The chief difference is that the first electron is transferred from the aminoquinol TPQ to Cu(II), generating a semiquinone radical and Cu(I) (**Mechanism I, Scheme 1-3**) (*15*). This property appears to be highly dependent on the source of the enzyme.

TPQ Biogenesis
Prior spectroscopic and structural studies have led to a working mechanism for TPQ biogenesis, summarized in **Scheme 1-2** (*2*). When Cu(II) is added to apo-enzyme anaerobically, an absorbance at 380 nm forms immediately and then decays to baseline. This absorbance has been attributed to a transient ligand to metal charge transfer between the Cu(II) and a residue en route to the active site. It is then proposed that binding of O_2 at the active site near the precursor tyrosine causes a conformational change that promotes the deprotonation of the tyrosine and ligation of the resulting tyrosinate to Cu(II) (*2*). Next, dioxygen reacts with the "activated" precursor tyrosine in the form of a tyrosinate-Cu(II) ligand-to-metal charge transfer (LMCT) complex (**bracketed species, Scheme 1-2**) (*2*). Due to the nature of the oxygen-copper bond in this complex, partial radical character is expected to be imparted onto the tyrosyl ring, thus circumventing the spin-forbidden nature of direct reaction between singlet tyrosine and triplet dioxygen. Experimental evidence for the LMCT complex comes from the observation of a spectral intermediate (λ_{max} = 350 nm) that forms rapidly upon aeration of HPAO pre-bound with Cu(II) and decays rapidly concomitantly with the appearance of TPQ (*2*). The 350-nm intermediate represents the species that reacts with the first mole of oxygen, the rate-limiting step in Cu(II)-catalyzed TPQ biogenesis (*2*). It should be noted that this 350-nm intermediate has only been seen in HPAO and not other well-studied CAOs from *E. coli* (ECAO) and *Arthrobacter globiformis* (AGAO). This is most likely due to the considerably slower rate of TPQ biogenesis in HPAO, which allows for detection of the intermediate using a conventional UV-vis spectrophotometer. In the other two enzymes, stopped-flow techniques would likely be necessary to detect any intermediates. O–O bond cleavage leads to the formation of the dopaquinone intermediate. Subsequent Michael addition of hydroxide/water at the C-2 position, followed by tautomerization yields 2,4,5-trihydroxyphenylalanine (topa). Oxidation by a second molecule of O_2 generates the oxidized TPQ form and H_2O_2 (*2*).

Structural Properties

Structural studies have contributed greatly to the interpretation of the wealth of kinetic and spectroscopic data in the literature on CAOs. As previously mentioned, CAOs are ubiquitous and found in bacteria, plants, fungi, and animals. Structures of CAOs have been solved from a variety of sources, including *Escherichia coli* (ECAO), pea seedling (PSAO), *Hansenula polymorpha* (HPAO), bovine serum (BSAO), *Arthrobacter globiformis* (AGAO), *Pichia pastoris* (PPLO), and human (human vascular adhesion protein-1) (*16*). The overall three-dimensional structure for all solved CAO structures is similar (HPAO shown in **Figure 1-2**) (*17*). In all cases, the CAOs are homodimers of ~70 kDa subunits that contain a carboxy-terminal domain that folds into a β-sandwich with twisted β-sheets (*17*). The overall shape of the dimer resembles a mushroom cap. The active site is buried deeply within each subunit and contains a TPQ cofactor, which is not directly liganded to the Cu but rather has hydrogen bonding between O-2 and a water molecule and between O-4 and another conserved Tyr in the active site (Y305 in HPAO) (**Figure 1-1**). In addition, O-5 of the cofactor is oriented close to the catalytic base (Asp319 in HPAO) in the amine substrate binding pocket (*17*). The Cu(II) is liganded in a distorted square pyramidal geometry with three histidine side chains (H456, H458 and H624 in HPAO) providing N ligands ~2.0 Å away, an axial water at a distance of ~2.4 Å, and sometimes a labile equatorial water ligand ~2.0 Å away (*17*).

Biogenesis intermediates

Biogenesis of TPQ can be studied structurally by preparing enzyme in the absence of copper, as TPQ formation is a self-processing event. What has been particularly insightful is the identification of intermediates along the pathway by freeze-trapping techniques (*18*) reviewed in (*17*). In the first of these structures, that of apo-enzyme, the His metal ligands along with the TPQ precursor Tyr residue are arranged in a tetrahedral geometry, poised to bind copper (*18*). When Cu is added anaerobically, another structure can be trapped that is virtually identical to that of apo-enzyme, with the Cu now coordinated by the three His residues and TPQ precursor Tyr residue (*18*). After exposing these anaerobic crystals to oxygen for a short period (10 min), the next intermediate that is trapped is that of 3,4-dihydroxyphenylalanine (or the oxidized quinone form) (*18*). In this structure, an oxygen atom of either water or hydroxide is located in an equatorial position to the Cu. When anaerobic crystals were instead exposed to oxygen for a longer period (100 min), a different, later-stage intermediate is observed, which now has three oxygens and can be modeled as either the reduced or oxidized form of TPQ (*18*). This structure also shows that the structure has rotated 180º about the Cβ-Cγ bond. Evidence that this structure is the reduced cofactor comes from single crystal microspectrophotometry, which shows no evidence of a 480 nm absorbance characteristic of oxidized TPQ (*18*). To visualize the final step of TPQ biogenesis, anaerobic crystals were aerobically soaked in copper solutions for a week, which resulted in pink crystals indicative of oxidized TPQ formation (*18*). In the final structure, the TPQ is clearly in an "off-copper" conformation, with the O-4 pointed away from the Cu.

Structural data and catalysis

Structural studies have also been insightful in studying intermediates of both the reductive and oxidative half reactions. The structure of a substrate Schiff base with the inhibitor 2-hydrazinopyridine (2-HP) has been solved (*17*). Hydrazines irreversibly inhibit CAO activity and can be used to derivatize the TPQ cofactor for spectral analysis (e.g. phenylhydrazine generates a strongly absorbing hydrazone). In this structure, 2-HP is covalently bound to the C-5 that is

also the site of nucleophilic attack by natural amine substrates (*17*). This structure also shows N-2 of 2-HP hydrogen bonded to the carboxylate side chain of the catalytic base (Asp383 in ECAO). This position is analogous to the methylene carbon of a primary amine substrate where a proton is abstracted by the active site base in the conversion of substrate Schiff base to product Schiff base. To examine the aminoquinol form of the enzyme, crystals were prepared anaerobically and subsequently reduced with substrate (2-phenethylamine). In this structure, the aminoquinol form of the cofactor is ordered and in the same position as the oxidized form of TPQ.

In order to study the oxidative half reactions, studies were conducted in which crystals were reduced with substrate anaerobically, reduced with substrate anaerobically in the presence of nitric oxide (NO), or aerobically trapped. In the substrate reduced structure, previously mentioned with respect to the reductive half reaction, there is clearly the presence of product phenylacetaldehyde in the active site (*17*). This is consistent with the ping-pong kinetics of the enzyme in which irreversible formation of product occurs prior to oxygen binding. In the structure with NO, NO takes the place of the axial water, and is situated between the copper and the O2 of the aminoquinol (*17*). Thus, the dioxygen mimic NO appears capable of interaction with both the copper ion and the aminoquinol, consistent with a mechanism of electron transfer from either Cu(I) or aminoquinol to O_2. In the aerobically trapped structure, oxygen occupies the same site as NO did, with an electron density compatible with the peroxide product (*17*).

1.3 Unnatural Amino Acids

Background

Natural proteins are generally composed of only the twenty canonical amino acids. In order to expand on this limited repertoire, nature employs post-translational modifications as well as organic and inorganic cofactors in order to add additional functions. The ability to incorporate noncanonical amino acids into proteins is a powerful method not only to investigate protein structure and function but also to engineer proteins with novel functions. The first work on noncanonical amino acid incorporation dates back to the 1950s, where it was demonstrated that selenomethionine could be incorporated into bacterial proteins as a surrogate for methionine (*19*). This method has since been extended to the field of protein x-ray crystallography, where incorporation of a heavy atom helps in solving the phase problem (*20*). Since then, several different methods have been developed and applied to the incorporation of unnatural amino acids into proteins.

Expressed Protein Ligation (EPL)

The origins of EPL are rooted in classical solid phase peptide synthesis, first pioneered in the 1960s by Robert Bruce Merrifield (*21*). An important extension of these initial methods was reported in 1994, when the Muir group reported a native chemical ligation (NCL) approach, in which a peptide with N-terminal cysteine reacts with a second peptide with a C-terminal thioester to give a peptide bond after rearrangement (*22*) (**a**, **Figure 1-3**). This method has the advantages of being able to synthesize small proteins beyond the 50-70 residue limit of solid phase synthesis, working with fully deprotected peptides, working in the presence of free cysteines, and going to completion in seconds at pH 7 (*22*). Taking advantage of the phenomenon of natural protein splicing, in which an internal protein fragment (intein) is excised, and the remaining protein fragments (exteins) are ligated together (**b**, **Figure 1-3**), a technique called expressed protein ligation (EPL) was developed (*23, 24*). In this method, a mutated intein is used that only allows for the first step in splicing, allowing for cleavage by thiols and the generation of a thioester. The thioester can then react with a second peptide that contains an N-terminal cysteine to generate the product (**c**, **Figure 1-3**). ECL is useful for incorporating unnatural amino acids, and has been used to study such diverse proteins as GTPases, ion channels, histones, and ribonucleotide reductases (*25*).

Residue-Specific Incorporation

Residue-specific incorporation results in the partial or total replacement of a particular canonical amino acid with a non-canonical analog. This method was pioneered by the Tirrell group, and has been reviewed in detail (*26, 27*) (**Figure 1-4**). Typically, protein expression is carried out in bacteria auxotrophic for the natural amino acid and grown in media where the natural amino acid is exchanged for the analog of interest. These methods allow for facile incorporation of unnatural amino acid at multiple sites, offering the potential to substantially alter the physical or chemical properties of the natural protein. In addition, no genetic manipulation is necessary, nor any separate chemical synthesis steps. This method also allows for the modification of all cellular proteins, regardless of whether their identity or sequence is known, and has been applied to the labeling of proteins in response to different stimuli at the proteomic level (*28*).

Site-Specific Incorporation

Although the ability to replace part or all of a given amino acid population within a protein (or a proteome) is useful, it is easy to see the limitations. These include the production of mixed populations of proteins, some with greater incorporation than others, and the lack of positional specificity. There are many applications where, in contrast, the site-specific incorporation of an unnatural amino acid would be more useful. Techniques for site-specific incorporation have been pioneered by the Schultz group over the past two decades (*29-32*). In the first iteration of this technique, unnatural amino acids were incorporated using chemically acylated amber suppressor tRNA (tRNA$_{CUA}$) that inserted the unnatural amino acid in response to an amber stop codon that had been generated at the site of replacement (*33*). This stop codon suppression technique takes advantage of the fact that the amino acid code is redundant, with the other stop codons being used with much greater frequency than the amber stop codon (*34*). The other advantage of this technique is that virtually any amino acid can be used, since the acylation is done chemically rather than by the cellular machinery. Unfortunately, this method suffers from low yields during the acylation step as well as during the *in vitro* protein synthesis step (*34*). In order to characterize these novel proteins using protein-intensive physical techniques such as x-ray crystallography, NMR, and EPR, a different approach for incorporation must be taken.

Taking this method a step further, a method was developed where the unnatural amino acids would be acylated and incorporated totally *in vivo* (*35*). In order for this method to work, new components of the cellular biosynthetic machinery must be engineered, including an orthogonal tRNA-aminoacyl-tRNA synthetase pair that specifically incorporates the unnatural amino acid in response to the cognate codon (*29*). The same amber stop codon used in the *in vitro* method can also be used for this *in vivo* method. However, a new orthogonal tRNA-synthetase pair is necessary. The first such pair for incorporation into *E. coli* was derived from a tyrosyl-tRNA synthetase (TyrRS)-tRNA^{Tyr} pair from the archaea *Methanococcus jannaschii* (Mj) (*35*). Archael tRNAs have distinct aminoacyl-tRNA synthetase recognition sites when compared to those from *E. coli* such that they do not react with the endogenous bacterial synthetases during expression. In addition, the Mj Tyr RS has a small anticodon loop binding domain, making it easy to edit the anti-codon loop of the corresponding tRNA (to pair with the UAG stop codon) with little loss in binding affinity. Lastly, the synthetase lacks an editing mechanism such as those seen in phenylalanyl-tRNA syntheases that would deacylate the unnatural amino acid (*29*). This method has been extended to incorporate unnatural amino acids into not only *E. coli* but also yeast (*36*) and mammalian cells (*37, 38*). The range of unnatural amino acids that have been incorporated continues to grow, and includes fluorophores, sugar analogs, photoactive side chains, heavy atom labeled residues for NMR, and residues with altered redox potential (reviewed in *31*) (**Figure 1-5**).

9
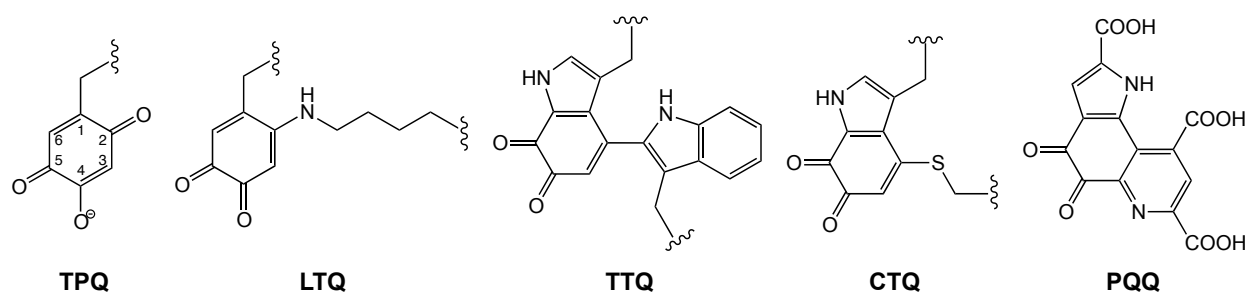
Scheme 1-1. Structures of quinocofactors. The structures of topa quinone (TPQ), lysine tyrosylquinone (LTQ), tryptophan tryptophylquinone (TTQ), cysteine tryptophylquinone (CTQ), and pyrroloquinoline quinone (PQQ) are shown.
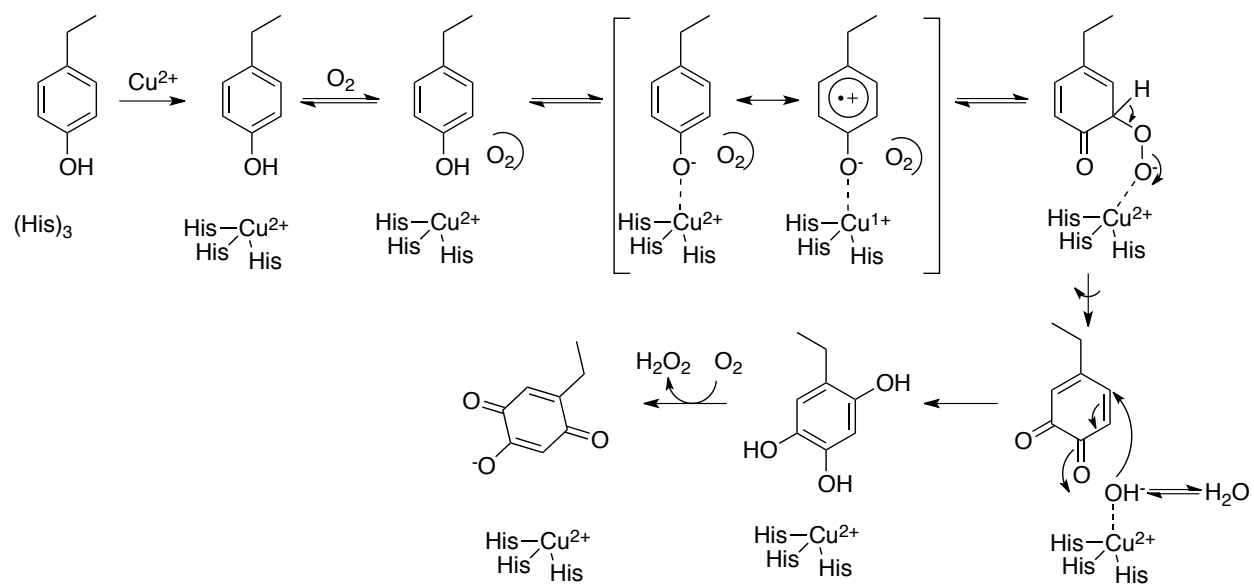
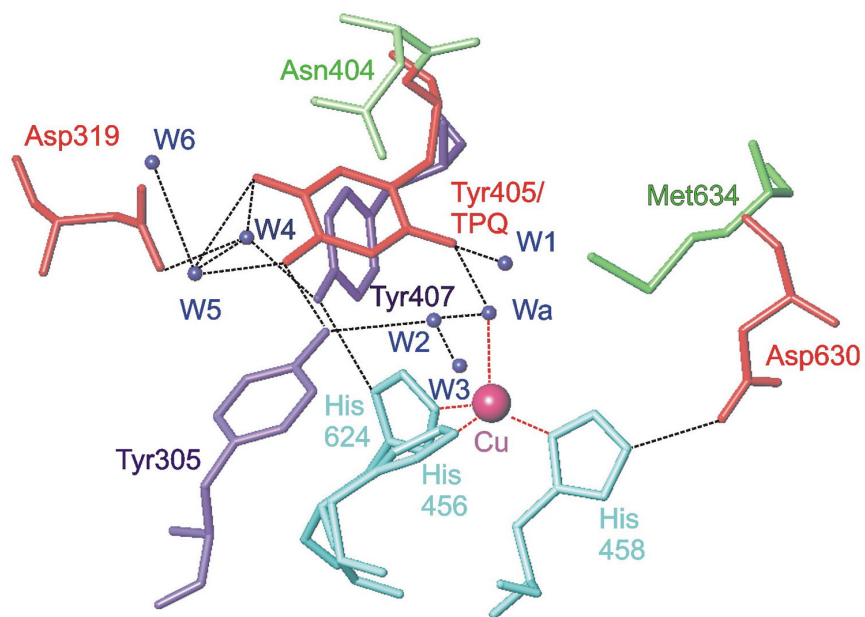**Scheme 1-2**. Proposed mechanism for TPQ biogenesis (*2*).

Figure 1-1. Mature HPAO active site with TPQ in the reactive conformation. Acidic chains are in red, basic in cyan, aromatic in purple, neutral hydrophilic in lime, TPQ cofactor in red, and Cu(II) in crimson. A network of six active site water molecules (W1-W6) and one axial copper-coordinating water (Wa) that forms hydrogen bonds to TPQ and side chain atoms are shown in blue. Hydrogen and metal coordination bonds are shown as black and red dashed lines, respectively. Reprinted with permission from (*39*). Copyright 2006 American Chemical Society.
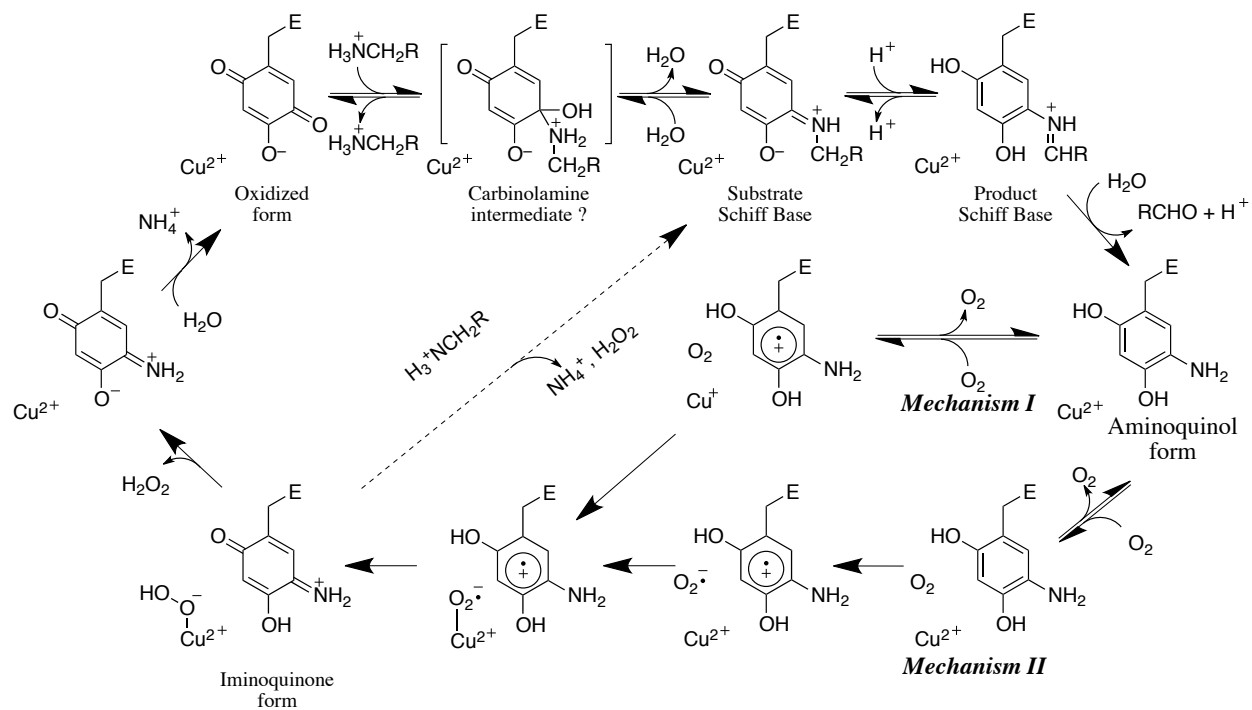
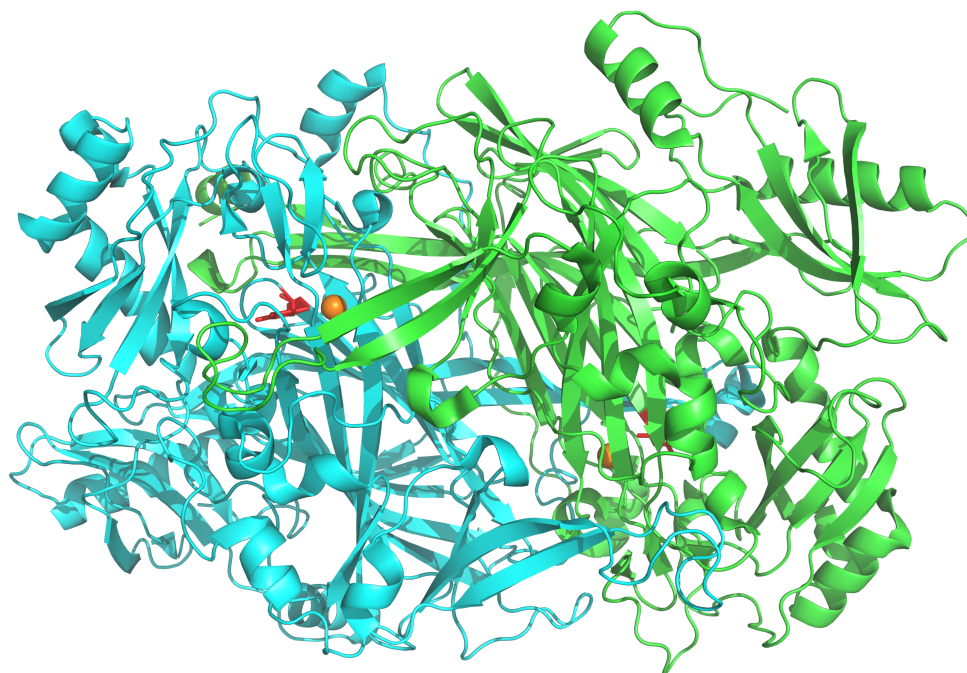**Scheme 1-3.** Proposed catalytic mechanism of the CAOs (*14, 15*).

Figure 1-2. Ribbon diagram of HPAO (PDB entry; 2OOV). One monomer is colored cyan, the other green. Copper ions are shown as orange spheres. TPQ is colored red.
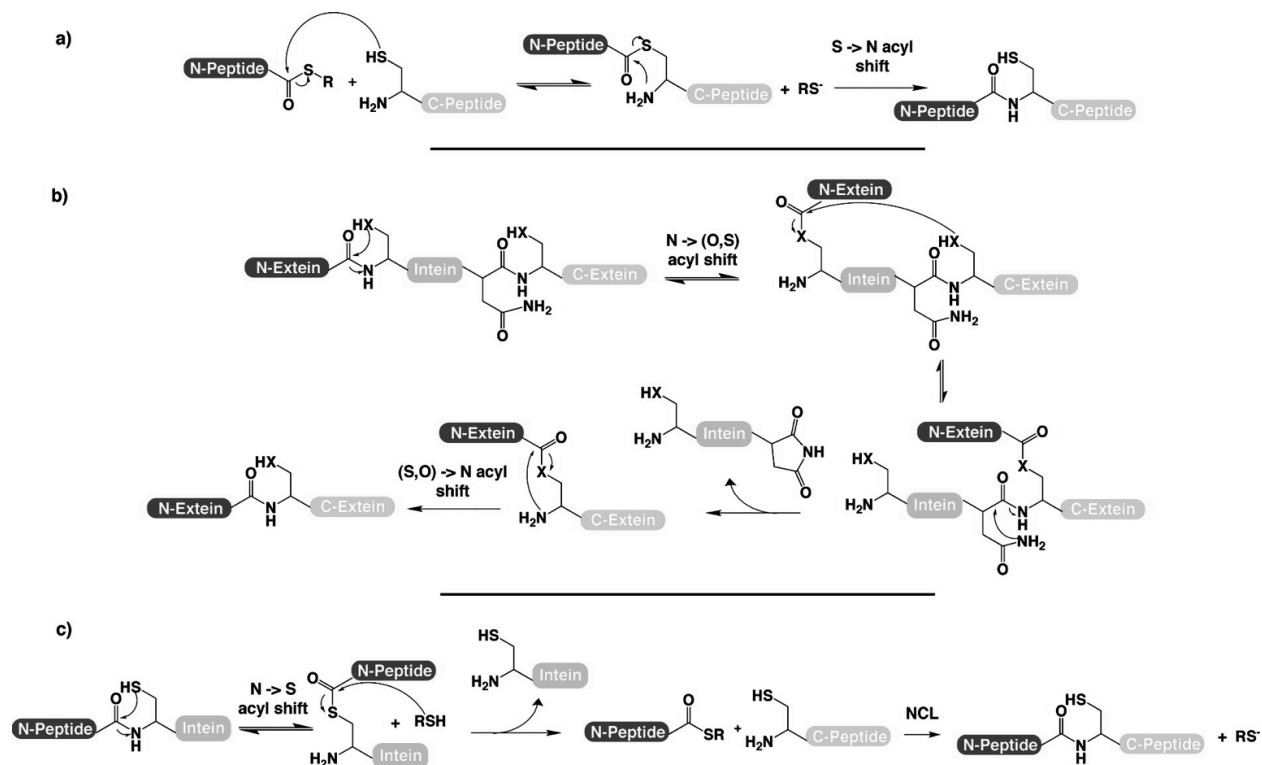
Figure 1-3. (a) Mechanism of NCL. In NCL, transthioesterification by the N-terminal cysteine is followed by an S → N acyl shift, generating a native peptide bond. **(b)** Mechanism of protein splicing. In protein splicing, a N → S or O acyl shift at the N-terminal residue of the intein is followed by *trans*(thio)-esterification to the residue C-terminal to the intein, generating a branched intermediate. The C-terminal asparagine of the intein then cleaves the C-terminal intein-extein bond, generating a succinimide product, and the fused exteins undergo an (S,O) → N acyl shift to create a native peptide bond. **(c)** Mechanism of EPL. In EPL, a thiol is used to generate a thioester from a mutated intein. The thioester can then react by NCL with an N-terminal cysteine peptide. R = alkyl, phenyl, benzyl, $CH_2CH_2SO_3Na$; X = O, S. Reprinted (adapted) with permission from (*40*). Copyright 2009 American Chemical Society.
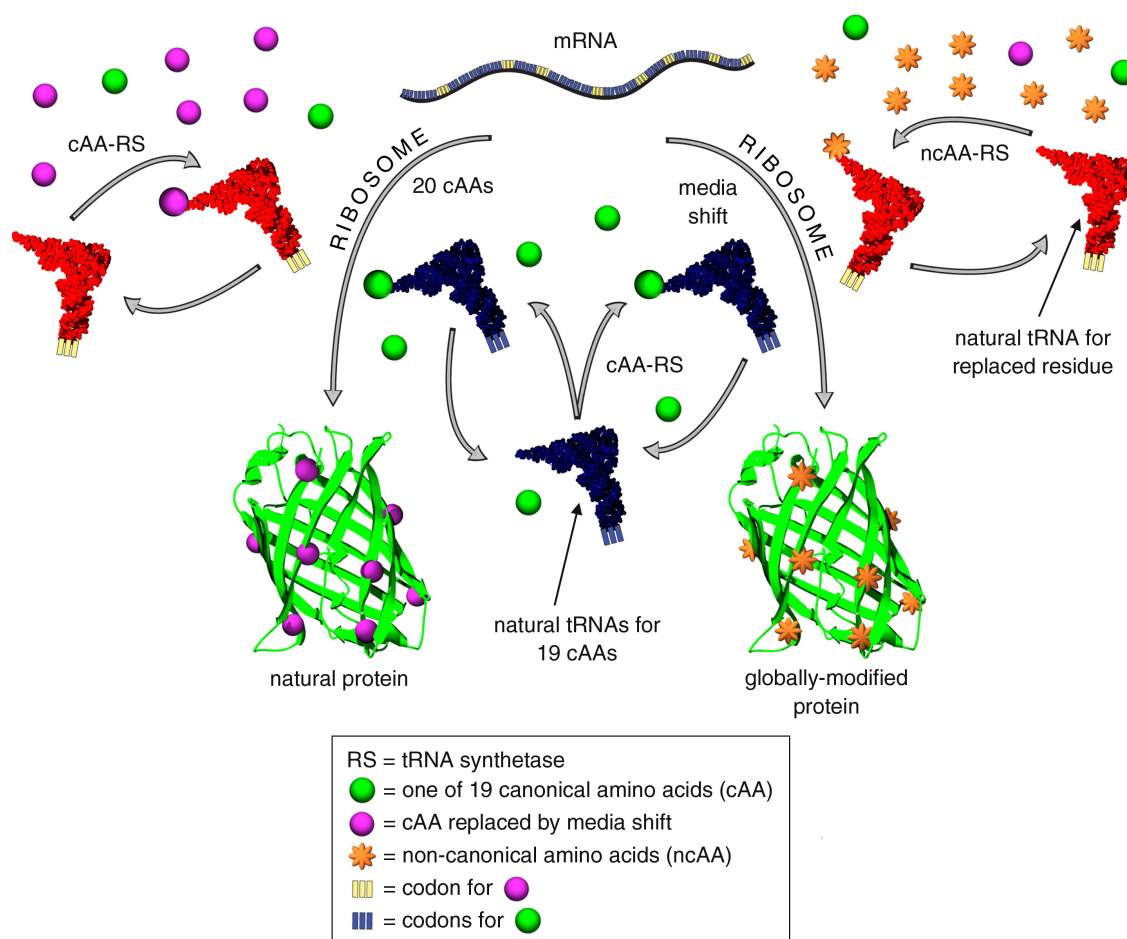
Figure 1-4. Schematic for residue-specific incorporation of non-canonical amino acids (ncAAs) into proteins. A natural mRNA contains codons for the 20 canonical amino acids (cAAs). A cAA (purple sphere) assigned to one of those codons (yellow) is replaced with an ncAA (orange star). A medium shift is performed to remove the cAA to be replaced (purple sphere) and to introduce the ncAA (orange star) along with the remaining 19 cAAs (green spheres). The ncAA is charged to the appropriate tRNA (red) by either the wild-type or a mutant aminoacyl-tRNA synthetase (aaRS). The correctly aminoacylated tRNA^{CAA} (blue with green sphere) and the misacylated tRNA (red with orange star) are processed by the ribosome to give a globally modified protein. The left path depicts normal protein synthesis with 20 cAAs for comparison. Reprinted from (*27*) with permission from Elsevier.

1

2

3

4

5

6

7

8

9

10

11

12

13

14

15

16

17

18

19

20

21

22

23

24

25

26

27

28

29

30
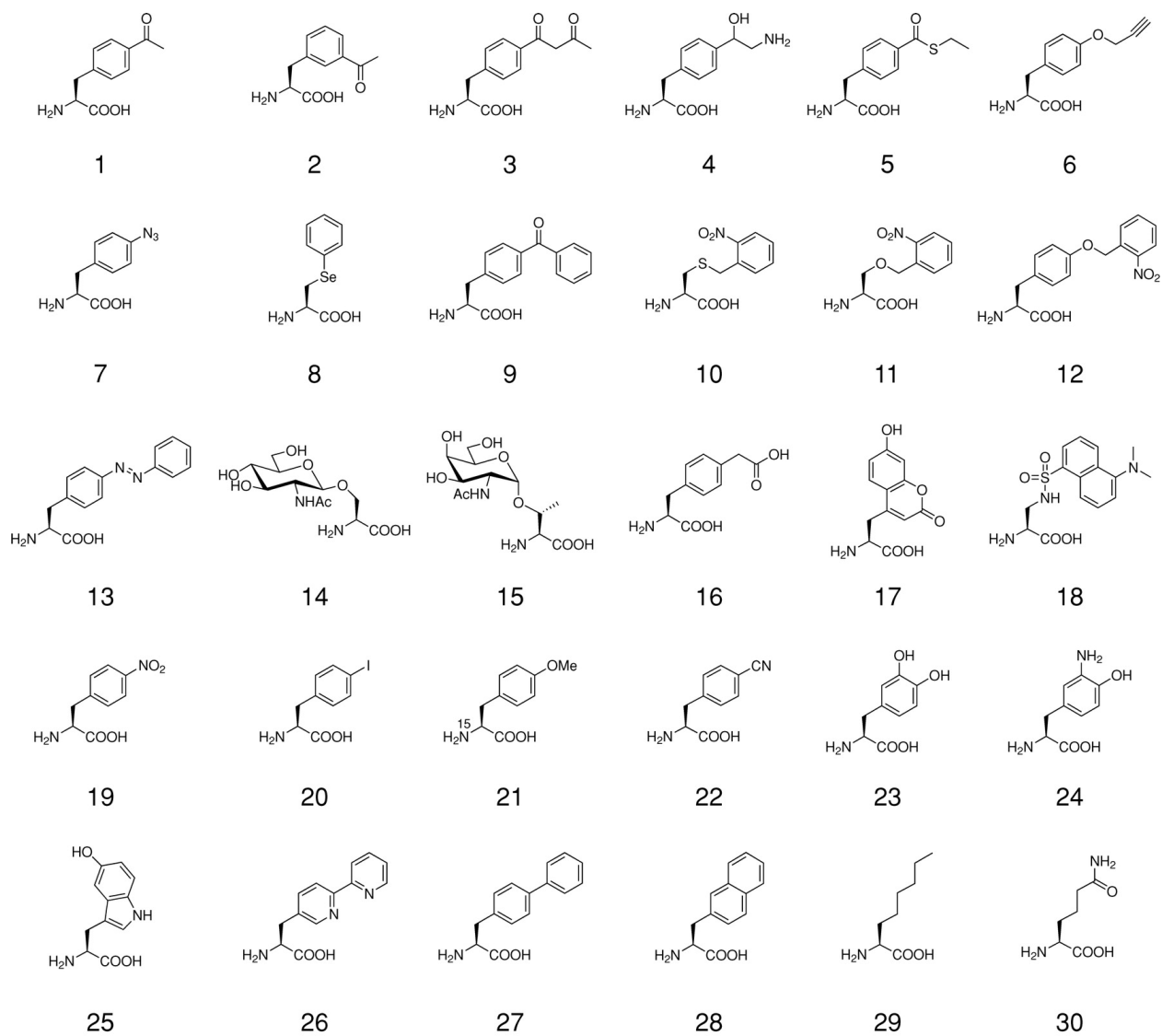
Figure 1-5. Unnatural amino acids that have been added to the genetic codes of *E. coli*, yeast, or mammalian cells. Reproduced with permission of Annual Reviews in the format Republish in a thesis/dissertation via Copyright Clearance Center (*41*).

References

1. Davidson, V. L. (2007) Protein-Derived Cofactors. Expanding the Scope of Post-Translational Modifications, *Biochemistry 46*, 5283–5292.
2. DuBois, J. L., and Klinman, J. P. (2005) Mechanism of post-translational quinone formation in copper amine oxidases and its relationship to the catalytic turnover, *Archives of Biochemistry and Biophysics 433*, 255–265.
3. Stubbe, J., and van Der Donk, W. A. (1998) Protein Radicals in Enzyme Catalysis, *Chem. Rev. 98*, 705–762.
4. Boomsma, F., de Kam, P. J., Tjeerdsma, G., van den Meiracker, A. H., and van Veldhuisen, D. J. (2000) Plasma semicarbazide-sensitive amine oxidase (SSAO) is an independent prognostic marker for mortality in chronic heart failure, *Eur. Heart J. 21*, 1859–1863.
5. Boomsma, F., van den Meiracker, A. H., Winkel, S., Aanstoot, H. J., Batstra, M. R., Man in 't Veld, A. J., and Bruining, G. J. (1999) Circulating semicarbazide-sensitive amine oxidase is raised both in type I (insulin-dependent), in type II (non-insulin-dependent) diabetes mellitus and even in childhood type I diabetes at first clinical diagnosis, *Diabetologia 42*, 233–237.
6. Marttila-Ichihara, F., Auvinen, K., Elima, K., Jalkanen, S., and Salmi, M. (2009) Vascular adhesion protein-1 enhances tumor growth by supporting recruitment of Gr-1+CD11b+ myeloid cells into tumors, *Cancer Res. 69*, 7875–7883.
7. Shen, S. H., Wertz, D. L., and Klinman, J. P. (2012) Implication for functions of the ectopic adipocyte copper amine oxidase (AOC3) from purified enzyme and cell-based kinetic studies, *PLoS ONE 7*, e29270.
8. Klinman, J. P., and Mu, D. (1994) Quinoenzymes in biology, *Annu. Rev. Biochem. 63*, 299–344.
9. Salmi, M., and Jalkanen, S. (1992) A 90-kilodalton endothelial cell molecule mediating lymphocyte binding in humans, *Science 257*, 1407–1409.
10. Ruggiero, C. E., and Dooley, D. M. (1999) Stoichiometry of the topa quinone biogenesis reaction in copper amine oxidases, *Biochemistry 38*, 2892–2898.
11. Cai, D., Williams, N. K., and Klinman, J. P. (1997) Effect of metal on 2,4,5-trihydroxyphenylalanine (topa) quinone biogenesis in the *Hansenula polymorpha* copper amine oxidase, *J. Biol. Chem. 272*, 19277–19281.
12. Mu, D., Janes, S. M., Smith, A. J., Brown, D. E., Dooley, D. M., and Klinman, J. P. (1992) Tyrosine codon corresponds to topa quinone at the active site of copper amine oxidases, *J. Biol. Chem. 267*, 7979–7982.
13. Li, R., Klinman, J. P., and Mathews, F. S. (1998) Copper amine oxidase from *Hansenula polymorpha*: the crystal structure determined at 2.4 Å resolution reveals the active conformation, *Structure 6*, 293–307.
14. Mure, M., Mills, S. A., and Klinman, J. P. (2002) Catalytic Mechanism of the Topa Quinone Containing Copper Amine Oxidases, *Biochemistry 41*, 9269–9278.
15. Dooley, D. M., McGuirl, M. A., Brown, D. E., Turowski, P. N., McIntire, W. S., and Knowles, P. F. (1991) A Cu(I)-semiquinone state in substrate-reduced amine oxidases, *Nature 349*, 262–264.
16. Guss, J. M., Zanotti, G., and Tiina, S. A. (2009) Copper Amine Oxidase Crystal Structures, in *Copper Amine Oxidases: Structures, Catalytic Mechanisms and Role in*

Pathophysiology (Floris, G., and Mondovi, B., Eds.). CRC Press.

17. Brazeau, B. J., Johnson, B. J., and Wilmot, C. M. (2004) Copper-containing amine oxidases. Biogenesis and catalysis; a structural perspective, *Archives of Biochemistry and Biophysics 428*, 22–31.

18. Kim, M., Okajima, T., Kishishita, S., Yoshimura, M., Kawamori, A., Tanizawa, K., and Yamaguchi, H. (2002) X-ray snapshots of quinone cofactor biogenesis in bacterial copper amine oxidase, *Nat. Struct Biol. 9*, 591–596.

19. Cowie, D. B., and Cohen, G. N. (1957) Biosynthesis by *Escherichia coli* of active altered proteins containing selenium instead of sulfur, *Biochim. Biophys. Acta 26*, 252–261.

20. Hendrickson, W. A., Horton, J. R., and LeMaster, D. M. (1990) Selenomethionyl proteins produced for analysis by multiwavelength anomalous diffraction (MAD): a vehicle for direct determination of three-dimensional structure, *EMBO J. 9*, 1665–1672.

21. Merrifield, R. B. (1963) Solid Phase Peptide Synthesis. I. The Synthesis of a Tetrapeptide, *J. Am. Chem. Soc. 85*, 2149–2154.

22. Dawson, P. E., Muir, T. W., Clark-Lewis, I., and Kent, S. B. (1994) Synthesis of proteins by native chemical ligation, *Science 266*, 776–779.

23. Muir, T. W., Sondhi, D., and Cole, P. A. (1998) Expressed protein ligation: a general method for protein engineering, *Proc. Natl. Acad. Sci. U.S.A. 95*, 6705–6710.

24. Severinov, K., and Muir, T. W. (1998) Expressed protein ligation, a novel method for studying protein-protein interactions in transcription, *J. Biol. Chem. 273*, 16205–16209.

25. Pellois, J.-P., and Muir, T. W. (2006) Semisynthetic proteins in mechanistic studies: using chemistry to go where nature can't, *Current Opinion in Chemical Biology 10*, 487–491.

26. Link, A. J., Mock, M. L., and Tirrell, D. A. (2003) Non-canonical amino acids in protein engineering, *Curr. Opin. Biotechnol. 14*, 603–609.

27. Johnson, J. A., Lu, Y. Y., Van Deventer, J. A., and Tirrell, D. A. (2010) Residue-specific incorporation of non-canonical amino acids into proteins: recent developments and applications, *Current Opinion in Chemical Biology 14*, 774–780.

28. Dieterich, D. C., Link, A. J., Graumann, J., Tirrell, D. A., and Schuman, E. M. (2006) Selective identification of newly synthesized proteins in mammalian cells using bioorthogonal noncanonical amino acid tagging (BONCAT), *Proc. Natl. Acad. Sci. U.S.A. 103*, 9482–9487.

29. Xie, J., and Schultz, P. G. (2005) Adding amino acids to the genetic repertoire, *Current Opinion in Chemical Biology 9*, 548–554.

30. Liu, C. C., and Schultz, P. G. (2010) Adding new chemistries to the genetic code, *Annu. Rev. Biochem. 79*, 413–444.

31. Young, T. S., and Schultz, P. G. (2010) Beyond the canonical 20 amino acids: expanding the genetic lexicon, *J. Biol. Chem. 285*, 11039–11044.

32. Wang, L., and Schultz, P. G. (2005) Expanding the Genetic Code, *Angew. Chem. Int. Ed. 44*, 34–66.

33. Noren, C. J., Anthony-Cahill, S. J., Griffith, M. C., and Schultz, P. G. (1989) A general method for site-specific incorporation of unnatural amino acids into proteins, *Science 244*, 182–188.

34. Anthony-Cahill, S. J., Griffith, M. C., Noren, C. J., Suich, D. J., and Schultz, P. G. (1989) Site-specific mutagenesis with unnatural amino acids, *Trends Biochem. Sci. 14*, 400–403.

35. Wang, L., Brock, A., Herberich, B., and Schultz, P. G. (2001) Expanding the Genetic Code of *Escherichia coli*, *Science 292*, 498–500.

36. Chin, J. W., Cropp, T. A., Anderson, J. C., Mukherji, M., Zhang, Z., and Schultz, P. G. (2003) An expanded eukaryotic genetic code, *Science 301*, 964–967.
37. Sakamoto, K., Hayashi, A., Sakamoto, A., Kiga, D., Nakayama, H., Soma, A., Kobayashi, T., Kitabatake, M., Takio, K., Saito, K., Shirouzu, M., Hirao, I., and Yokoyama, S. (2002) Site-specific incorporation of an unnatural amino acid into proteins in mammalian cells, *Nucleic Acids Res. 30*, 4692–4699.
38. Hino, N., Okazaki, Y., Kobayashi, T., Hayashi, A., Sakamoto, K., and Yokoyama, S. (2005) Protein photo-cross-linking in mammalian cells by site-specific incorporation of a photoreactive amino acid, *Nat Meth 2*, 201–206.
39. DuBois, J. L., and Klinman, J. P. (2006) Role of a Strictly Conserved Active Site Tyrosine in Cofactor Genesis in the Copper Amine Oxidase from *Hansenula polymorpha*, *Biochemistry 45*, 3178–3188.
40. Flavell, R. R., and Muir, T. W. (2009) Expressed protein ligation (EPL) in the study of signal transduction, ion conduction, and chromatin biology, *Acc. Chem. Res. 42*, 107–116.
41. Wang, L., Xie, J., and Schultz, P. G. (2006) Expanding the genetic code, *Annu Rev Biophys Biomol Struct 35*, 225–249.

Chapter 2

Expression and Characterization of HPAO-Y405pAF

2.1 Introduction

Though much is known about the mechanism of TPQ biogenesis, replacing the precursor tyrosine with unnatural amino acids provides a subtle method to perturb and further probe the biogenesis pathway. In recent years, techniques for unnatural amino acid incorporation have progressed to the point where expression levels in *E. coli* are relatively high, making them amenable to producing protein for detailed kinetic and spectroscopic analysis. While much of the initial work with unnatural amino acids focused on adding new functions to proteins, this method has tremendous potential to probe protein structure and function beyond what is possible with site-directed mutagenesis (*1-4*). In particular, we are quite interested in the nature of the Y405/Cu(II) charge transfer complex (**bracketed species, Scheme 1-2**) that activates the tyrosine sufficiently for O_2 insertion.

Toward this end, we sought to incorporate *para*-aminophenylalanine (pAF) (**Scheme 2-1**) into position 405, that of the TPQ precursor tyrosine. The replacement of a tyrosine phenol functionality with an aniline functionality found in pAF has both acid/base and redox potential implications (**Scheme 2-1**). Compared to tyrosine, which is relatively easy to deprotonate to the tyrosinate form, aniline will be much more difficult to deprotonate to its anion form ($pK_a \simeq 31$ for pAF vs. ca. 10 for Tyr) (*5*). In contrast, the one electron oxidation of neutral aniline is energetically similar to that of neutral and deprotonated Tyr ($E^o \simeq 1.0$ V for pAF vs. ca. 0.9 V for Tyr-OH, 0.7 V for Ty-O$^-$) (*6, 7*). Therefore, by studying the pAF-incorporated version of HPAO (HPAO-Y405pAF), we can test the importance of pK_a vs. redox potential for the formation of a charge transfer complex that can support O_2 insertion.

The method of unnatural amino acid incorporation we used is the stop codon suppression method developed by Schultz et al. in which an orthogonal tRNA delivers the unnatural amino acid in response to an amber stop codon, and a new aminoacyl-tRNA synthetase selectively aminoacylates the orthogonal tRNA (*1, 2*). The tRNA/synthetase pair developed for the incorporation of pAF (*8*) has been applied to providing a handle for an oxidative coupling reaction specific to aniline (*9*) and is known to incorporate pAF with high fidelity, in contrast to some other tRNA/synthetase pairs that suffer from "leakage" i.e. incorporation of the native amino acid.

2.2   Materials and Methods

Mutagenesis
Mutations were made to the pET3a-HPAO plasmid (*10*) in order to substitute an amber stop codon for the sequence that encodes for the precursor Tyr at position 405. The pET expression system relies on the bacteriophage T7 RNA polymerase to drive expression, which is induced with Isopropyl β-D-1-thiogalactopyranoside (IPTG). Site-directed mutagenesis was performed using the Stratagene QuikChange II XL kit. HPLC-purified primers were purchased from Eurofins MWG Operon. The forward primer is listed in the 5' to 3' direction, and the reverse primer is listed in the 3' to 5' direction. The mutated codon is in bold, and the changed bases are in italics. DNA mutation was confirmed by automated sequencing at the UC Berkeley Sequencing Facility.

HPAO Y405pAF:
```
5'– AATATTTACTGCTGCCAATTAGGAGTACTGTCTGTACTGG–3'
3'– TTATAAATGACGACGGTTAATCCTCATGACAGACATGACC–5'
```

Protein Expression
Dr. Matt Francis (UC Berkeley) supplied the second plasmid for unnatural amino acid incorporation, which encodes for an orthogonal aminoacyl-tRNA synthetase and tRNA that incorporates pAF in response to the amber stop codon UAG in *E. coli* (original material provided by Dr. Peter Schultz, Scripps) (*8*). This plasmid, designated pDule-pAF, a p15A Tet[R] plasmid, was co-transformed with the pET3a-HPAO Y405pAF plasmid, which encodes for HPAO with a single amber stop codon at amino acid position 405, into BL21(DE3) *E. coli* competent cells (Stratagene). Successfully transformed colonies were picked and grown in 5 mL LB+Amp+Tet cultures, and shaken overnight at 37ºC. The next day, 400 μl of these overnight cultures were mixed with 400 μl 30% glycerol and snap frozen in liquid N_2 to generate glycerol stocks, stored at -80ºC.

These glycerol stocks were used to inoculate 3x150 mL minimal growth medium cultures, made with the components listed below (adapted from (*8, 9*). These cultures were shaken at 37ºC overnight. The following day, these 3x150 mL cultures were used to inoculate 6x1.5 L cultures prepared with the components listed below. Within an hour of starting the large cultures,15 mL of 100 mM pAF (final [1 mM]) were added to each flask. This 100 mM pAF solution was made by dissolving 1.95 g pAF• HCl (Bachem) into 90 mL autoclaved water, followed by addition of 1.44 mL 10 M NaOH. These large cultures were grown to an OD_{600} ~0.6 (after ~4 h) at 37ºC, and then induced with IPTG to a final concentration of 0.4 mM. Induction was allowed to proceed for 20 h before the cell paste was collected by centrifugation and stored at -20ºC.

	For 150 ml cultures	For 1.5 L cultures
Glycerol (10% w/v)	7.5 mL	75 mL
Dextrose (40% w/v)	180 μl	1.8 mL
50xM Salts	3 mL	30 mL
$MgSO_4$ (1M)	300 μl	3 mL
L-Asparate, pH 7.5 (5%)	7.5 mL	75 mL
L-Leucine pH 7.5 (4 mg/mL)	3 mL	30 mL
25x 18-amino acid mix	6 mL	60 mL
Trace metal mix	150 μl	1.5 mL
Water	123 mL	1.224 mL
Ampicillin (100 mg/mL)	150 μl	750 μl
Tetracycline (12.5 mg/mL)	300 μl	300 μl

Flasks were first autoclaved with water, then supplemented with the components above.

25x 18-amino acid solution (Add 5g of each amino acid except for Cys and Tyr)
- Glutamate sodium salt   - Proline   - Valine
- Aspartate   - Glycine   - Leucine
- Lysine-HCl   - Threonine   - Isoleucine
- Arginine-HCl   - Serine   - Phenylalanine
- Histidine-HCl-H_2O - Glutamine   - Tryptophan
- Alanine   - Asparagine-H_2O - Methionine

Brought up to 1 L with water, sterile filtered, and stored at 4°C, covered in foil.

Trace metal stock solution (1L) (recipe modified from (11).
- 500 mg Na_2MoO_4 • $2H_2O$ - 2.45 g $Fe(NH_4)(SO_4)_2$ • $6H_2O$
- 1 g $MnSO_4$ • H_2O - 1.5 g $CaCl_2$
- 8.75 g $MgSO_4$ • $7H_2O$ - 1 g H_3BO_3

Brought up to 1L in 1M HCl and sterile filtered.

Protein Purification
Protein was prepared as previously described (*12*, *13*) with some modifications. Frozen cell paste was thawed on ice and disrupted by sonication (Branson 450: duty cycle = 30%, output = 8) for 10 min, off for 5 min, then repeated two more times (three total). The soluble portion was separated from cellular debris by centrifugation at 22,000 x *g* for 1 h at 4°C. The supernatant was

then dialyzed against 4 L of 5 mM potassium phosphate buffer supplemented with 1 mM EDTA and 1 mM diethyldithiocarbamate (DDC) (pH 7) at 4°C. Dialysis tubing comes pre-treated to minimize trace levels of heavy metals (Spectra/Por 7, Spectrum Labs). Following dialysis, the liquid was briefly centrifuged to pellet any material that had precipitated out of solution (22,000 x g for 15 min at 4ºC).

Dialysate was loaded onto a DEAE sepharose fast flow column pre-equilibrated with 5 mM potassium phosphate plus 1 mM EDTA and 1 mM DDC (pH 7). After binding, the column was washed with 600 mL of the same 5 mM potassium phosphate buffer, followed by elution using a gradient of 5 mM to 100 mM potassium phosphate (1L total volume). Fractions ~10 mL were collected at 1 min/fraction (elution by gravity) and evaluated by SDS-PAGE, with those containing HPAO pooled and concentrated to ~2-3 mL using Amicon concentrators. This concentrated pool of protein was loaded onto a S-300 sephacryl column pre-equilibrated with 50 mM potassium phosphate plus 1 mM EDTA and 1 mM DDC (pH 7). The same buffer was pumped over the column at ~0.2 ml/min, and fractions were collected overnight (10 min/fraction, ~2 mL/fraction). The fractions from the sizing column were analyzed by SDS-PAGE, and those >90% in HPAO were pooled and concentrated using an Amicon concentrator. Protein was concentrated to a volume of ~500 µl, then resuspended in 7 mL 50 mM HEPES, pH 7. Cycles of concentration and resuspension were repeated 3 more times in order to fully exchange the protein into 50 mM HEPES, pH 7. The final protein was concentrated to ~10-20 mg/ml, and either aliquoted to be snap-frozen in liquid nitrogen and kept at -80ºC for storage or kept on ice to be used within 1-2 weeks.

Protein Characterization

Protein quantitation
Protein concentration was measured by the Bradford assay (Bio-Rad) (*14*). Typical protein yields were ~3-5 mg/9 L cell culture (in comparison to ~10-20 mg/9 L for WT apo-protein).

N-terminal sequencing
The sequence of purified HPAO-Y405pAF was verified by N-terminal sequencing (Edman degradation) at the Stanford Protein and Nucleic Acid (PAN) Biotechnology Facility (http://pan.stanford.edu/index.html) (*15*).

Metal analysis
Copper and zinc content were measured on a Perkin-Elmer Optima 7000 DV ICP-OES Spectrometer (Department of Chemistry, UC Berkeley). Calibration was performed using commercially available metal reference solutions (Fisher Scientific). Specifically, the zinc reference standard solution was 1000 ppm ±1% zinc oxide in dilute nitric acid for atomic absorption. The copper reference standard solution was 1000 ppm ±1% copper nitrate in dilute nitric acid for atomic absorption. Apo samples were measured as purified. For reconstituted samples, 1 equivalent of $CuSO_4$ was added to protein, which was then dialyzed overnight against 1 mM EDTA at 4ºC to remove any adventitiously bound metal. The next day, dialyzed protein was briefly centrifuged at 14k rpm, 4ºC to remove any precipitated protein before analysis.

Redox staining

To test for the presence of TPQ or another redox active cofactor, reaction with nitroblue tetrazolium (NBT) was used (*13*). Purified HPAO-Y405pAF was run on SDS-PAGE, then electroblotted onto a nitrocellulose membrane, and incubated with 0.24 mM NBT in 2M sodium glycinate (pH 10), covered in foil.

Phenylhydrazine reaction

For a more sensitive test for the presence of TPQ, reaction with an excess of phenylhydrazine HCl was used. 1 µl 5 mg/ml phenylhydrazine was added to 40 µM enzyme reconstituted with Cu(II) (see protocol below), and the reaction was monitored at 448 nm on a Varian Cary 50 Bio UV-Vis spectrophotometer. An extinction coefficient of 40,500 $M^{-1}cm^{-1}$ (wild type value) was used to quantitate phenylhydrazone formation (*13*).

Aerobic Cu^{2+} reconstitution

HPAO-Y405pAF was diluted with 50 mM CHES, pH 9.0 to 110 µl at 40 µM (3 mg/mL) Spectral changes to this sample after addition of 4.4 µl $CuSO_4$ (1 equivalent) were monitored over 1 h in a Varian Cary 50 Bio UV-Vis spectrophotometer.

Anaerobic reconstitution

A solution of protein (40 µM, 150 µl, in 50 mM CHES pH 9.0) was prepared in a gas-tight, septum-sealed cuvette. This solution was then made anaerobic, either by purging the sample on ice with a slow flow of argon gas for 1 h or by several cycles of evacuation followed by argon back filling (*13*). A stock solution of 1 mM $CuSO_4$ was similarly made anaerobic by continuous bubbling or argon or alternating cycles of vacuum and argon. An equivalent of Cu(II) was added to the sample by gas-tight syringe, and the sample was mixed gently. Spectral changes were monitored over 1 h in a Varian Cary 50 Bio UV-Vis spectrophotometer. At this point, the septum was removed from the cuvette, and the sample was flushed with air. Spectra were then measured for another hour.

As an alternative method to establish anaerobiosis, a glucose oxidase/catalase scrubbing system was used (*16, 17*). Specifically, a solution of 50 u/mL glucose oxidase (from *Aspergillus niger*, 5.6 units/mg, Sigma) and 50 u/mL catalase (from bovine liver, 1780 units/mg, Sigma) was purged using cycles of Ar and vacuum (1 min, 3 cycles total) in a cuvette capped with a rubber septum. Separately, a solution of 200 mM glucose was made anaerobic with the same cycling of Ar and vacuum. Then, glucose was added to the glucose oxidase/catalase mixture (final concentration of glucose = 20 mM) using a gas-tight syringe, and the entire mixture was incubated at room temperature overnight, scrubbing any residual oxygen. The next day, the cocktail was removed from the cuvette using a gas-tight syringe. 40 µM HPAO-Y405pAF was then dissolved in a solution of fresh glucose oxidase and catalase and subjected to cycles of Ar and vacuum (1 min each, 3 cycles total). Separately, 10x glucose (200 mM), and 1 mM $CuSO_4$ solutions were also subject to the same cycling of Ar and vacuum in separate vials. Then, glucose was added to the glucose oxidase/catalase mixture (final concentration glucose = 20 mM) using a gas-tight syringe to initiate the activity of glucose oxidase (which consumes O_2). Then, 1 equivalent of $CuSO_4$ was added using a gas-tight syringe, and spectra were collected every 2 min for 1 h.

Kinetic Measurements

To test for activity toward benzylamine, benzaldehyde formation was monitored at 250 nm (ε = 12,800 M^{-1}cm^{-1}) on a Varian Cary 50 Bio UV-Vis spectrophotometer (*18*). Standard conditions were as follows: 50 mM CHES, pH 9.0 at 25ºC, with a total volume of 1 mL and initiation of the reaction by addition of 5 µl Cu(II) reconstituted enzyme. To test for enzyme activity toward ethylamine, oxygen consumption was monitored with a Clark-type oxygen electrode and a YSI-5300 biological oxygen monitor (*19*). Standard conditions were as follows: 50 mM CHES, pH 9.0 at 25ºC, with a final volume of 1 mL and initiation of reaction by addition of 5µl of Cu(II) reconstituted enzyme.

Proteolytic Digestions

Trypsin digests
1.62 -3.24 nmol protein was added to 10 M urea in 100 mM Tris-HCl, pH 8.5 such that the final concentration of urea was 8 M in a total volume of 80 µl. For example, 16 µl protein was added to 64 µl of 10 M urea. The final concentration of digested protein was 5-10 µM. To the denatured protein, 4 µl of 100 mM (*tris*(2-carboxyethyl)phosphine) (TCEP) (final concentration 5 mM) was added to reduce disulfide bonds, and allowed to incubate at room temperature (RT) for 20 min. Next, 1.6 µl freshly made 500 mM iodoacetate was added (final concentration 10 mM) to cap the reduced disulfides, and allowed to incubate at RT for 15 min, wrapped in foil. 240 µl of 100 mM Tris-HCl, pH 8.5 was then added, diluting the concentration of urea to 2 M, followed by 3.2 µl of 100 mM CaCl$_2$ to a final concentration of 1 mM. 1 µl of trypsin at 0.5 µg/µl was added, and the final mixture was incubated at 37ºC overnight.

Thermolysin digests
1.62 -3.24 nmol protein was added to 10 M urea in 100 mM NH$_4$HCO$_3$ such that the final concentration of urea was 8 M in a total volume of 80 µl. For example, 16 µl protein was added to 64 µl of 10 M urea. The final concentration of digested protein was 5-10 µM. To the denatured protein, 4 µl of 100 mM (*tris*(2-carboxyethyl)phosphine) (TCEP) (final concentration 5 mM) was added to reduce disulfide bonds, and allowed to incubate at room temperature (RT) for 20 min. Next, 1.6 µl freshly made 500 mM iodoacetate was added (final concentration 10 mM) to cap the reduced disulfides, and allowed to incubate at RT for 15 min, wrapped in foil, followed by 240 µl of 100 mM NH$_4$HCO$_3$, diluting the concentration of urea to 2 M. 2% thermolysin (w/w) was added, and the final mixture was incubated at 37ºC overnight.

Chymotrypsin digests
1.62 -3.24 nmol protein was added to 10 M urea in 100 mM Tris-HCl, pH 7.8 such that the final concentration of urea was 8 M in a total volume of 80 µl. For example, 16 µl protein was added to 64 µl of 10 M urea. The final concentration of digested protein was 5-10 µM. To the denatured protein, 4 µl of 100 mM (*tris*(2-carboxyethyl)phosphine) (TCEP) (final concentration 5 mM) was added to reduce disulfide bonds, and allowed to incubate at room temperature (RT) for 20 min. Next, 1.6 µl freshly made 500 mM iodoacetate was added (final concentration 10 mM) to cap the reduced disulfides, and allowed to incubate at RT for 15 min, wrapped in foil, followed by 240 µl of 100 mM Tris-HCl, pH 7.8, diluting the concentration of urea to 2 M. 3.2 ul of 100 mM CaCl$_2$ was then added to a final concentration of 1 mM. 1 µl of 4 mg/ml chymotrypsin (1:60 w/w) was added, and the final mixture was incubated at 30ºC overnight.

Mass Spectrometry

Proteolytic digests of HPAO were analyzed using an ultraperformance liquid chromatograph (nanoAcquity UPLC, Waters, Milford, MA) that was connected in-line with a quadrupole time-of-flight mass spectrometer equipped with a nanoelectrospray ionization (nanoESI) source (Q-Tof Premier, Waters).

The UPLC was equipped with C_{18} trapping (20 mm × 180 μm, 5 μm particles, Waters Symmetry) and analytical (100 mm × 100 μm, 1.7 μm particles, Waters BEH130) columns and a 10 μL sample loop. Solvent A was 99.9% water/0.1% formic acid and solvent B was 99.9% acetonitrile/0.1% formic acid (v/v). Following sample injection, trapping was performed for 3 min with 100% A at a flow rate of 15 μL/min. The elution program consisted of a linear gradient from 5% to 30% B over 100 min, a linear gradient to 95% B over 0.33 min, isocratic conditions at 95% B for 3.67 min, a linear gradient to 1% B over 0.33 min, and isocratic conditions at 1% B for 12.67 min, at a flow rate of 500 nL/min. The analytical column and sample compartment were maintained at 35 ºC and 8 ºC, respectively.

The column exit was connected to a Universal NanoFlow nanoESI emitter mounted in the ion source of the Q-Tof Premier. The Tof analyzer was operated in "V" mode. External mass calibration was performed immediately prior to analysis. Mass spectra were acquired in the positive ion mode over the range m/z = 350-1500, in continuum data format, using a 0.45 s scan integration and a 0.05 s interscan delay. Real-time deisotoping and charge state recognition were used to select 1+, 2+, 3+, 4+, and 5+ charge state precursor ions for tandem mass spectrometry (MS/MS) analysis. Collision energies for collisionally activated dissociation (CAD) were automatically selected based on the mass and charge state of a given precursor ion. MS/MS spectra were acquired over the range m/z = 100-2000 using a 0.15 s scan integration and a 0.05 s interscan delay. Data were processed using MassLynx software (version 4.1, Waters) and ProteinLynx Global Server software (version 2.3, Waters).

2.3   Results

Purification and Initial Characterization
Following purification by ion-exchange and size-exclusion chromatography, HPAO-Y405pAF runs as a single band on SDS-PAGE and similarly to apo-WT HPAO (also purified from *E. coli*) and holo-HPAO (purified from *S. cerevisiae*) (**Figure 2-1**). N-terminal sequencing matched the expected N-terminal sequence from WT-HPAO, verifying that the purified protein is indeed HPAO rather than another protein that ran at a similar size on SDS-PAGE (also see **Figure 2-2**):

```
WT-HPAO              AASAAPARPAHPLDPLSTAE
HPAO-Y405pAF         AASAAPARPAHPLDPLSTAE
```

Proteolytic Digestions and Mass Spectrometry
Though SDS-PAGE and N-terminal sequencing verified that the purified protein was indeed HPAO, we turned to mass spectrometry to give direct evidence that pAF had been incorporated at position 405. Given the large size of HPAO (~74 kDa), detecting the difference in mass between intact WT HPAO and HPAO-Y405pAF, that of 1 Da, would be extremely challenging. Moreover, a mass measurement of the intact HPAO protein, by itself, would not indicate the location of the pAF residue within the protein sequence. To definitively determine the identity and position of the pAF residue, we chose to digest the intact, purified protein using different proteases and subjected the resulting peptides to liquid chromatography tandem mass spectrometry (LC-MS/MS) in collaboration with Dr. Tony Iavarone (Chemistry/QB3 Mass Spectrometry Facility, UC Berkeley). Initial work was done with trypsin and thermolysin, the former given its reliability and widespread use for proteolytic digestions and the latter given its use in the original identification of TPQ in copper amine oxidase from bovine serum (BSAO) (*20*). While both of these enzymes resulted in very good sequence coverage by LC-MS/MS (50-70%), no peptides containing residue 405 were observed. Turning to chymotrypsin, which cleaves proteins on the carboxyl side of aromatic residues, we were able to observe a $[M+H]^+$ ion corresponding to a peptide that contained pAF (but not Tyr) at residue 405 (**Figure 2-3**). Collisionally activated dissociation (CAD) of this positively charged ion at $m/z = 830.37$ produced b and y ions which confirmed that the mass of the residue at position 405 corresponds to pAF and not Tyr (**Figure 2-4**).

Further Characterization of HPAO-Y405pAF

Metal analysis
Purified HPAO-Y405pAF was analyzed for both zinc and copper content by elemental analysis (ICP-OAS). As with purified apo-WT HPAO, apo-HPAO-Y405pAF is purified with very low levels (~5%) of both Cu and Zn. Apo-HPAO-Y405pAF that has been reconstituted with Cu(II), then dialyzed against 1 mM EDTA overnight shows 1 mole of copper per monomer of protein, and again, very low levels of Zn. This result is comparable to what was observed with reconstituted apo-WT HPAO.

Aerobic reconstitution and quinone cofactor detection

Aerobic reconstitution of HPAO-Y405pAF at pH 9.0 generated a species with a λ_{max} ~450 nm (WT HPAO λ_{max}TPQ = 480 nm) that grew in over an hour and was stable for several hours afterward at RT (**Figure 2-5**). This new 450 nm-species did not react with phenylhydrazine to form a hydrazone as TPQ does, however, suggesting that it is not a quinone. In addition, Cu-reconstituted protein did not react with NBT to form a purple band as TPQ-containing holo-HPAO does (**Figure 2-6**), further suggesting that this new species is not a quinone.

Activity toward benzylamine and ethylamine
Cu(II)-reconstituted protein was also tested for activity toward known substrates of HPAO, the aliphatic amine ethylamine and the aromatic amine benzylamine. When benzylamine was added to Cu(II) reconstituted HPAO-Y405pAF, no increase in absorbance at 250 nm (where benzaldehyde product absorbs) was observed. To test for activity toward ethylamine, which does not allow for easy spectrophotometric detection of product, O_2 depletion was monitored with a Clark-type electrode. No O_2 consumption was seen, further indicating that the protein is not active toward primary amine substrates and that it does not contain a mature TPQ cofactor.

Anaerobic reconstitution
In order to characterize the 450-nm species further, we sought to determine whether its formation is oxygen-dependent. When protein is reconstituted with Cu(II) anaerobically using Ar purging, a 450 nm-species appears that is similar to what is seen with aerobic reconstitution (**A**, **Figure 2-7**). No further spectra changes were observed after subsequent exposure to air (data not shown). Similar results were seen when anaerobiosis was established using a glucose oxidase/catalase oxygen scrubbing system (*16*, *17*) (**B**, **Figure 2-7**).

2.4   Discussion

We were very excited to successfully incorporate pAF into position 405 of HPAO given the large size of HPAO (~74 kDa). Much of the initial work with mutant tRNA/synthetase pairs was done with smaller proteins such as dihydrofolate reductase (DHFR), and on residues much closer to the N-terminus of proteins (*21*). In particular, we did not encounter any problems with the misincorporation of other amino acids, namely tyrosine, into position 405, nor any truncation due to the incorporation of an amber stop codon. Thus, we felt confident that all further biochemical and spectroscopic studies would be carried out with protein that contains pAF at position 405.

It was originally hypothesized that the incorporation of pAF into HPAO would possibly result n the biogenesis of a novel cofactor that retained an amino group (rather than a hydroxyl group) at the 4-position (**Scheme 2-2**). If dioxygen can insert into the phenyl ring due to radical character imparted by an NH_2/Cu(II) LMCT complex, an intermediate iminoquinone will form. While this could undergo hydrolysis to yield an *ortho*-quinone, the addition of hydroxide ion (representing the normal pathway) may be expected to greatly out-compete such a hydrolysis because the active site is normally poised for imine hydrolysis at the 5- rather than 4-position during the catalytic cycle. Hydrolysis would yield TPQ; hydroxide addition would yield a 4-aminoquinol. The formation of a 4-aminoquinol would be of great interest since the normal catalytic pathway of the enzyme leads to an oxidized quinone that is ionized at the C-4 position, while oxidation of the aniline-derived cofactor should yield a neutral 4-aminoquinone. Given that the 4-postion of TPQ does not exchange with solvent water under turnover conditions, catalytic turnover by the 4-aminoquinone product would be expected to retain the nitrogen functionality at the 4-position, very likely yielding some unexpected catalytic properties.

All evidence, however, points to HPAO-Y405pAF not forming a quinone after addition of Cu(II). Instead, a new species forms with λ_{max} ~450 nm, which differs from that of TPQ (~480 nm). This new species, however, does not react with phenylhydrazine to form a strongly absorbing hydrazine as TPQ does. In addition, this new species fails to react with NBT/glycinate after transfer to a nitrocellulose membrane, and shows no activity toward either benzylamine or ethylamine substrates. This led to the possibility that biogenesis with pAF proceeds through an alternate pathway, one analogous to that seen in the Y305F mutant (*12*). In the Y305F mutant a new spectroscopic intermediate forms that absorbs at ~420 nm, which was then crystallized and demonstrated to be a novel trihydroperoxy species rather than TPQ (*22*). Drawing on these data, we can postulate that the new 450-nm species observed in HPAO-Y405pAF arises from the partitioning of an aryl-peroxy intermediate between concomitant proton abstraction and O-O bond cleavage to generate an iminoquinone (**b**, **Scheme 2-3**), and proton loss and ring aromatization to yield a hydroperoxo-product (**a**, **Scheme 2-3**).

The most provocative result of these initial studies was that the 450-nm species formed even when Cu(II) reconstitution was carried out anaerobically (**Figure 2-7**). Given this finding, we must consider that the species being formed is not a hydroperoxo-species or any other structure that requires oxygen insertion into the pAF ring. It is not possible, however, to totally exclude the possibility of a small amount of oxygen leakage in these experiments. What can be said is that similar results were seen when Cu(II)-reconstitution was carried out anaerobically using either Ar purging alone (**A**, **Figure 2-7**) or a glucose oxidase/catalase oxygen scavenging system

to remove residual oxygen (*16*, *17*) (**B**, **Figure 2-7**). Also, when the same conditions were carried out with WT apo-protein, whether anaerobiosis was established using Ar purging only or a GO/catalase scrubbing system, no TPQ was observed (data not shown). If there was some oxygen leakage during addition of Cu(II), we should see the formation of TPQ as a peak that grows in at 480 nm. Instead, we saw similar results to what was previously reported i.e. after WT-apo-HPAO is reconstituted with Cu(II) anaerobically, no TPQ was observed, and only upon subsequent exposure to air did a 350-nm species grow in, then decay rapidly and concomitantly with the appearance of TPQ (data not shown) (*23*). We cannot rule out that HPAO-Y405pAF is more sensitive to oxygen than the WT protein, but can say that under the same conditions sufficient for anaerobiosis in the WT protein, a 450-nm species was clearly observed in HPAO-Y405pAF.

To provide additional information about the nature and identity of this 450-nm species, we turned to more physical spectroscopic methods, to be discussed in Chapter 3.

para-aminophenylanine (pAF)

$pK_a(\text{Ph-NH}_3^+)$	4.6		$pK_a(\text{Tyr-OH})$	10
$pK_a(\text{Ph-NH}_2)$	31		$E°(\text{Tyr-OH})$	0.9 V
$E°(\text{Ph-NH}_2)$	1.0 V		$E°(\text{Tyr-O}^-)$	0.7 V
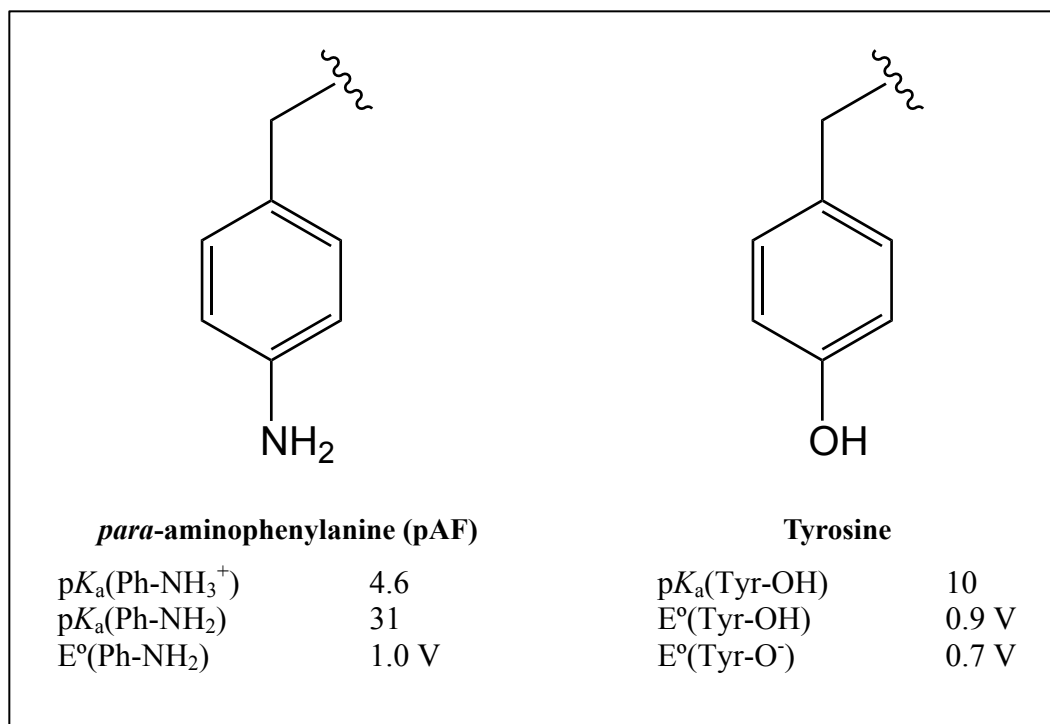
Tyrosine

Scheme 2-1. Comparison of *para*-aminophenylalanine (pAF) and tyrosine (*5-7*). Adapted with permission from (*24*). Copyright 2004 American Chemical Society.
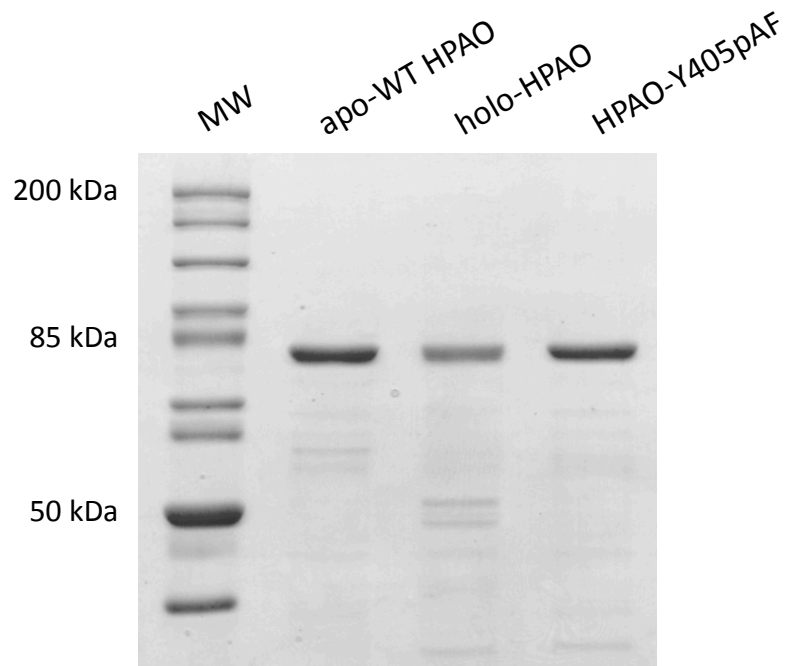
Figure 2-1. SDS-PAGE analysis of purified apo-WT HPAO, holo-HPAO, and HPAO-Y405pAF. 1 μg of each protein loaded. MW = molecular weight marker (PageRuler Unstained, Fermentas).

Res.#	AMINO ACIDS				YIELD (in pmoles)			
1	A				240			
2	A				280			
3	S				100			
4	A				220			
5	A				200			
6	P				100			
7	A				120			
8	R				100			
9	P				70			
10	A				90			
11	H				50			
12	P				40			
13	(L)	(G)			60	30		
14	D				60			
15	(P)	(I)			20	20		
16	(L)	(F)	(V)		25	20	15	
17	S				25			
18	(T)				20			
19	(A)				60			
20	(E)				15			

Figure 2-2. N-terminal sequencing results for HPAO-Y405pAF. On the left hand side is the sequence of amino acids measured, with alternate residues listed in subsequent columns. On the right hand side is the yield of each amino acid, including possible alternate residues at each position. Figure prepared by Stanford PAN Facility.
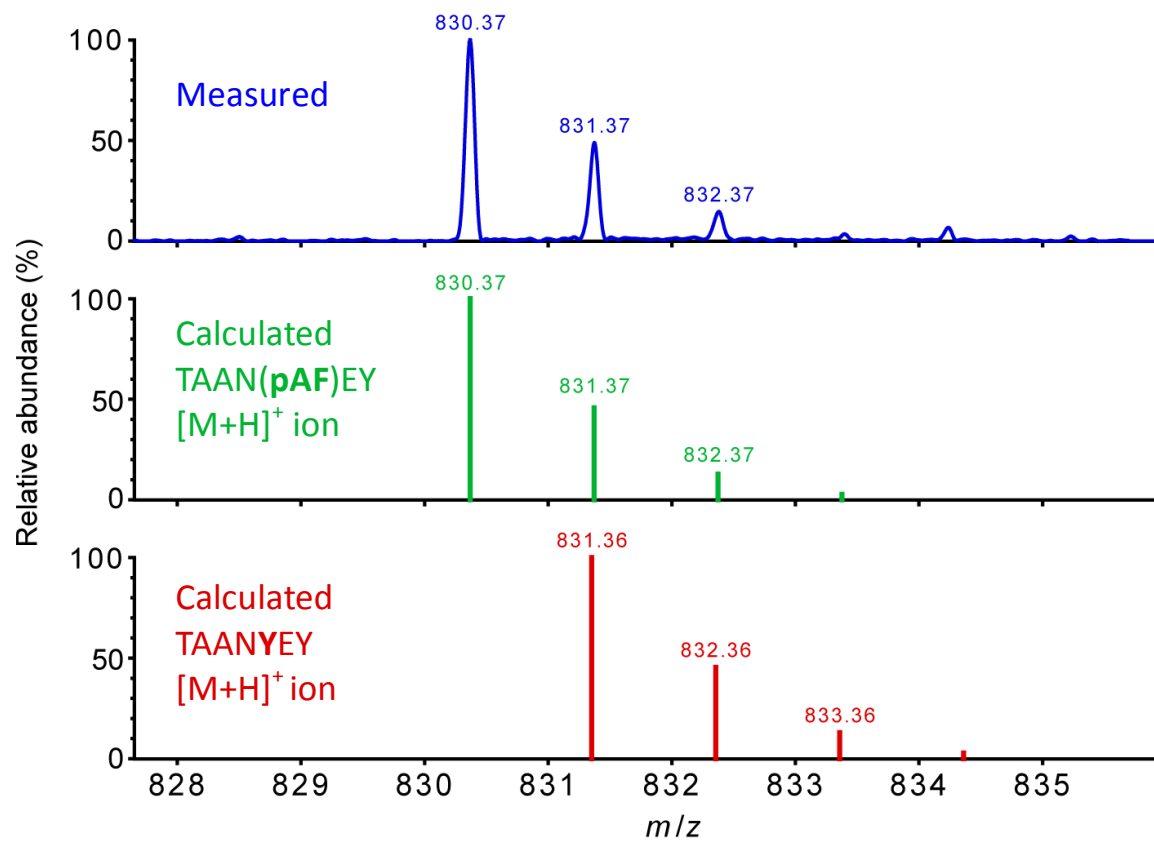
Figure 2-3. Precursor ion mass spectrum (formed by positive ESI) of HPAO-Y405pAF chymotryptic peptide. Figure generated by Dr. Tony Iavarone (QB3/Chemistry Mass Spectrometry Facility).
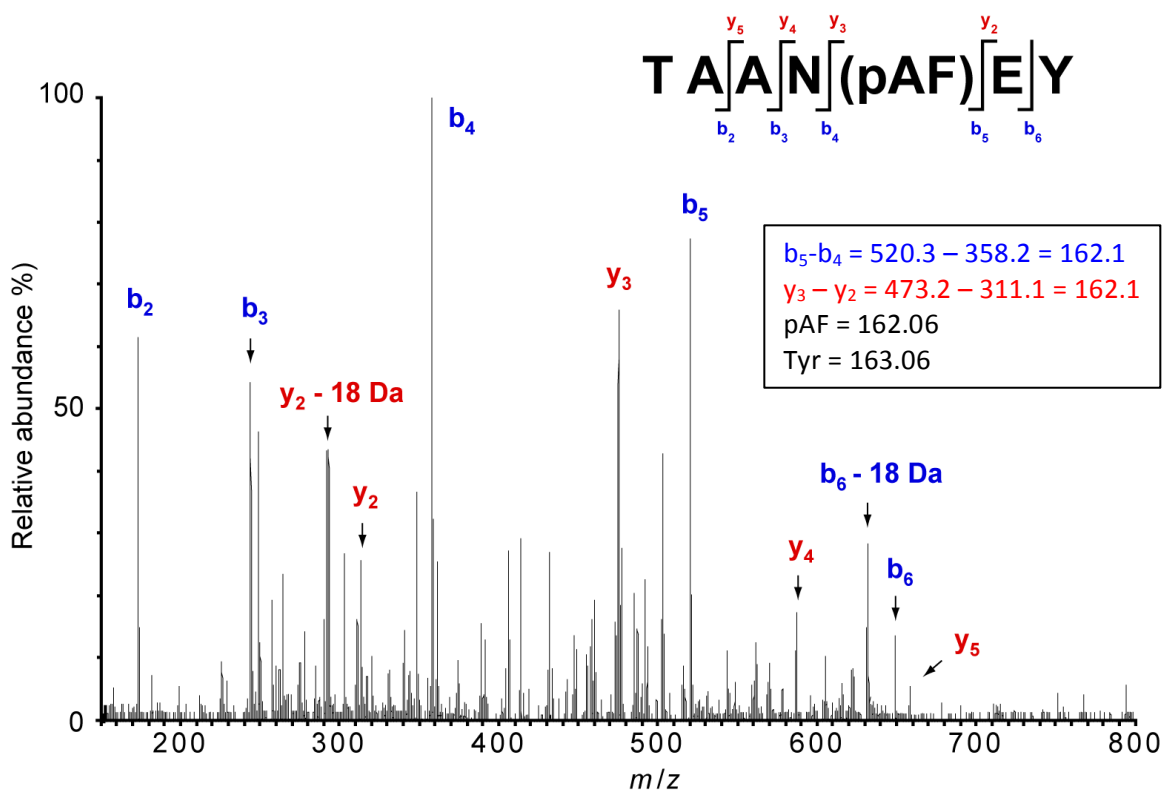
Figure 2-4. MS/MS spectrum of pAF-containing precursor ion. Labels indicate b and y fragment ions generated as a result of collisionally activated dissociation (CAD). Legend shows the b and y fragment ions that can be used to verify that position 405 contains an amino acid with a mass equal to that of pAF and not Tyr. Figure generated by Tony Iavarone (QB3/Chemistry Mass Spectrometry Facility).
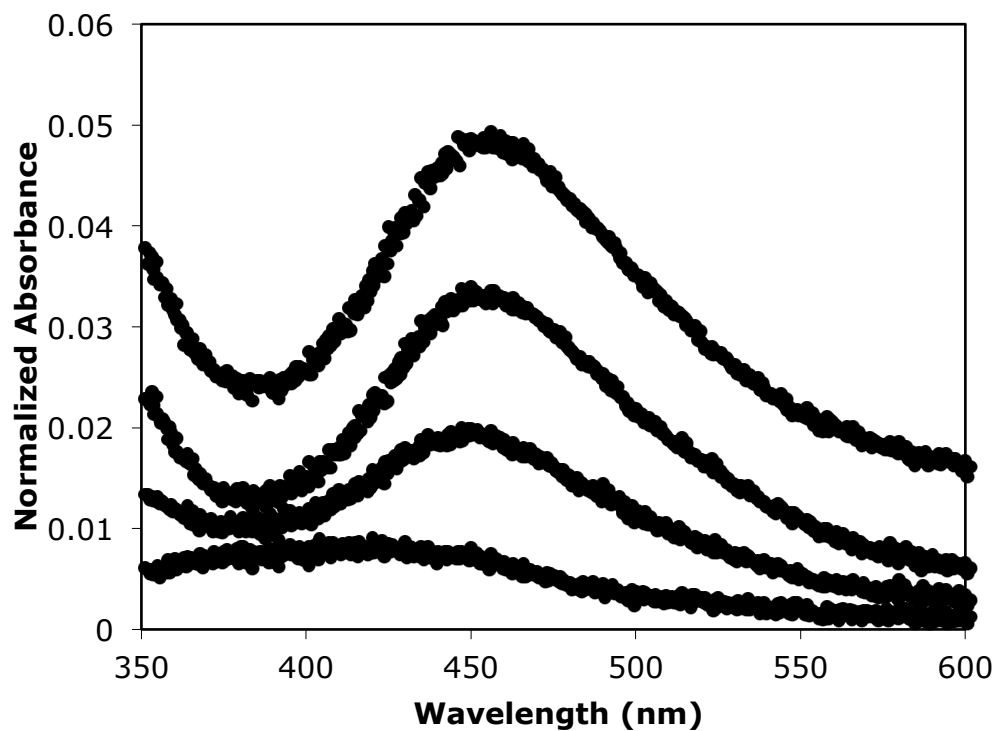
Figure 2-5. Spectral changes after addition of Cu(II) to apo-HPAO-Y405PAF at pH 9.0. The initial spectrum has been subtracted from each subsequent spectrum to emphasize the spectral changes. Spectra were measured every 2 min for 60 min. Shown are spectra at $t = 2$ min, 10 min, 30 min, and 60 min.
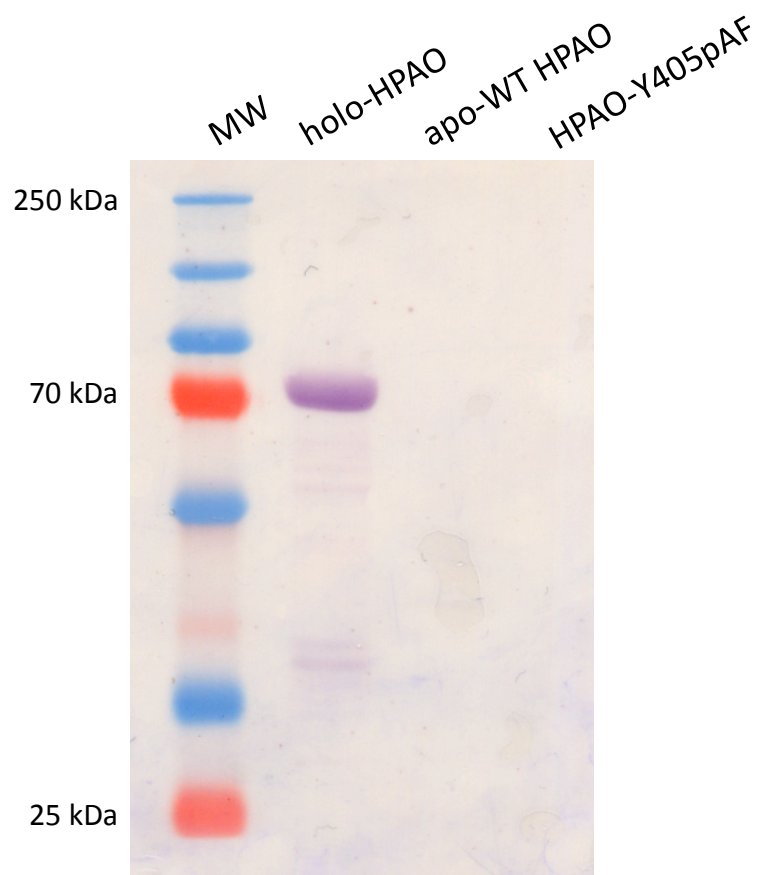
Figure 2-6. Nitrocellulose membrane stained for quinone detection. Proteins loaded were holo-HPAO, apo-WT HPAO, and HPAO-Y405pAF. MW = molecular weight marker (PageRuler Plus Prestained, Fermentas).
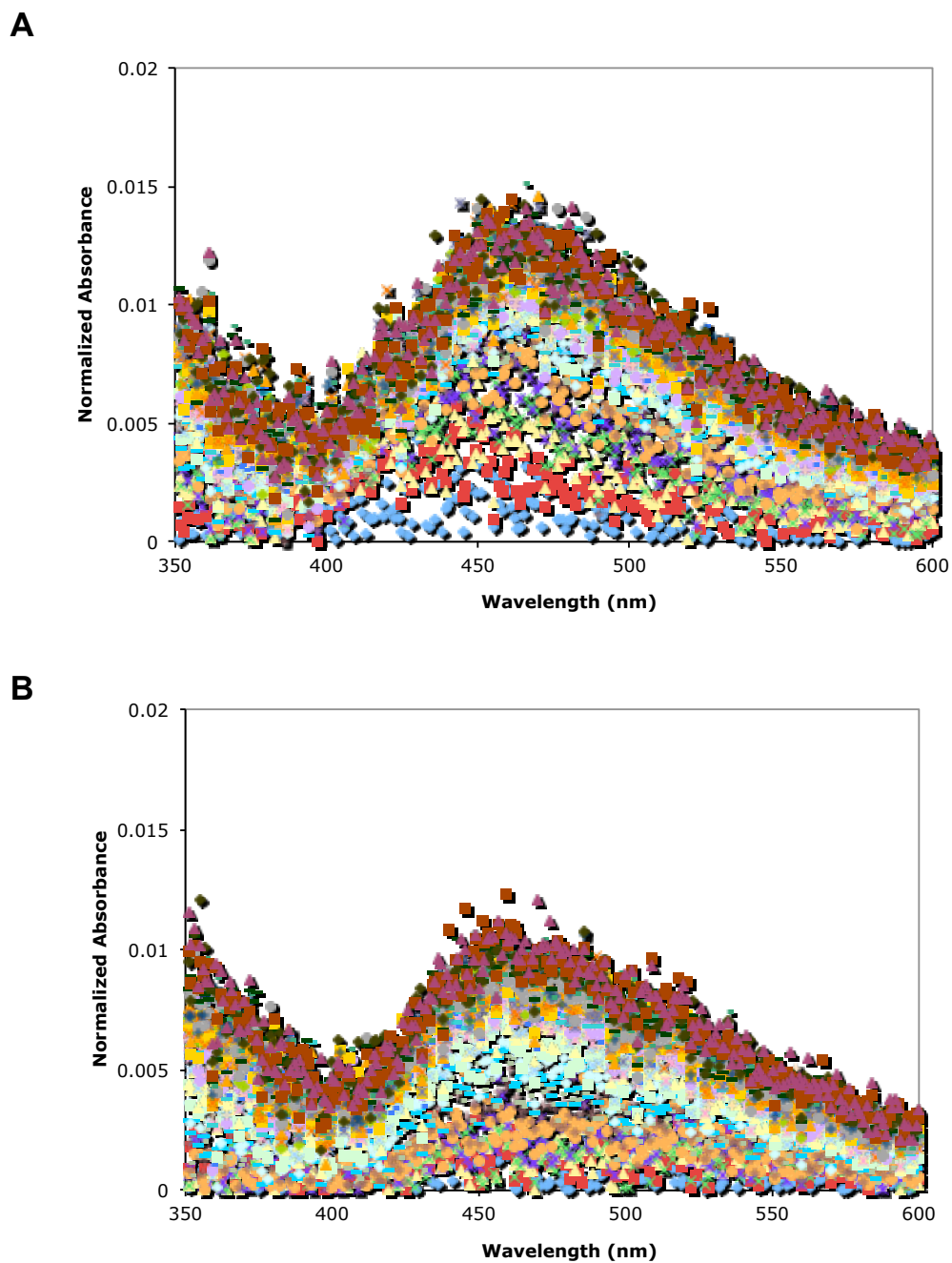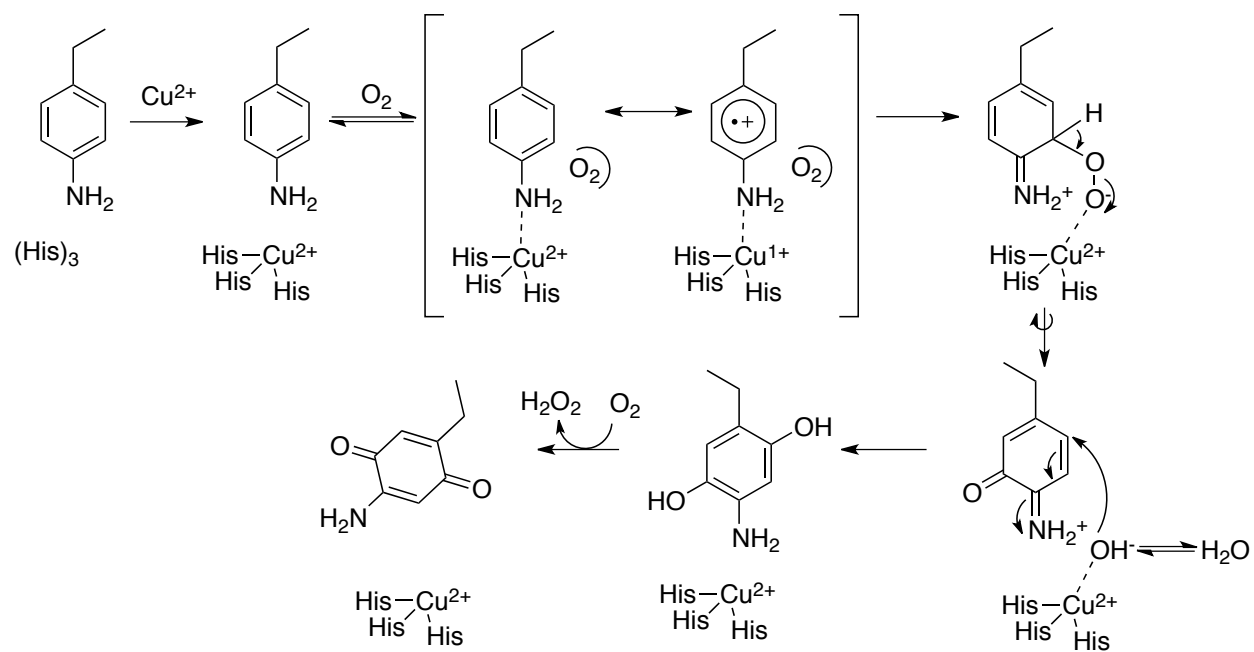
A

B

Figure 2-7. Spectral changes after anaerobic addition of Cu(II) to apo-HPAO-Y405PAF at pH 9.0. In **A**, Ar purging was used. In **B**, Glucose Oxidase/Catalase scrubbing system was used. The initial spectrum has been subtracted from each subsequent spectrum to emphasize the spectral changes. Spectra were measured every 2 min for 60 min.

Scheme 2-2. Hypothetical mechanism for the processing of pAF to an active site cofactor in HPAO.
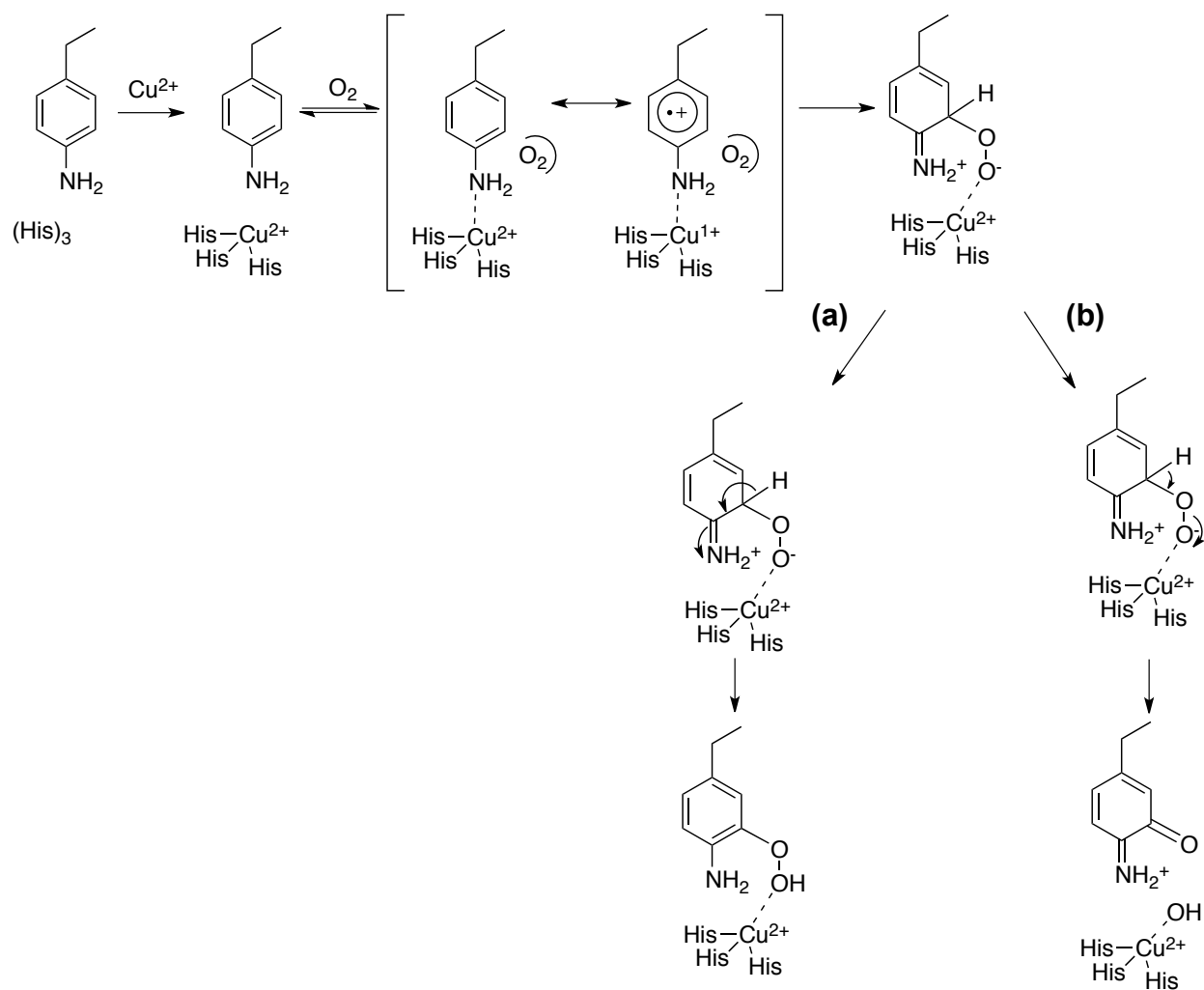
Scheme 2-3. Possible alternative mechanisms for the processing of pAF. One is the formation of a hydroperoxo-product could be generated by ring aromatization (pathway **a**). Pathway **b** shows O-O bond cleavage to generate an *o*-iminoquinone, which could then be processed into a final 4-aminoquinone product (Scheme 2-2).

References

1. Xie, J., and Schultz, P. G. (2005) Adding amino acids to the genetic repertoire, *Current Opinion in Chemical Biology 9*, 548–554.
2. Liu, C. C., and Schultz, P. G. (2010) Adding new chemistries to the genetic code, *Annu. Rev. Biochem. 79*, 413–444.
3. Young, T. S., and Schultz, P. G. (2010) Beyond the canonical 20 amino acids: expanding the genetic lexicon, *J. Biol. Chem. 285*, 11039–11044.
4. Wang, L., and Schultz, P. G. (2005) Expanding the Genetic Code, *Angew. Chem. Int. Ed. 44*, 34–66.
5. Smith, M., and March, J. (2007) March's Advanced Organic Chemistry, John Wiley & Sons.
6. Jonsson, M., Lind, J., Eriksen, T. E., and Merenyi, G. (1994) Redox and Acidity Properties of 4-Substituted Aniline Radical Cations in Water, *J. Am. Chem. Soc. 116*, 1423–1427.
7. DeFelippis, M. R., Murthy, C. P., Faraggi, M., and Klapper, M. H. (1989) Pulse radiolytic measurement of redox potentials: the tyrosine and tryptophan radicals, *Biochemistry 28*, 4847–4853.
8. Mehl, R. A., Anderson, J. C., Santoro, S. W., Wang, L., Martin, A. B., King, D. S., Horn, D. M., and Schultz, P. G. (2003) Generation of a bacterium with a 21 amino acid genetic code, *J. Am. Chem. Soc. 125*, 935–939.
9. Carrico, Z. M., Romanini, D. W., Mehl, R. A., and Francis, M. B. (2008) Oxidative coupling of peptides to a virus capsid containing unnatural amino acids, *Chem. Commun. (Camb.)* 1205–1207.
10. Samuels, N. M., and Klinman, J. P. (2005) 2,4,5-Trihydroxyphenylalanine Quinone Biogenesis in the Copper Amine Oxidase from *Hansenula polymorpha* with the Alternate Metal Nickel, *Biochemistry 44*, 14308–14317.
11. Farrell, I. S., Toroney, R., Hazen, J. L., Mehl, R. A., and Chin, J. W. (2005) Photo-cross-linking interacting proteins with a genetically encoded benzophenone, *Nat Meth 2*, 377–384.
12. DuBois, J. L., and Klinman, J. P. (2006) Role of a Strictly Conserved Active Site Tyrosine in Cofactor Genesis in the Copper Amine Oxidase from *Hansenula polymorpha*, *Biochemistry 45*, 3178–3188.
13. DuBois, J. L., and Klinman, J. P. (2004) Methods for characterizing TPQ-containing proteins, *Meth. Enzymol. 378*, 17–31.
14. Bradford, M. M. (1976) A rapid and sensitive method for the quantitation of microgram quantities of protein utilizing the principle of protein-dye binding, *Anal. Biochem. 72*, 248–254.
15. Edman, P. (1950) Method for determination of the amino acid sequence in peptides, *Acta chem scand. 4*, 283–293.
16. Gibson, Q. H., Swoboda, B. E., and Massey, V. (1964) Kinetics and Mechanism of Action of Glucose Oxidase, *J. Biol. Chem. 239*, 3927–3934.
17. Fabian, J. J. (1965) Simple Method of Anaerobic Cultivation, with Removal of Oxygen by a Buffered Glucose Oxidase-Catalase System, *J Bacteriol 89*, 921–921.
18. Hartmann, C., and Klinman, J. P. (1991) Structure-function studies of substrate oxidation by bovine serum amine oxidase: relationship to cofactor structure and mechanism,

Biochemistry 30, 4605–4611.

19. Cai, D., and Klinman, J. P. (1994) Copper amine oxidase: heterologous expression, purification, and characterization of an active enzyme in *Saccharomyces cerevisiae*, *Biochemistry 33*, 7647–7653.

20. Janes, S. M., Mu, D., Wemmer, D., Smith, A. J., Kaur, S., Maltby, D., Burlingame, A. L., and Klinman, J. P. (1990) A new redox cofactor in eukaryotic enzymes: 6-hydroxydopa at the active site of bovine serum amine oxidase, *Science 248*, 981–987.

21. Wang, L., Brock, A., Herberich, B., and Schultz, P. G. (2001) Expanding the Genetic Code of *Escherichia coli*, *Science 292*, 498–500.

22. Chen, Z.-W., Datta, S., DuBois, J. L., Klinman, J. P., and Mathews, F. S. (2010) Mutation at a strictly conserved, active site tyrosine in the copper amine oxidase leads to uncontrolled oxygenase activity, *Biochemistry 49*, 7393–7402.

23. Dove, J. E., Schwartz, B., Williams, N. K., and Klinman, J. P. (2000) Investigation of Spectroscopic Intermediates during Copper-Binding and TPQ Formation in Wild-Type and Active-Site Mutants of a Copper-Containing Amine Oxidase from Yeast, *Biochemistry 39*, 3690–3698.

24. Chang, M. C. Y., Yee, C. S., Nocera, D. G., and Stubbe, J. (2004) Site-specific replacement of a conserved tyrosine in ribonucleotide reductase with an aniline amino acid: a mechanistic probe for a redox-active tyrosine, *J. Am. Chem. Soc. 126*, 16702–16703.

Chapter 3

Further Characterization of Y405pAF and Comparison to Y305pAF

3.1   Introduction

Further Characterization of HPAO-Y405pAF
Having established that HPAO Y405pAF does not form a quinone but does form a new species that absorbs at 450 nm, we sought to pursue a full range of spectroscopic methods to further probe this species. Preliminarily, we assigned this new species as an aniline radical cation, given previous work showing that a 4-methylaniline radical cation had a spectra with λ_{max} ~450 nm (*1*). In addition, this species was reported to have an extinction coefficient of ~7500 $M^{-1}cm^{-1}$, which when applied to the data in **Figure-2-4**, gives a percentage of this species compared to total protein of ~15%. This value is similar to what is seen for the %TPQ seen when apo-WT HPAO is reconstituted with Cu(II) (*2*).

Therefore, we entered into several collaborations with groups that specialize in spectroscopic techniques that could provide insight beyond UV-Vis spectrophotometry. First, we pursued Resonance Raman spectroscopy in collaboration with the Mathies and Marletta Groups at UC Berkeley, which could provide information about bond stretches unique to an aryl hydroperoxy or aniline radical cation species. We also pursued electron paramagnetic resonance (EPR) spectroscopy in collaboration with the Britt Group at UC Davis, seeking to detect the appearance of an organic-based radical species concomitant with the disappearance of Cu(II) to Cu(I) due to electron transfer from the Cu(II) to aniline. As an alternative and possible more sensitive approach, we have also initiated a collaboration with the Solomon Group at Stanford to monitor the formation of a Cu(I) edge absorption directly by X-ray Absorption Near Edge Structure (XANES). We have also pursued crystallographic studies with the Wilmot group at University of Minnesota, with whom we have a long-standing collaboration on copper amine oxidase (*3-5*).

Role of Y305 in Cofactor Biogenesis
A common O_2 binding site in the copper amine oxidases has been proposed to link cofactor biogenesis to catalysis (*6*). This raises the provocative question of how a single O_2 binding site can lead to disparate activities: monooxygenation of tyrosine to generate TPQ and oxidation of amines to aldehydes and reduction of O_2 to hydrogen peroxide during catalytic turnover. Because the same active site facilitates both reactions, individual active site residues may serve multiple roles. One residue of interest is a strictly conserved tyrosine (Y305 in HPAO) that hydrogen bonds to the O-4 of TPQ in the mature enzyme (**Figure 1-1**).

The role of Y305 in cofactor biogenesis has been studied by analyzing the properties of Y305A and Y305F mutant proteins (*7*). It was found that the Y305F mutant gave rates for TPQ production that were close to that of WT (reduced ~3-fold), while the Y305A mutant was significantly more hindered, with a rate ~30-fold slower than WT (*7*). In biogenesis, the fairly high rate for Y305F in relation to Y305A implicates a role for steric bulk and hydrophobicity at this position in steering the position of Y405 and its oxygenated intermediates that form en route to TPQ. It is also possible that this Tyr residue acts as a general acid to help facilitate breakdown of the aryl-peroxide intermediate or as a general base to abstract a proton from C-3 of the cofactor ring to drive breakdown of this intermediate (*7*). Furthermore, an additional product was detected that absorbed at ~400 nm in the case of Y305A and at ~420 nm for Y305F. In the case of Y305F, the alternate species forms 4-fold more quickly than TPQ at pH 7, facilitating its preferential crystallization and characterization by x-ray crystallography (*8*). In this crystal

structure, a novel 2,3,4-trihydroperoxo, 5-hydroxo derivative was detected (**Figure 3-1**). Formation of this new species is postulated to involve the partitioning of the normal, aryl-peroxy intermediate (**E-I**) between concomitant proton abstraction and O-O bond cleavage to generate dopaquinone and ultimately TPQ (**top of Scheme 3-1**), and proton loss and ring aromatization to yield an off-path hydroperoxo-product (TPO) (**bottom of Scheme 3-1**).

By incorporating pAF into position 305, we can further investigate the role of this residue in cofactor biogenesis and catalysis. pAF is nearly isosteric to Tyr, providing a unique probe that differs from site-directed mutagenesis of Tyr to Phe or Ala. By incorporating pAF into another residue in the active site, we will also be able to make interesting comparisons to our results with HPAO Y405pAF.

3.2 Materials and Methods

HPAO-Y305pAF Mutagenesis
Mutations were made to the pET3a-HPAO plasmid (*9*) in order to substitute an amber stop codon for the sequence that encodes for Tyr at position 305. The pET expression system relies on the bacteriophage T7 RNA polymerase to drive expression, which is induced with Isopropyl β-D-1-thiogalactopyranoside (IPTG). Site-directed mutagenesis was performed using the Stratagene QuikChange II XL kit. HPLC-purified primers were purchased from Eurofins MWG Operon. The forward primer is listed in the 5' to 3' direction, and the reverse primer is listed in the 3' to 5' direction. The mutated codon is in bold, and the changed bases are in italics. DNA mutation was confirmed by automated sequencing at the UC Berkeley Sequencing Facility.

HPAO Y305pAF:
```
5'–CCGAGATGATTGTTCCTTAGGGCTCGCCAG–3'
3'–GGCTCTACTAACAAGGAATCCCGAGCGGTC–5'
```

HPAO-Y305pAF Expression
Expression of HPAO-Y305pAF was carried out identically to Y405pAF (see Chapter 2) with the exception that cell paste was not frozen before purification. Instead it was kept on ice to be lysed that same day or overnight to be lysed the next day. This was done due to instability seen with Y305F and Y305A mutant protein, where freezing the cell pellets or the purified protein did not yield spectroscopically detectable TPQ (λ_{max} ~480 nm) (*7*).

HPAO-Y305pAF Purification
Protein purification of HPAO-Y305pAF was carried out identically to Y405pAF, using ion-exchange and size-exclusion chromatography (see Chapter 2).

HPAO Y305pAF Characterization

Protein quantitation
Protein concentration was measured by the Bradford assay (Bio-Rad) (*10*). Typical protein yields were ~2-4 mg/9 L cell culture (in comparison to ~10-20 mg/9 L for WT apo-protein).

Phenylhydrazine reaction
For a more sensitive test for the presence of TPQ, reaction with an excess of phenylhydrazine HCl was used. 1 μl 5 mg/ml phenylhydrazine was added to 40 μM enzyme reconstituted with Cu(II) (see protocol below), and the reaction was monitored at 448 nm on a Varian Cary 50 Bio UV-Vis spectrophotometer. An extinction coefficient of 40500 $M^{-1}cm^{-1}$ was used to quantitate phenylhydrazone formation (*2*).

Aerobic Cu^{2+} reconstitution
HPAO-Y305pAF was diluted with 50 mM CHES, pH 9 to 110 μl at 40 μM (3 mg/mL) Spectral changes to this sample after addition of 4.4 μl $CuSO_4$ (1 equivalent) were monitored over 1 h in a Varian Cary 50 Bio UV-Vis spectrophotometer.

Anaerobic Cu^{2+} reconstitution

A solution of protein (40 µM, 150 µl) was prepared in a gas-tight, septum-sealed cuvette. This solution was then made anaerobic, either by purging the sample on ice with a slow flow of argon gas for 1 h or by several cycles of evacuation followed by argon back filling (*2*). A solution of 1 mM $CuSO_4$ was similarly made anaerobic by continuous bubbling or argon or alternating cycles of vacuum and argon. An equivalent of Cu(II) was added to the sample by gas-tight syringe, and the sample was mixed gently. Spectral changes were monitored over 1 h in a Varian Cary 50 Bio UV-Vis spectrophotometer. At this point, the septum was removed from the cuvette, and the sample was flushed with air. Spectra were then measured for another hour.

HPAO-Y305pAF Kinetic Measurements
To test for activity toward benzylamine, benzaldehyde formation was monitored at 250 nm ($\varepsilon = 12800$ $M^{-1}cm^{-1}$) on a Varian Cary 50 Bio UV-Vis spectrophotometer (*11*). Standard conditions were as follows: 50 mM CHES, pH 9.0 at 25ºC, with a total volume of 1 mL and initiation of the reaction by addition of 5 µl Cu(II) reconstituted enzyme. To test for enzyme activity toward ethylamine, oxygen consumption was monitored with a Clark-type oxygen electrode and a YSI-5300 biological oxygen monitor (*12*). Standard conditions were as follows: 50 mM CHES, pH 9.0 at 25ºC, with a final volume of 1 mL and initiation of reaction by addition of 5µl of Cu(II) reconstituted enzyme.

HPAO-Y305pAF Chymotrypsin Digestion
Y305pAF was digested with chymotrypsin similarly to Y405pAF (see Chapter 2).

Mass Spectrometry
Y305pAF samples were processed similarly to Y405pAF (see Chapter 2).

Resonance Raman Spectroscopy
All spectra were obtained using the 457.9 nm excitation line from an Ar^+ laser (Spectra-Physics model 2020). Raman scattering was collected with a cooled, back-illuminated CCD detector (LN/CCD-1100/PB; Roper Scientific) and controller (ST-133; Princeton Instruments) coupled to a subtractive dispersion double spectrograph (*13*). The laser power at the sample was ~30-90mW. Data acquisition times were 1 h and 4 h for the native WT and reconstituted enzymes, respectively. To minimize photodegradation, the protein samples were loaded into a microspinning sample cell at a 90° scattering geometry, described previously (*14*). The sample temperature was maintained at ~8-10°C by flowing cooled N_2 gas over the spinning cell. The Raman spectra were corrected for wavelength dependence of the spectrometer efficiency using a white lamp, and the instrument was calibrated using the Raman frequencies from cyclohexane, carbon tetrachloride, and toluene. For each Raman spectrum, the raw data were baseline-corrected. The reported frequencies are accurate to ±1 cm^{-1} and the spectral bandpass was set to 6.5 cm^{-1}. Spectral analysis was performed using Igor Pro (Wavemetrics).

EPR Characterization
HPAO-Y405pAF was buffer exchanged into 50 mM CHES, pH 9.0 by concentrating in an Amicon Ultra-4 spin concentrator to ~500 µl, followed by diluting with 4 mL 50 mM CHES, pH 9.0, then repeating three more times (4x total). Final concentration of protein used was ~70-120 µM, volume ~300 µl. 0.5 or 0.75 equivalents of $CuSO_4$ were added, and the samples were incubated at RT for 1 h. After incubation, 150 µl of Cu(II)-reconstituted protein was added to 30

μl glycerol (final concentration ~20%), and the sample was loaded in EPR tubes, capped with a rubber septum, and flash frozen in liquid N_2. For the apo-HPAO Y405pAF sample, protein alone was mixed with glycerol and flash frozen. For the buffer only sample, 50 mM CHES, pH 9.0 was mixed with glycerol and flash frozen. EPR tubes were previously cleaned and prepared by being soaked in 1M NaOH for 1 h, rinsed with ddH_2O, soaked in 1 M HNO_3 for 1 h, rinsed with ddH_2O, soaked in 1 mM EDTA for 1 h, then rinsed with ddH_2O. The tubes were left to dry in an oven for 2 h before use.

EPR experiments were conducted at the CalEPR center at the University of California, Davis, using a Bruker ECS106 X-band spectrometer equipped with a TE102 cavity (ER4102ST) resonating at ~9.38 GHz and an Oxford ESR900 helium cryostat with an ITC503 temperature controller. The field modulation frequency and amplitude were 100 kHz and 10 G peak-to-peak, respectively. Cu(II) quantitation was carried out by comparing the double integral of an EPR spectrum with the double integrals of the EPR spectra of Cu^{2+}-EDTA solutions at known concentrations between 25 μM - 200 μM. The double integral of a spectrum (area underneath the integrated EPR spectrum) is proportional to the number of spins contributing to the spectrum.

X-Ray Absorption Spectroscopy

The Cu K-edge X-ray absorption spectra of HPAO were measured at the Stanford Synchrotron Radiation Lightsource (SSRL) on the unfocused 20-pole, 2.0-T wiggler beamline 7-3 under storage ring conditions of 3 GeV and 350 mA. A Rh-coated pre-monochromator mirror was used for harmonic rejection and vertical collimation. A Si(220) double-crystal monochromator was used for energy selection. The samples were loaded into 2 mm Delrin XAS cells with a 38 μm Kapton window. The samples were maintained below a temperature of 10 K during data collection using an Oxford Instruments CF 1208 continuous-flow liquid-helium cryostat. A Canberra solid-state Ge 30-element array detector was used to collect Kα fluorescence data. Internal energy calibration was performed by the simultaneous measurement of the absorption of the Cu foil placed between two ionization chambers located after the sample. The first inflection point of the foil spectrum was assigned to 8980.3 eV.

Several scans were collected at the same spot and the subsequent scans revealed no substantial photoreduction. The energy-calibrated data were processed by fitting a second-order polynomial to the pre-edge region and subtracting this from the entire spectrum as a background. The spectra were normalized by assigning the edge jump at 9000 eV to 1.0. This background subtraction and normalization were done using PySpline (*15*).

Crystallization

Crystals of HPAO-Y405pAF and Y305pAF were grown by hanging drop vapor diffusion using a 1:1 volume ratio of purified protein and the crystallization solution (2-6 μl total volume; 7.0-8.5% w/v polyethylene glycol 8000, 0.25-0.28 M potassium phosphate, pH 7.0). These conditions are similar to those used for the crystallization of holo-HPAO and apo-HPAO. Although the absorbance feature in the aniline-substituted HPAO-pAF at 450 nm is strongest at higher pH values (9.0), attempts to grow diffraction-quality crystals of Y405pAF HPAO at a pH above 7.0 were unsuccessful. After equilibrating for ~24 h, drops were seeded with a streak-seeding technique using a native HPAO-1 crystal as seed donor (*16*). Colorless crystals grew to full size after 7-9 days. Once formed, crystals were transferred every other day into a new drop

of crystallization solution at an increasingly higher pH (pH was increased by 0.5 for each transfer) until a final pH of 9.0 was reached. HPAO-Y405pAF crystals at a variety of final pH values were soaked in 25% glycerol mixed with well solution for ~5-10 sec for cryoprotection before flash-freezing in liquid N_2.

Data Collection and Refinement
Diffraction data collection, processing, and refinement statistics for the structure of HPAO-Y405pAF in complex with Cu(II) from a crystal harvested at pH 7.0 are given in **Table 3-1**. Diffraction data were collected at the Advanced Photon Source in Argonne, IL (beamline 23-ID, General Medical Sciences and National Cancer Institute Collaborative Access Team (GM/CA-CAT) to a resolution of 1.57 Å and processed using HKL2000 and SCALEPACK (*17*). HPAO Y405pAF protein was found to crystallize in space group $C222_1$, which is different than that of native HPAO, which crystallizes in space group $P2_1$. Molecular replacement using the program PHASER in the CCP4 suite with a holo HPAO monomer from the native structure as a search model (PDB code 2oov with solvent molecules, metal, and the side chain of TPQ removed) was used to solve the HPAO-Y405pAF structure (*3, 18*). Manual model building was performed using COOT, and refinement was carried out using the program REFMAC in the CCP4 suite (*19, 20*). The structure of pAF was incorporated into each polypeptide chain (PDB residue HOX) based on peaks in the *$2F_o$-F_c* and *F_o-F_c* electron density maps. Cycles of manual model building continued until peaks in the *F_o-F_c* electron density were at the level of noise.

Single Crystal UV-Visible Spectrophotometry
All crystals were flash frozen in liquid nitrogen for storage before data collection and single crystal UV/visible spectroscopy. Spectra were measured at 100 K after X-ray exposure with a microspectrophotometer (4DXray Systems AB) linked to an Oxford CryoStream system (OxfordCryosystems) that had been manually calibrated using a holmium filter (Abbota Corporation). Spectroscopic data were recorded using the program Andor MCD (http://www.andor.com).

3.3 Results

Spectroscopic Studies of HPAO Y405pAF

Resonance Raman spectroscopy
Initially, we sought to analyze WT holo-HPAO (which contains mature TPQ cofactor), as a control before moving on to HPAO Y405pAF. The underivatized protein, however, did not generate enough signal-to-noise (data not shown), most likely due to the low molar extinction coefficient of TPQ (ε_{480} = 2400 $M^{-1}cm^{-1}$) (*2*). In previous experiments with underivatized CAO, a very high concentration of protein was used (~400 μM) (*21*). In these experiments, only ~100 μM protein was used, providing a possible explanation for the low signal. Thus, we turned to derivatizing the TPQ-containing WT holo-HPAO with phenylhydrazine, which provides an intensely absorbing chromophore in the form of a phenylhydrazone (ε = 40500 $M^{-1}cm^{-1}$) (*22*) (**Figure 3-2**). The observed results, including peaks at ~1300 cm^{-1}, ~1600 cm^{-1}, and between 400-500 cm^{-1} are comparable to what was previously seen with phenylhyrazone-derivatized copper amine oxidases from bovine serum and *Arthrobacter* P1 (**Figure 3-2**) (*22*)

Given our ability to reproduce previous work with WT holo-HPAO, we then turned to analyzing HPAO-Y405pAF. This unnatural amino acid-incorporated protein, unlike WT, cannot be derivatized with phenylhydrazine to form a strongly absorbing hydrazone (see Chapter 2). Thus, we used high concentration of protein ~300 μM in order to study the weakly absorbing 450-nm species previously seen by UV-Vis spectrophotometry (see Chapter 2). As controls, we also analyzed the spectra of pAF by itself and CHES buffer. What we observed was fairly low signal to noise, with most of significant features found in the HPAO-Y405pAF spectra, including peaks ~800-850 cm^{-1}, 1044 cm^{-1}, 1209 cm^{-1}, 1357 cm^{-1}, and 1618 cm^{-1}, being attributable to either the pAF alone spectrum or CHES buffer spectrum (**Figure 3-3**).

EPR spectroscopy
Our initial work with lower concentration of protein (~70 μM) shows that Cu(II)-reconstituted HPAO-Y405pAF has a clear Cu(II) signal at g = 2.06, and that apo-protein contains very little Cu(II) signal, a result verified by our previous ICP data (Chapter 2) (**Figure 3-4**). Unfortunately, we were unable to see the presence of a an organic radical, which would be centered around g = 2.002 – 2.008 (*23*). The next attempt was carried out with more concentrated protein (~125 μM). The temperature chosen was 40K, as the signal saturates at 20K and has poor signal-to-noise at 80K (data not shown). Looking at the spectra of Cu(II)-reconstituted HPAO-Y405pAF, we can see a clear Cu(II) signal in the holo-protein, whereas the apo-protein and buffer control are essentially free of spin (**Figure 3-5**). There is a high-field shoulder at 340 mT visible at low powers in the holo-protein. At higher powers, this shoulder saturates and cannot be observed. Also visible is the fact that the holo signal extends down to at least 270 mT.

Looking at the power dependence of the signal at 40K, it can be seen that the signal saturates at 1 mW and above (**Figure 3-6**). This means that at 40K, 100 μW is probably the optimum power that minimizes saturation and maximizes signal-to-noise without saturating the signal more than a few percent. The shoulder at ~340 mT is also visible at the lower powers. Using Cu^{2+}-EDTA solutions as standards, we can quantitate the amount of Cu(II) signal in the holo-protein, apo-protein, and buffer control. Given the saturation of signal for the standards at 100 μW (at 40K),

the standards were measured at 10 μW, and the resulting spectra corrected for the modified power. The results are 41 μM for the holoprotein and 3 μM for the apoprotein (**Figure 3-7**). Total protein concentration was 125 μM, which was reconstituted with 0.75 equivalents of Cu(II), or 94 μM.

X-Ray Absorption Spectroscopy
As an alternative to EPR, we also sought to monitor the formation of a Cu(I) edge absorption directly by XANES in collaboration with the Solomon Lab at Stanford University. Toward this end, we sought to examine Cu(II)-reconstituted HPAO Y405-pAF at an early time point, such that Cu(II) is able to enter the active site, and a later time point, after chemistry happens i.e. the same phenomenon seen in the UV-Vis spectrophotometer in the form of a 450-nm species growing in. From the spectra (**Figure 3-8**) it appears that both samples contain the same amount of reduced Cu. A closer examination reveals that the longer time incubation (1 h) contains ~2-3% more reduced Cu, though this is most likely within experimental error.

HPAO-Y305pAF Characterization

Expression and purification
The same expression and purification conditions used for Y405pAF were used for the Y305pAF variant. Following purification by ion-exchange and size-exclusion chromatography, HPAO-Y305pAF runs as a single band on SDS-PAGE and similarly to HPAO Y405pAF (data not shown). No issues with truncation due to incorporation of an amber stop codon at residue 305 were seen.

Chymotrypsin Digestion and Mass Spectrometry
In collaboration with Dr. Tony Iavarone (Chemistry/QB3 Mass Spectrometry Facility, UC Berkeley), we used mass spectrometry to provide direct evidence that pAF had been incorporated at position 305. Given our previous success with using chymotrypsin on the Y405pAF protein (Chapter 2), we used the same protease to digest Y305pAF. Analysis of chymotryptic peptides by LC-MS/MS revealed a $[M+2H]^{2+}$ ion with $m/z = 653.86$. The isotopic distribution for this peptide matches that of the peptide RISLSEMIVP(**pAF**), containing a pAF residue at position 305, and does not match that calculated for the peptide containing Tyr (**Figure 3-9**). Collisionally activated dissociation of this peptide gives b and y ions that confirm the presence of pAF (but not Tyr) at position 305 (**Figure 3-10**). No analogous peptides containing Tyr instead of pAF i.e. RISLSEMIVP**Y** was measured from the sample by MS/MS.

Aerobic reconstitution and quinone cofactor detection
Aerobic reconstitution of HPAO-Y305pAF at pH 9.0 generated a species with a λ_{max} ~450 nm (WT HPAO λ_{max}TPQ = 480 nm) that grew in over an hour and was stable for several hours afterward at RT (**Figure 3-11**). This new 450 nm-species did not react with phenylhydrazine to form a hydrazone as TPQ does, however, suggesting that it is not a quinone. In addition, Cu-reconstituted protein did not react with NBT to form a purple band as TPQ does (data not shown), further suggesting that this new species is not a quinone.

Activity toward benzylamine and ethylamine
Cu(II)-reconstituted protein was also tested for activity toward benzylamine and ethylamine.

When benzylamine was added to Cu(II) reconstituted HPAO-Y305pAF, no increase in absorbance at 250 nm (where benzaldehyde product absorbs) was observed. To test for activity toward ethylamine, which does not allow for easy spectrophotometric detection of product, O_2 depletion was monitored with a Clark-type electrode. No O_2 consumption was seen, further indicating that the protein is not active toward primary amine substrates and that it does not contain a mature TPQ cofactor.

Anaerobic reconstitution
In order to characterize the 450-nm species further, we sought to determine whether its formation is oxygen-dependent. When protein is reconstituted with Cu(II) anaerobically, a 450 nm-species appears that is similar to what is seen with aerobic reconstitution (**Figure 3-12**). No further spectra changes were observed after subsequent exposure to air.

X-ray Crystallography of Y405pAF
X-ray diffraction data, processing, and refinement statistics for HPAO-Y405pAF in complex with Cu(II) are listed in **Table 3-1**. The structure of HPAO Y405pAF contains three polypeptide chains, or 1.5 physiological dimers, in the ASU in space group $C222_1$. It is nearly identical in overall fold to that of native HPAO, with superimposition of corresponding main chain atoms resulting in a root-mean-square deviation (rmsd) of 0.31 Å (*3*). HPAO-Y405pAF adopts the archetypal CAO overall fold and is arranged in three domains located along the primary sequence, with all significant structural differences between it and the native HPAO structure located at the active site.

Distances and occupancies are reported as the range observed across the three polypeptides in the ASU following refinement. The active site of HPAO-Y405pAF contains copper bound at an occupancy of 0.8-0.85 as determined by test refinements in an identical position to that of the native structure (**Figure 3-13**). The copper ion is ligated by the imidazole groups of three conserved histidine ligands at distances of 2.1, 2.0, and 2.0 Å (His456, His458, and His624, respectively) as well as by the amine group of pAF at a distance of 2.3-2.4 Å in a distorted square pyramidal geometry. The pAF amino acid side chain adopts an orientation similar to that of TPQ in its "on-copper" conformation in the native enzyme, and is nearly superimposable with the unprocessed precursor tyrosine residue that is modified to produce TPQ during biogenesis found in the structure of apo-HPAO. The pAF side chain is also involved in a hydrogen bond with a well-ordered water molecule seen in many native CAO structures, including HPAO-1 (**W in Figure 3-13**). All other active site residues are identical in position to those in the native HPAO structure.

Single crystal UV-Visible Spectra
Single crystal UV/visible spectra collected from the Cu(II)-reconstituted HPAO-Y405pAF crystal after x-ray exposure revealed a broad absorbance feature centered at 450 nm that is similar to the feature observed in solutions of HPAO-Y405pAF protein reconstituted with Cu(II) (**Figure 3-14**).

3.4   Discussion

Resonance Raman spectroscopy has proven very useful for studies of copper amine oxidase. The various C—C, C=O, and C—H stretching modes of TPQ have been well-characterized ((*21*, *22*). This method has also been used to identify catalytic cycle reaction intermediates in CAOs (*24*). We were able to reproduce previous results with phenylhydrazine-derivatized holo-HPAO (*22*) (**Figure 3-2**). HPAO-Y405pAF, however, does not have the advantage of reactivity toward phenylhydrazine to provide a strongly absorbing hydrazone (Chapter 2). Instead, we had to examine the spectrum of the underivatized protein, reconstituted with Cu(II). If the 450-nm species is indeed an aniline radical cation, it has a fairly low extinction coefficient when compared to that of the TPQ-containing phenylhydrazone (ϵ ~7500 $M^{-1}cm^{-1}$ vs. 40500 $M^{-1}cm^{-1}$) (*1*, *2*), though it is greater than that of the underivatized TPQ cofactor (2400 $M^{-1}cm^{-1}$) (*2*). Unfortunately, the significant features of the Cu(II)-reconstituted protein were also found in the pAF sample or the buffer control (**Figure 3-3**). What might be of interest is that there are features found in pAF alone that are not found in the Cu(II)-reconstituted protein, including features at 643 cm^{-1} and 1133 cm^{-1}, though it not clear what these correspond to. In sum, we were not able to achieve enough signal-to-noise to gain additional insight about the 450-nm species, whether it might be an aniline radical cation, hydroperoxy species, or something different. Thus, we turned to other spectroscopic techniques to probe this species further.

In collaboration with Stefan Stoll in the Britt group at UC Davis, we sought to monitor the formation an organic based radical or the loss of Cu(II) signal by EPR. The detection of such behavior would contrast with biogenesis in WT protein, where an organic radical has never been seen. In theory, EPR can be used to determine the oxidation state of the Cu in the active site given that paramagnetic Cu(II) is EPR-detectable, whereas diamagnetic Cu(I) is EPR-silent. EPR has also been widely used to study organic based radicals in biology (*23*). Other than a shoulder at 340 mT (**Figure 3-5**) that is too broad to assign to an organic radical, the dominant signal observed is that of Cu(II). Signal-to-noise was definitely an issue, as this feature was not visible at lower protein concentration (**Figure 3-4**).

The fact that the Cu-quantitation gives values less than what would be expected (**Figure 3-7**) i.e. 94 µM for ½ equivalent Cu(II) expected vs. 41 µM measured, does not necessarily mean that Cu(II) has been converted to Cu(I). Experimental error with the Cu-EDTA standards is certainly possible. In addition, after these samples were measured by EPR, they were analyzed for metal content by ICP-OES. The values measured were 4.4 µM for the apo-sample and 44 µM for the holo-protein, in close agreement with the EPR-quantitation values. So, experimental error in the exact amount of Cu weighed out for the Cu solution used for reconstitution, and/or experimental error in the amount of Cu solution added for reconstitution are also possible explanations for the discrepancy.

Given that we believe the 450-nm species only forms in a small population of the total protein (see Introduction, Chapter 3), it was going to be challenging to observe the formation of a possible radical species by EPR unless very high concentrations of protein were used. It would have been similarly difficult to observe the redox change of the metal, given that we would be looking for the loss of a signal in the form of paramagnetic Cu(II) rather than an increase in signal.

Initial examination of Cu(II) addition to HPAO-Y405pAF by XAS shows that both early (~10 min) and later time point (1 h) incubations show the same amount of reduced copper. It is possible that the process of 450-nm species formation is faster than we expected, such that the process finished even by the early time point. Our original experimental design drew on the results of the UV-Vis experiments, where 450-nm species formation grows in over 1 h (**Figure 2-4**). Therefore, we wanted the early time point to proceed long enough for the Cu(II) to migrate to the active site but not to undergo any reaction to a large extent. It is possible, however, that the majority of the reaction happens more quickly, with a non-specific reaction occurring afterward that contributes to the increase in absorbance at 450-nm. What will be of great interest is the result of Cu(I)-reconstituted HPAO-Y405pAF, which is under investigation. In this sample, both protein and Cu(I) were made anaerobic, then Cu(I) was added to the protein inside an inert atmosphere chamber. If the spectra of the Cu(I)-reconstituted sample looks substantially different from the two Cu(II)-reconstituted samples, we could infer that both of the Cu(II) samples are in the oxidized, Cu(II) state. If instead, the Cu(I) sample spectra looks similar to the two Cu(II) sample spectra, we could postulate that reduction of metal occurred in both of the Cu(II) samples.

Based on our biochemical, spectroscopic, and structural data, we propose that the 450-nm species represents an intramolecular electron transfer between the Cu(II) and pAF to form Cu(I) and an aniline radical (**Scheme 3-2**). Based on the structure of HPAO-Y405pAF (**Figure 3-13**), the distance between the amine group of pAF and the metal center (2.3-2.4 Å) is comparable to that of the precursor Tyr in WT protein (2.5 Å), further suggesting that intramolecular electron transfer is possible. Based on the single crystal UV-Vis spectrum (**Figure 3-14**), we can infer that the same process that happens in solution happens in the crystals. Thus, when we examine the crystal structure, which shows an unmodified pAF ring that is oriented toward the Cu, we can infer that that other types of chemistry e.g. oxygenation are also absent from the solution reaction. In addition, the 450-nm absorbance cannot be attributed to simple copper binding, as CAOs do not belong to the type 1 blue copper proteins, which show strong visible absorption at ~600 nm in the oxidized Cu(II) state (*25*). This strong absorption band (ε = 3000-6000 $M^{-1}cm^{-1}$) arises from a LMCT between the Cu and the S atom of a Cys ligand (*26*). Instead, CAOs are members of the type 2 or "non-blue" copper proteins, which have almost no visible absorption (ε ~ 40 $M^{-1}cm^{-1}$).

Our results with HPAO-Y305pAF were also quite unexpected, as this protein shows a similar UV-Vis absorbance upon Cu(II)-reconstitution (**Figure 3-11**) to that of the Y405pAF protein. This species grows in even under anaerobic conditions (**Figure 3-12**), a result also observed in Y405pAF. It should be noted that the same caveats relevant to anaerobic reconstitution of Y405pAF (see Discussion, Chapter 2) also apply to our results with Y305pAF. This 450-nm species was also similarly unreactive toward phenylhydrazine, suggesting that it is not a quinone. Cu(II)-reconstituted Y305pAF also showed no activity toward benzylamine or methylamine substrates. While the O-4 of Tyr405 is only ~2.5 Å from the metal center in the precursor structure, the O-4 of Y305 is ~4.9 Å away, too far to undergo inner sphere electron transfer with the metal. Thus, the phenomenon we observe with the Y305pAF protein might be instead outer sphere electron transfer from the Cu center to the aniline group, possibly mediated by active site

waters (possibly W in Figure 3-13). To study this further, the x-ray crystal structure of HPAO-Y305pAF in complex with Cu(II) is being pursued.
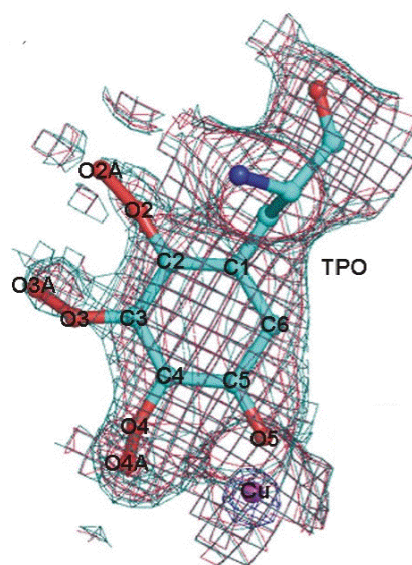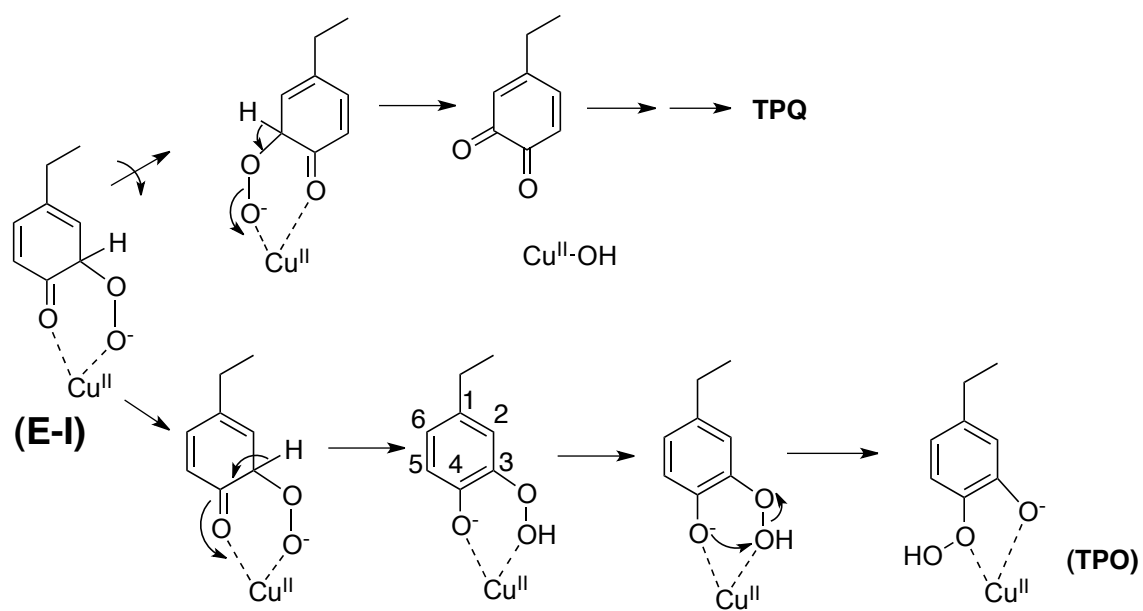
Figure 3-1. Simulated annealing omit map for a new active site structure observed during biogenesis of HPAO Y305F expressed in *E. coli*. Reprinted with permission from (*8*). Copyright 2010 American Chemical Society.

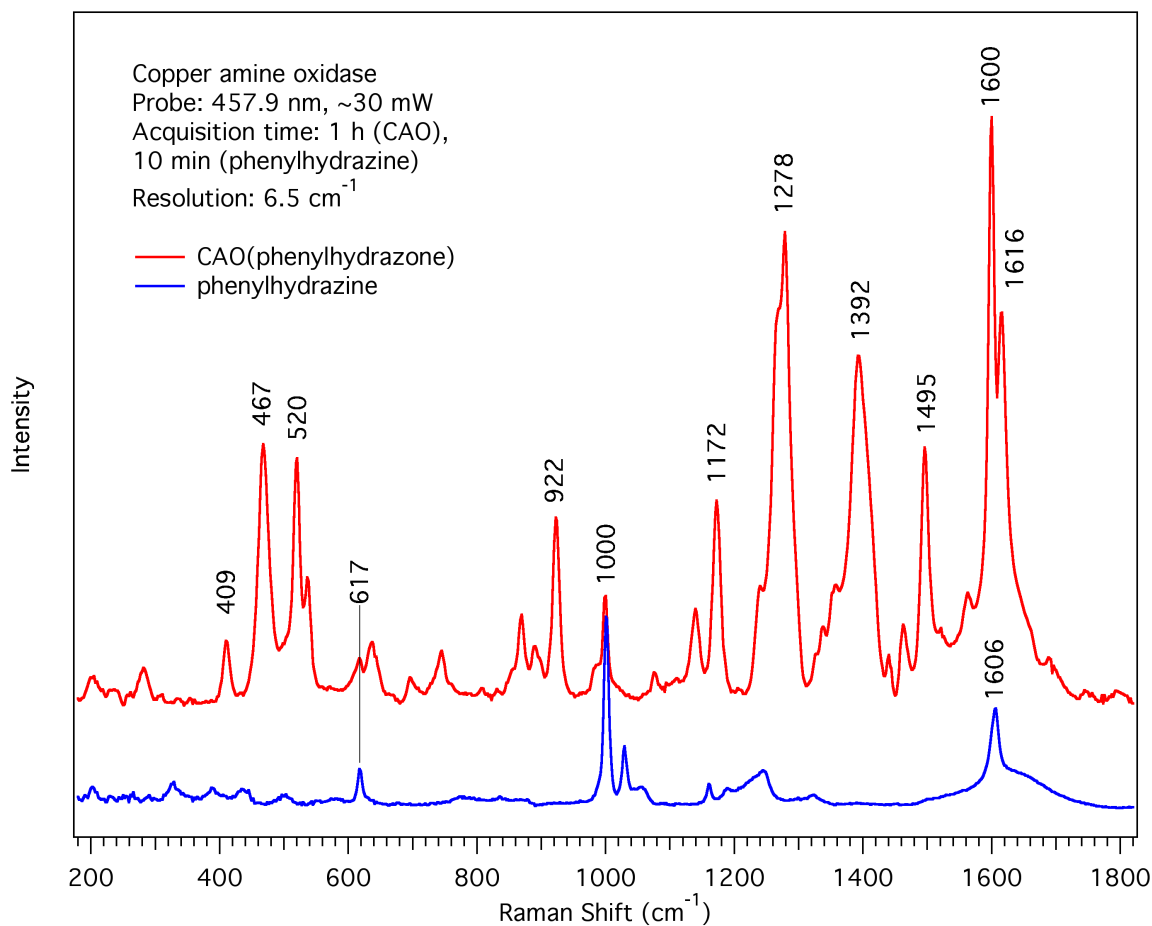**Scheme 3-1.** Postulated mechanism for the branching of a biogenesis intermediate to TPQ and TPO.

Figure 3-2. Resonance Raman spectra of WT HPAO derivatized with phenylhydrazine. Spectrum of phenylhydrazine alone is shown in blue. Excitation wavelength was 457.9 nm and the laser power was 30 mW.
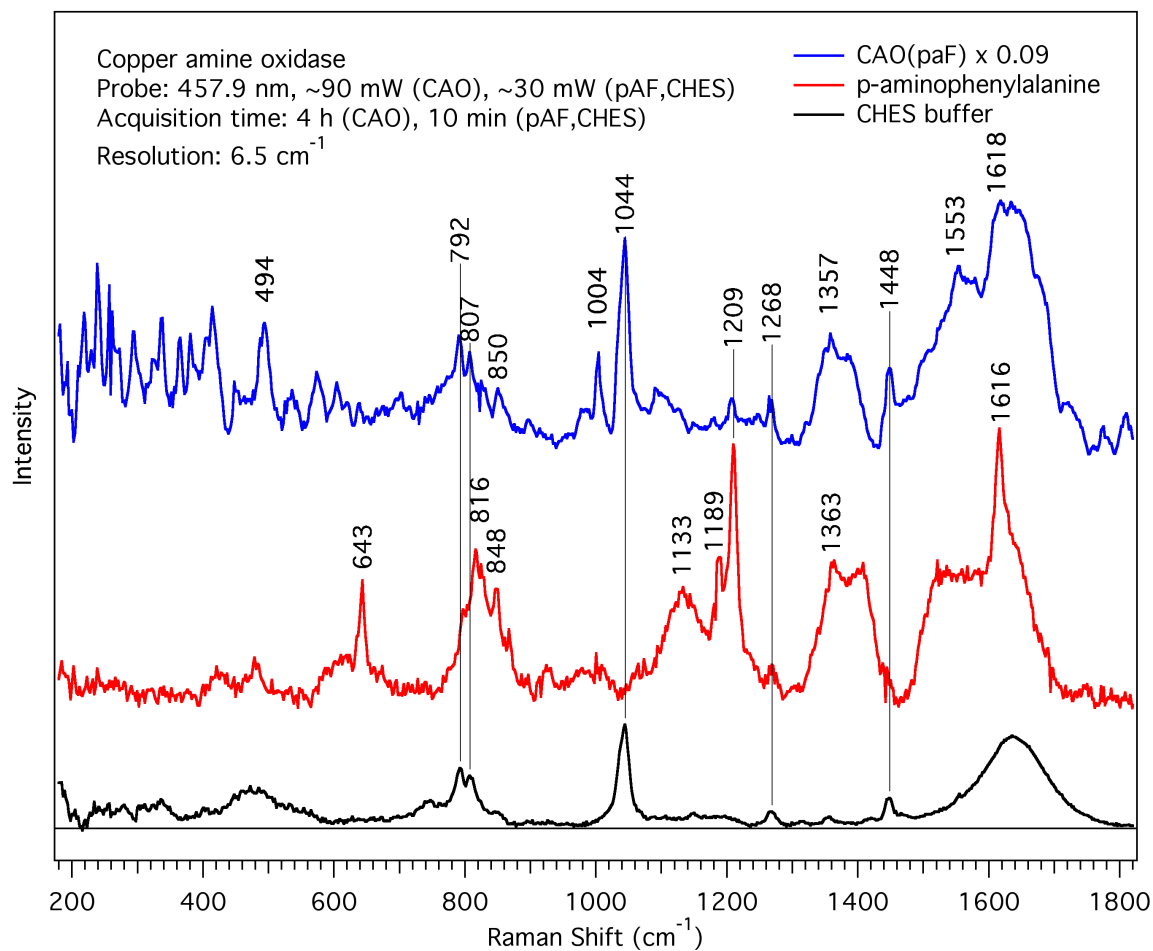
Figure 3-3. Resonance Raman spectra of HPAO-Y405pAF. Also shown are spectra for 100 mM pAF (red) and 50 mM CHES pH 9.0 (black). The spectrum for HPAO Y405pAF (blue) is scaled by a factor of 0.09 so it can be shown on the same plot as the other two spectra. Excitation wavelength was 457.9 nm and the laser power was 30 mW (pAF and buffer) and 90mW (HPAO-Y405pAF).
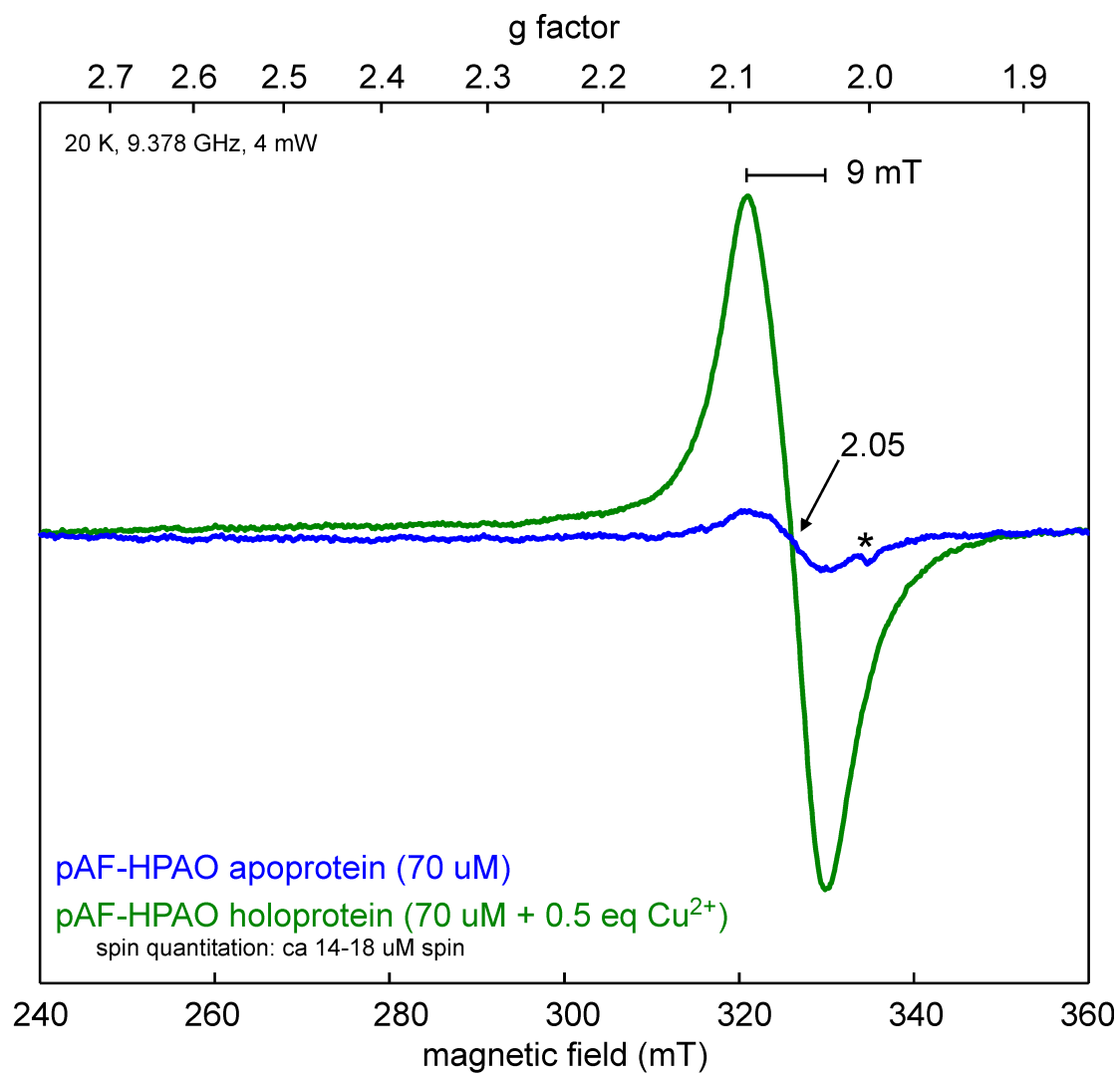
Figure 3-4. Continuous-wave X-band EPR spectra of apo-HPAO-Y405pAF (blue) and holo, Cu(II)-reconstituted HPAO-Y405pAF (green.) EPR conditions: temperature, 20K, microwave power, 4 mW, microwave frequency, 9.378 GHz.
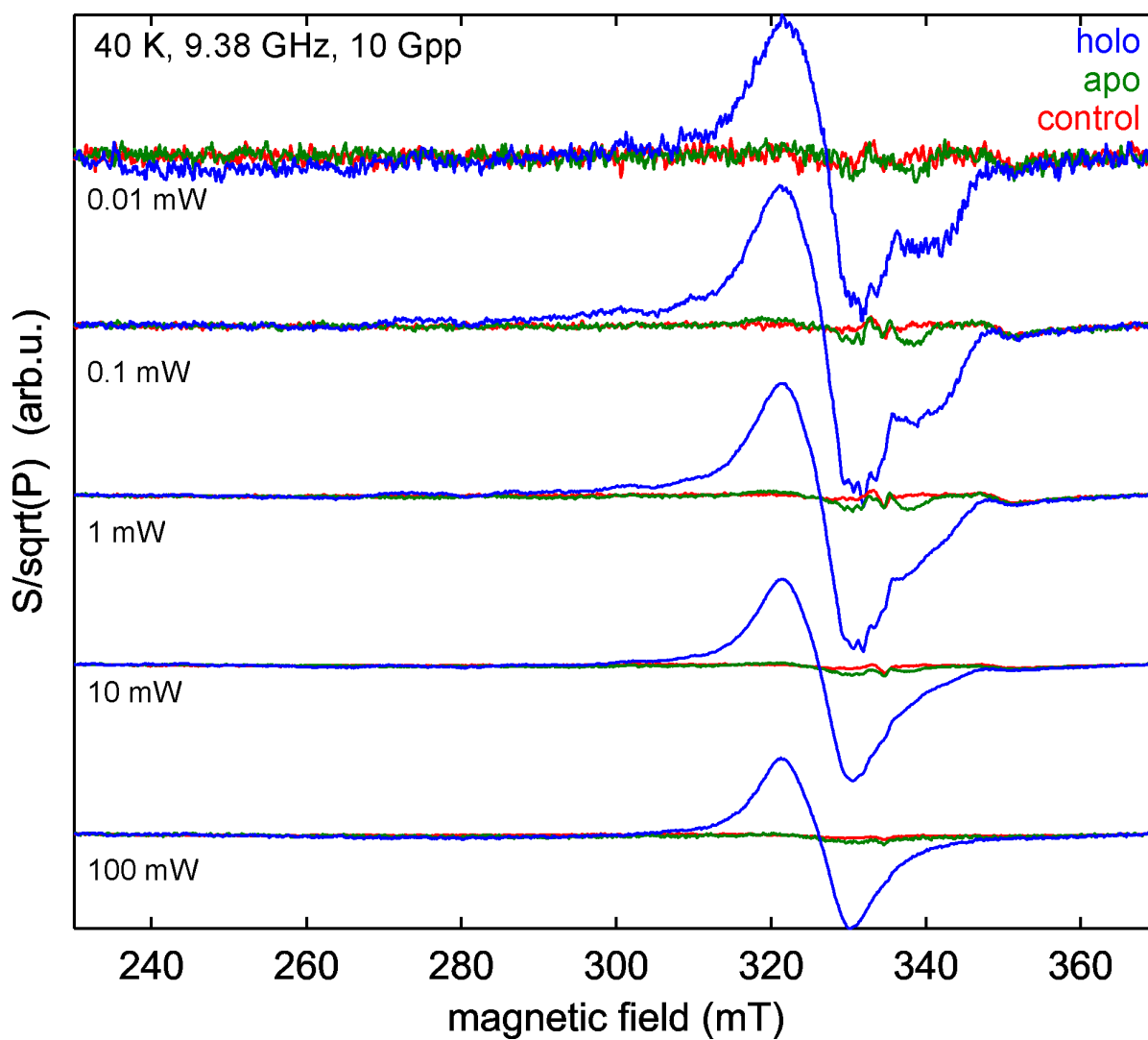
Figure 3-5. Continuous-wave X-band EPR spectra of Cu(II)-reconstituted holo-HPAO-Y405pAF (blue), apo-HPAO-Y405pAF (green), 50 mM CHES, pH 9.0 buffer control (red). EPR conditions: temperature, 40 K, microwave frequency, 9.38 GHz, field modulation amplitude, 10 G peak-to-peak. Microwave power varied from 0.01 mW – 100 mW.
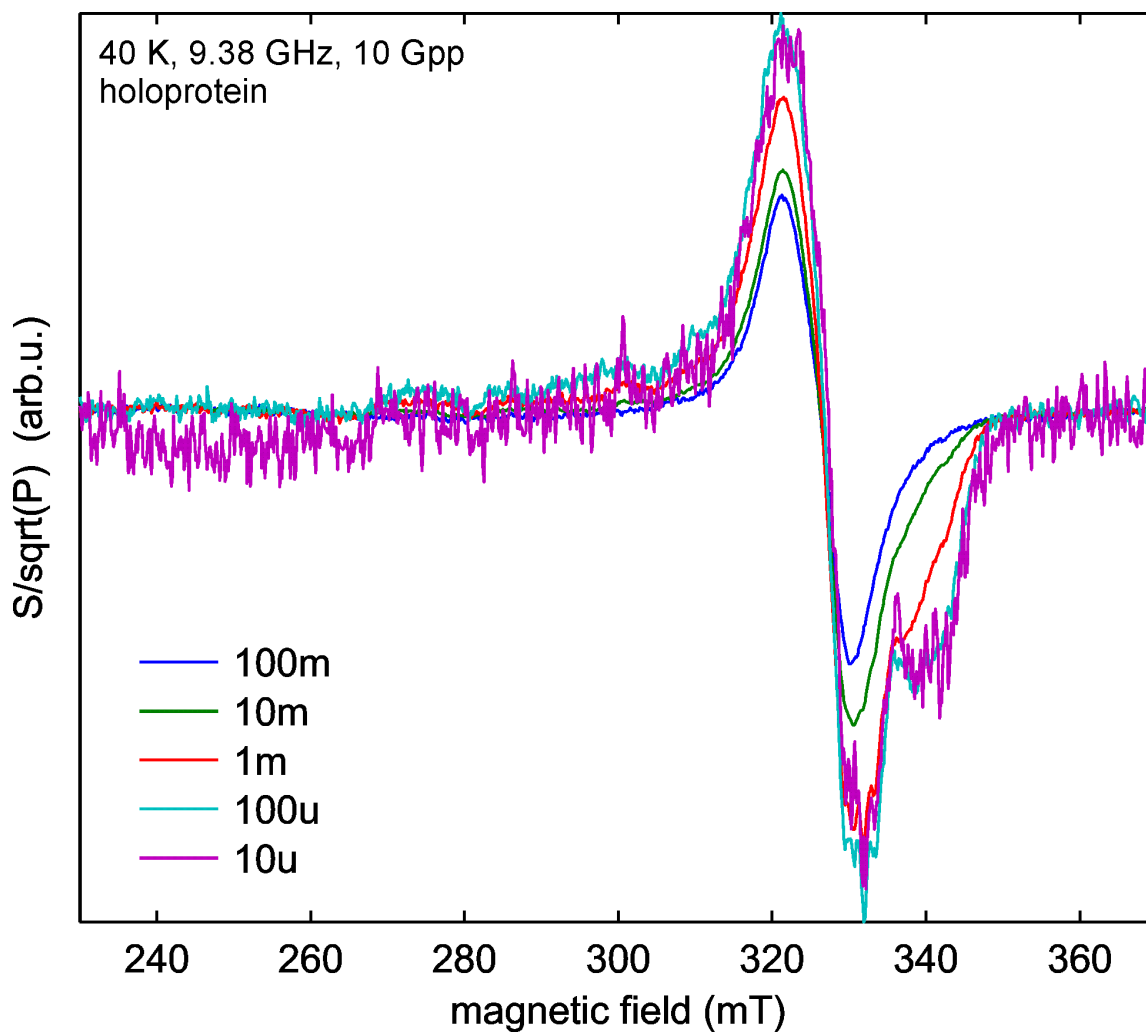
Figure 3-6. Power dependence of the continuous-wave, X-band EPR signal for Cu(II)-reconstituted, holo-HPAO-Y405pAF. EPR conditions: Temperature, 40 K, microwave frequency 9.38 GHz, field modulation, 10 Gpp. Microwave power ranged from 0.01 mW to 100 mW.
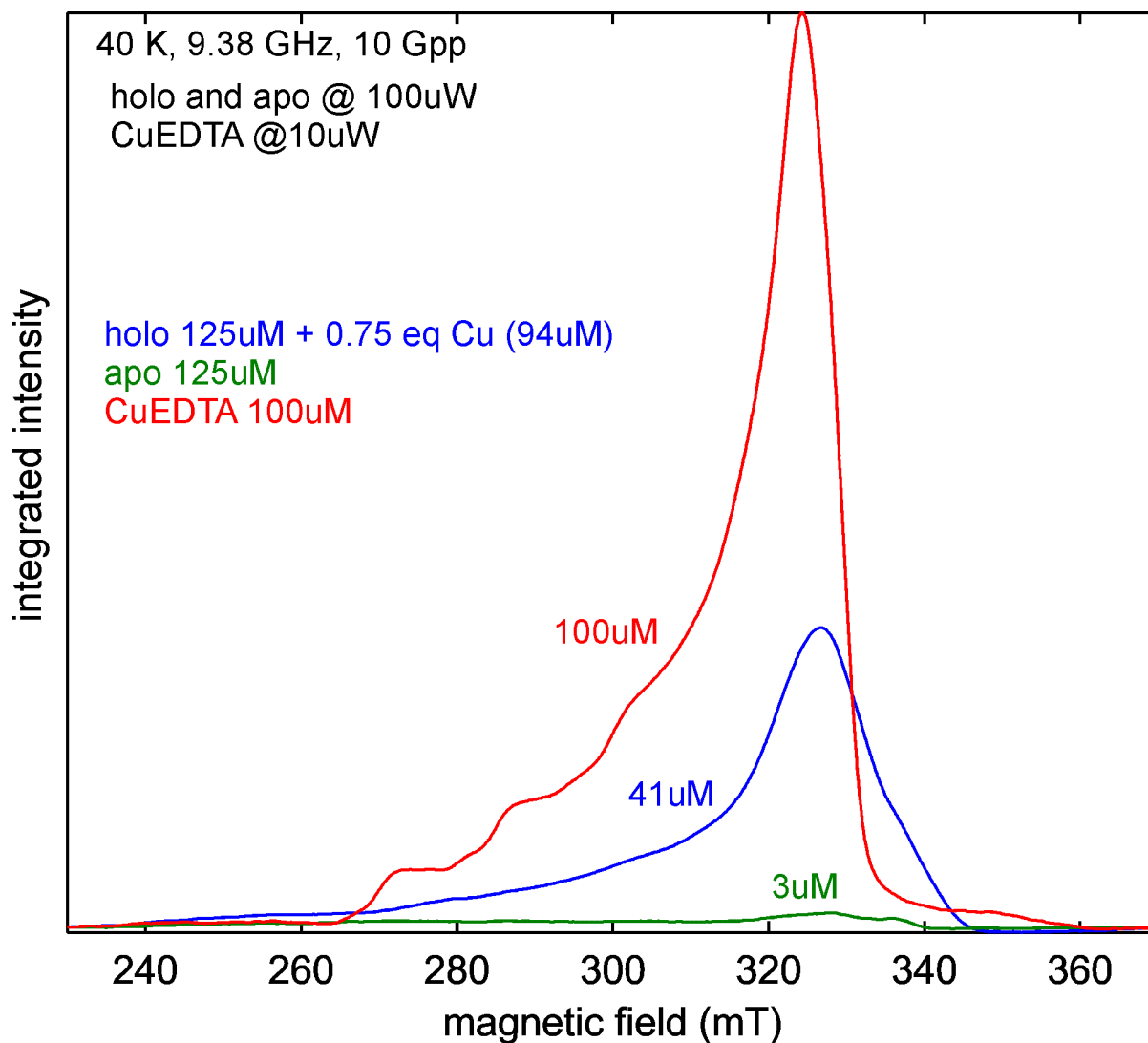
Figure 3-7. Integrated X-band EPR spectra for Cu-quantitation for apo-HPAO-Y405pAF (green) and Cu(II)-reconstituted, holo-HPAO-Y405pAF (blue). Also shown is the integrated spectrum of a Cu-EDTA standard at 100 μM (red). Quantitation was based on the areas underneath these spectra (double integrals of the original EPR spectra) by comparison to a calibration curve using Cu^{2+}-EDTA solutions at concentrations between 25 μM - 200 μM.
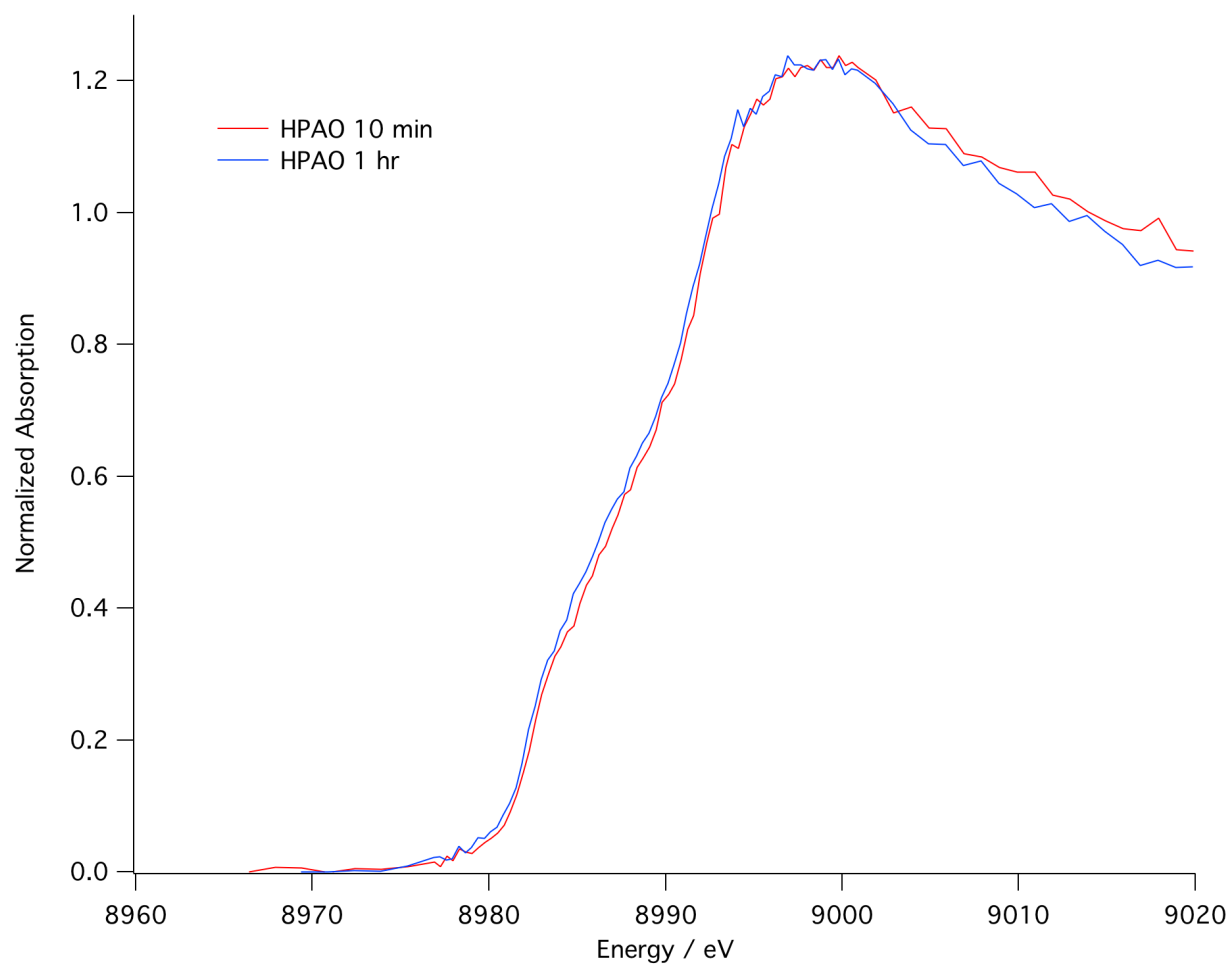
Figure 3-8. Cu K-edge XAS Spectra of HPAO-Y405pAF. HPAO-Y405pAF 10 min in red, HPAO-Y405pAF 1 hr in blue.
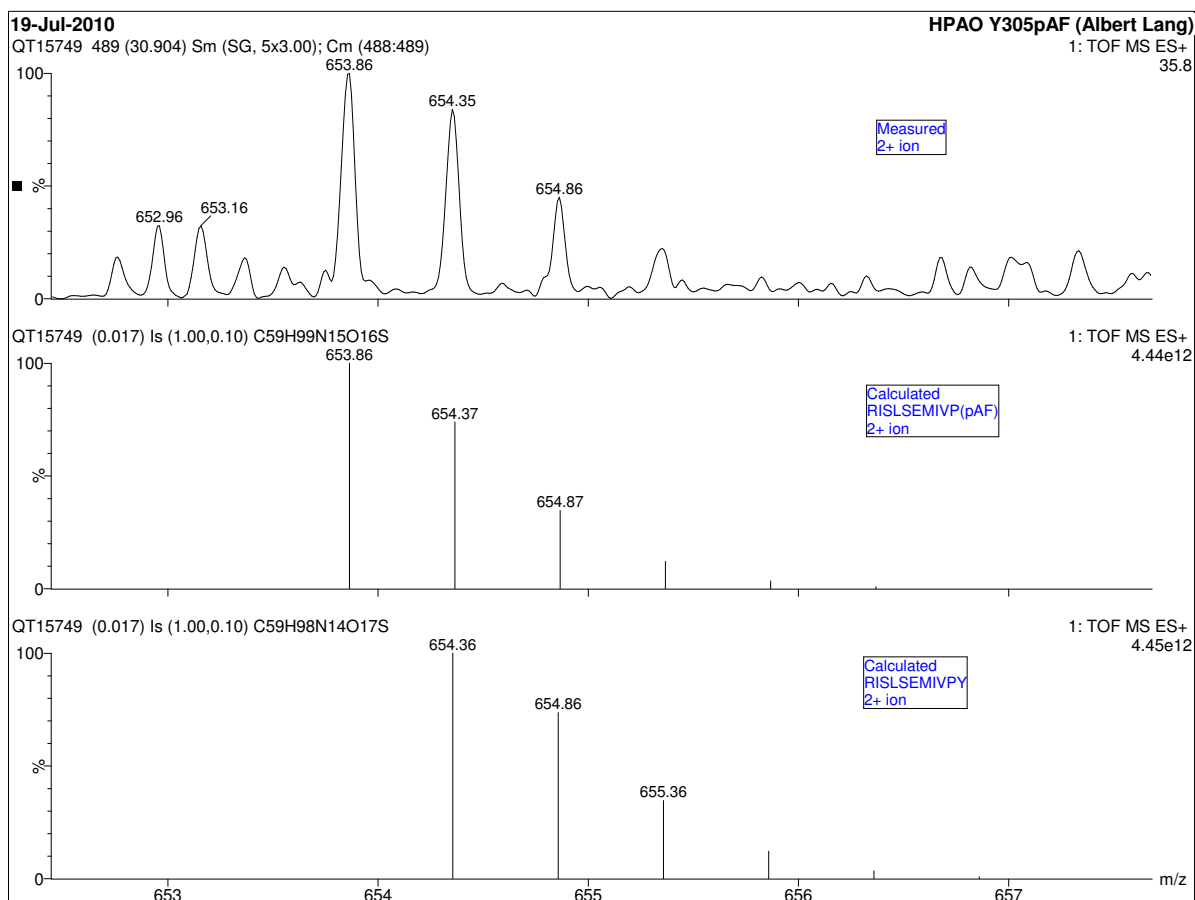
Figure 3-9. Precursor ion mass spectrum (formed by positive ESI) of HPAO-Y305pAF chymotryptic peptide. Figure generated by Dr. Tony Iavarone (QB3/Chemistry Mass Spectrometry Facility).
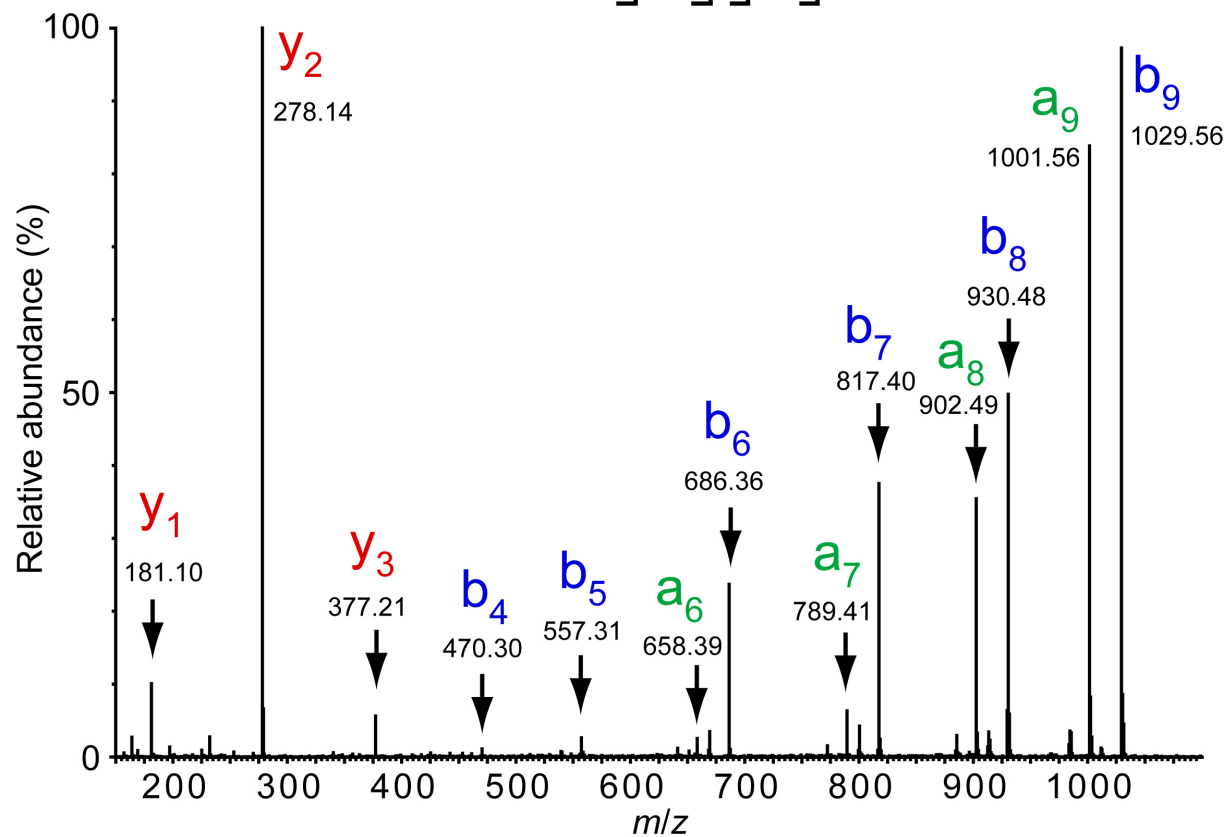
Figure 3-10. MS/MS spectrum of pAF-containing precursor ion derived from Y305pAF protein. Labels indicate b, y, and a fragment ions generated as a result of collisionally activated dissociation (CAD). Figure generated by Tony Iavarone (QB3/Chemistry Mass Spectrometry Facility).
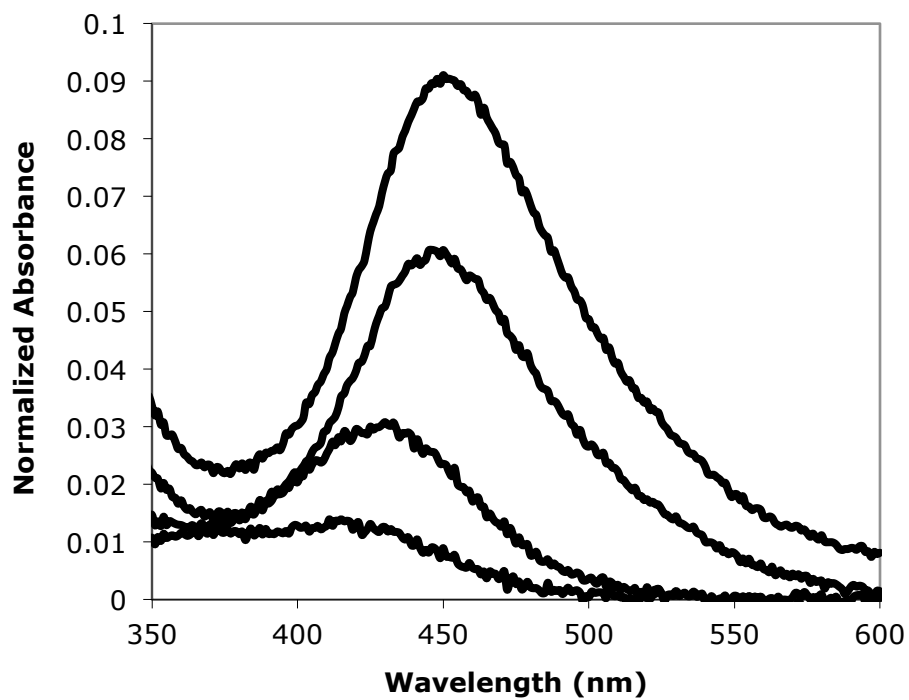
Figure 3-11. Spectral changes after addition of Cu(II) to apo-HPAO-Y305PAF at pH 9.0. The initial spectrum has been subtracted from each subsequent spectrum to emphasize the spectral changes. Spectra were measured every 2 min for 60 min. Shown are spectra at t = 2 min, 10 min, 30 min, and 60 min

Figure 3-12. Spectral changes after anaerobic addition of Cu(II) to apo-HPAO-Y305pAF at pH 9.0. The initial spectrum has been subtracted from each subsequent spectrum to emphasize the spectral changes. Spectra were measured every 2 min for 60 min. Shown are spectra at $t = 2$ min, 10 min, 30 min, and 60 min
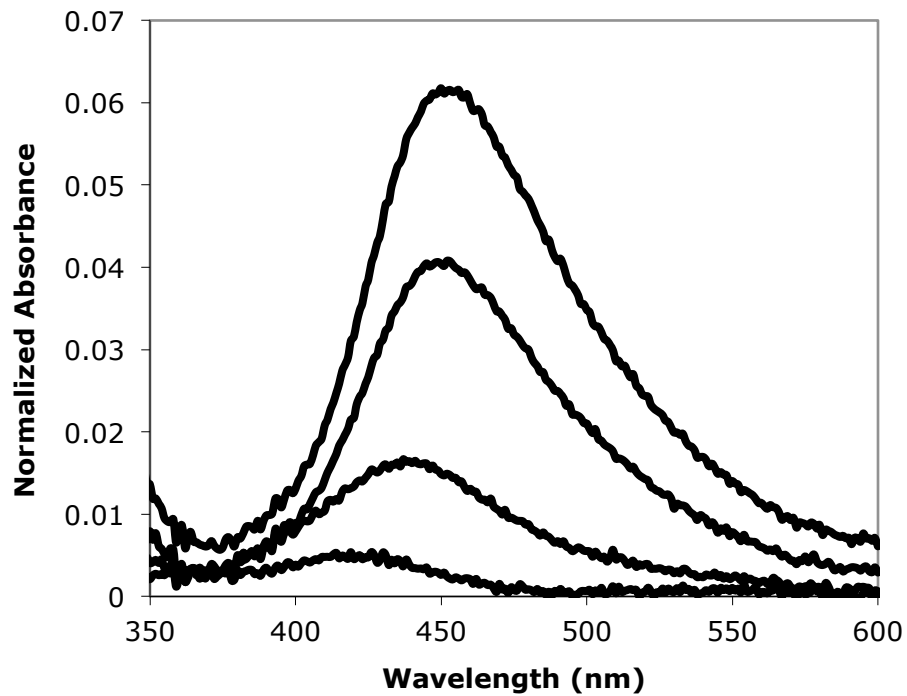
Table 3-1. X-ray crystallographic data collection, processing, and refinement statistics for HPAO-Y405pAF

Data collection and processing statistics	
	HPAO-Y405pAF
detector type	MARmosaic 300 CCD
beamline and source	23ID-D GM/CA-CAT, Advanced Photon Source
temperature (K)	100
space group	$C222_1$
unit cell dimensions	$a = 139.4$ Å, $b = 153.7$ Å, $c = 223.3$ Å
no. of molecules in the unit cell, Z	3
wavelength (Å)	1.0332
resolution (Å)[a]	50-1.57 (1.60-1.57)
no. of unique reflections	328,577
completeness (%)[a]	99.4 (87.7)
R_{merge}[a,b]	0.092 (0.566)
$I/\sigma I$[a]	37.6 (3.3)
redundancy[a]	7.9 (7.0)
Crystallographic refinement and model statistics	
resolution range (Å)[a]	29.12-1.57 (1.61-1.57)
no. of reflections in the working set[a]	311,940 (22,113)
no. of reflections in the test set[a]	16,564 (1,199)
current R_{work} (%)[a,c]	0.13.1 (0.210)
current R_{free} (%)[a,d]	0.160 (0.253)

[a]Numbers in parentheses refer to the highest-resolution shell. [b]$R_{merge} = \Sigma_{hkl}\Sigma_i|I_{hkl,I} - \langle I_{hkl}\rangle|/\Sigma_{hkl}\Sigma_i I_{hkl,I}$, where I is the observed intensity and $\langle I\rangle$ is the average intensity for multiple measurements. [c]$R_{work} = \Sigma\|F_o| -- |F_o\|/\Sigma|F_o|$, where $|F_o|$ is the observed structure factor amplitude and $|F_c|$ is the calculated structure factor amplitude for 95% of the data used in refinement. [d]R_{free} and R_{factor} based on 5% of the data excluded from refinement.
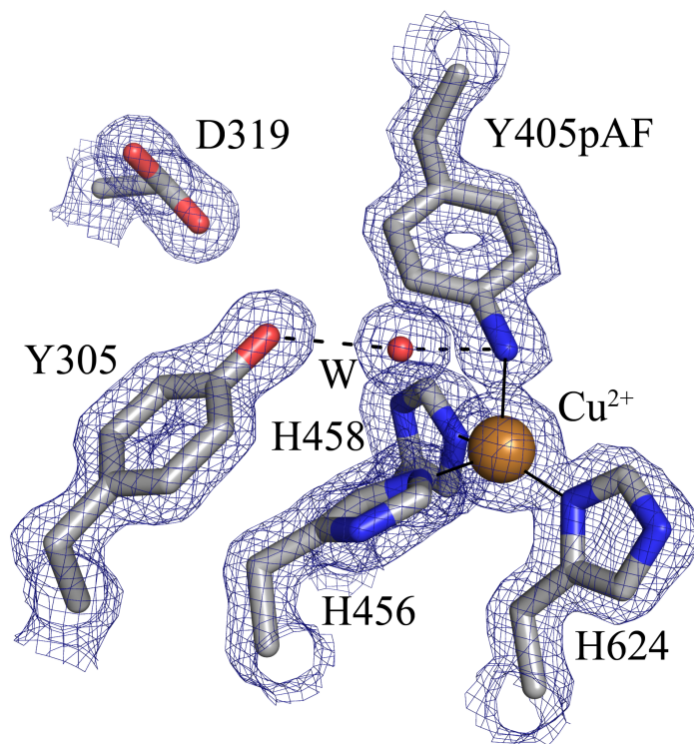
Figure 3-13. Active site of Y405pAF (crystal harvested at pH 7.0). Residues are shown in stick and colored by atom type (carbon, grey). A copper ion is shown as a gold sphere, and a water molecule is shown as a small red sphere. Metal-ligand interactions are shown as solid lines, and hydrogen bonds are shown as dashed lines. The *2F$_o$-F*c electron density map is shown as blue mesh and contoured to 1.5σ.
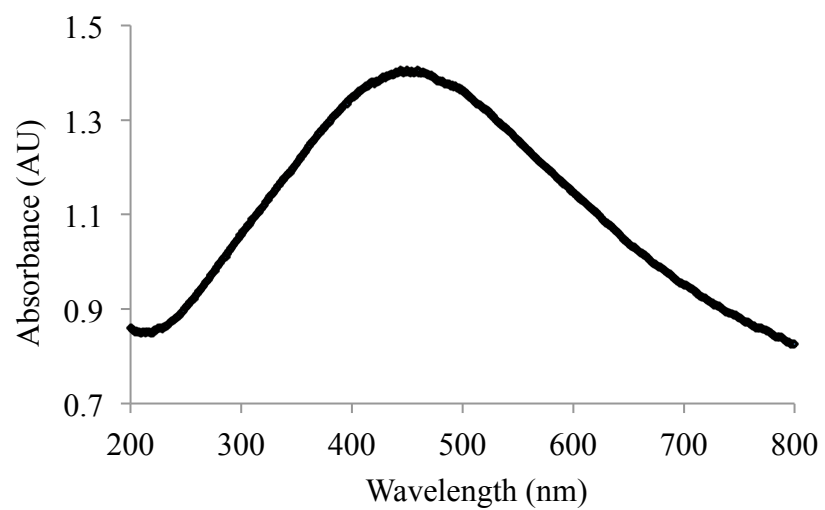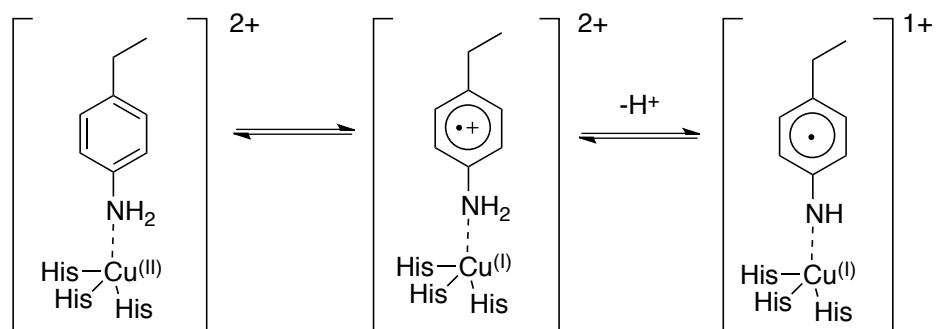
Figure 3-14. Single crystal UV/visible spectrum of Cu(II)-Y405pAF crystal after data collection revealing a broad absorbance feature centered at $\lambda_{max} = 450$ nm.

Scheme 3-2. Postulated mechanism for intramolecular electron transfer between Cu(II) and pAF to form Cu(I) and aniline radical.

References

1.   Jonsson, M., Lind, J., Eriksen, T. E., and Merenyi, G. (1994) Redox and Acidity Properties of 4-Substituted Aniline Radical Cations in Water, *J. Am. Chem. Soc. 116*, 1423–1427.
2.   DuBois, J. L., and Klinman, J. P. (2004) Methods for characterizing TPQ-containing proteins, *Meth. Enzymol. 378*, 17–31.
3.   Johnson, B. J., Cohen, J., Welford, R. W., Pearson, A. R., Schulten, K., Klinman, J. P., and Wilmot, C. M. (2007) Exploring molecular oxygen pathways in *Hansenula polymorpha* copper-containing amine oxidase, *J. Biol. Chem. 282*, 17767–17776.
4.   Chang, C. M., Klema, V. J., Johnson, B. J., Mure, M., Klinman, J. P., and Wilmot, C. M. (2010) Kinetic and structural analysis of substrate specificity in two copper amine oxidases from *Hansenula polymorpha*, *Biochemistry 49*, 2540–2550.
5.   Klema, V. J., Johnson, B. J., Klinman, J. P., and Wilmot, C. M. (2012) The precursor form of *Hansenula polymorpha* copper amine oxidase 1 in complex with Cu(I) and Co(II)., *Acta Crystallogr. Sect. F Struct. Biol. Cryst. Commun. 68*, 501–510.
6.   DuBois, J. L., and Klinman, J. P. (2005) The Nature of O_2 Reactivity Leading to Topa Quinone in the Copper Amine Oxidase from *Hansenula polymorpha* Its Relationship to Catalytic Turnover, *Biochemistry 44*, 11381–11388.
7.   DuBois, J. L., and Klinman, J. P. (2006) Role of a Strictly Conserved Active Site Tyrosine in Cofactor Genesis in the Copper Amine Oxidase from *Hansenula polymorpha*, *Biochemistry 45*, 3178–3188.
8.   Chen, Z.-W., Datta, S., DuBois, J. L., Klinman, J. P., and Mathews, F. S. (2010) Mutation at a strictly conserved, active site tyrosine in the copper amine oxidase leads to uncontrolled oxygenase activity, *Biochemistry 49*, 7393–7402.
9.   Samuels, N. M., and Klinman, J. P. (2005) 2,4,5-Trihydroxyphenylalanine Quinone Biogenesis in the Copper Amine Oxidase from *Hansenula polymorpha* with the Alternate Metal Nickel, *Biochemistry 44*, 14308–14317.
10.   Bradford, M. M. (1976) A rapid and sensitive method for the quantitation of microgram quantities of protein utilizing the principle of protein-dye binding, *Anal. Biochem. 72*, 248–254.
11.   Hartmann, C., and Klinman, J. P. (1991) Structure-function studies of substrate oxidation by bovine serum amine oxidase: relationship to cofactor structure and mechanism, *Biochemistry 30*, 4605–4611.
12.   Cai, D., and Klinman, J. P. (1994) Copper amine oxidase: heterologous expression, purification, and characterization of an active enzyme in *Saccharomyces cerevisiae*, *Biochemistry 33*, 7647–7653.
13.   Mathies, R., and Yu, N. (1978) Raman-Spectroscopy with Intensified Vidicon Detectors - Study of Intact Bovine Lens Proteins, *J Raman Spectrosc 7*, 349–352.
14.   Kim, M. M., Mathies, R. A. R., Hoff, W. D. W., and Hellingwerf, K. J. K. (1995) Resonance Raman evidence that the thioester-linked 4-hydroxycinnamyl chromophore of photoactive yellow protein is deprotonated, *Biochemistry 34*, 12669–12672.
15.   Tenderholt, A., Hedman, B., and Hodgson K. O. (2007) PySpline: A Modern, Cross-Platform Program for the Processing of Raw Averaged XAS Edge and EXAFS Data, *AIP Conf. Proc. 882*, 105-107.
16.   D'Arcy, A., Mac Sweeney, A., and Haber, A. (2003) Using natural seeding material to

generate nucleation in protein crystallization experiments, *Acta Crystallogr. D Biol. Crystallogr. 59*, 1343–1346.

17. Otwinowski, Z., and Minor, W. (1997) Processing of X-ray diffraction data collected in oscillation mode, *Method Enzymol 276*, 307–326.

18. Bailey, S. (1994) The Ccp4 Suite - Programs for Protein Crystallography, *Acta Crystallogr. D Biol. Crystallogr. 50*, 760–763.

19. Emsley, P., and Cowtan, K. (2004) *Coot*: model-building tools for molecular graphics, *Acta Crystallogr. D Biol. Crystallogr. 60*, 2126–2132.

20. Murshudov, G. N., Vagin, A. A., and Dodson, E. J. (1997) Refinement of macromolecular structures by the maximum-likelihood method, *Acta Crystallogr. D Biol. Crystallogr. 53*, 240–255.

21. Moënne-Loccoz, P., Nakamura, N., Steinebach, V., Duine, J. A., Mure, M., Klinman, J. P., and Sanders-Loehr, J. (1995) Characterization of the topa quinone cofactor in amine oxidase from *Escherichia coli* by resonance Raman spectroscopy, *Biochemistry 34*, 7020–7026.

22. Brown, D. E., McGuirl, M. A., Dooley, D. M., Janes, S. M., Mu, D., and Klinman, J. P. (1991) The organic functional group in copper-containing amine oxidases. Resonance Raman spectra are consistent with the presence of topa quinone (6-hydroxydopa quinone) in the active site, *J. Biol. Chem. 266*, 4049–4051.

23. Stubbe, J., and van Der Donk, W. A. (1998) Protein Radicals in Enzyme Catalysis, *Chem. Rev. 98*, 705–762.

24. Nakamura, N., Moënne-Loccoz, P., Tanizawa, K., Mure, M., Suzuki, S., Klinman, J. P., and Sanders-Loehr, J. (1997) Topaquinone-dependent amine oxidases: identification of reaction intermediates by Raman spectroscopy, *Biochemistry 36*, 11479–11486.

25. MacPherson, I. S., and Murphy, M. E. P. (2007) Type-2 copper-containing enzymes, *Cell. Mol. Life Sci. 64*, 2887–2899.

26. Solomon, E. I., Baldwin, M. J., and Lowery, M. D. (1992) Electronic-Structures of Active-Sites in Copper Proteins - Contributions to Reactivity, *Chem. Rev. 92*, 521–542.

Chapter 4

Second Sphere Ligands and Y407pAF

4.1 Introduction

While there is general agreement about the mechanism for the first half-reaction in CAOs, more than one mechanism has been proposed for the second, oxidative half reaction (*1*, *2*) (see Introduction, Chapter 1). The chief difference is the nature of the first electron transfer to O_2. In the first pathway (**Mechanism I**, **Scheme 1-3**), an electron is transferred from reduced TPQ to Cu(II), giving the semiquinone radical form of the cofactor and Cu(I). Dioxygen subsequently combines with Cu(I) to form Cu(II) superoxide. In the second pathway (**Mechanism II**, **Scheme 1-3**), O_2 is proposed to bind to a hydrophobic pocket near the metal center. Then, an electron is transferred directly from reduced TPQ to O_2 to form semiquinone cofactor and superoxide, respectively. Whereas the first pathway is seen in a variety of enzyme sources, including *Arthrobacter* PI and pea seedling (*2*), primary evidence for the second pathway comes from work on copper amine oxidase from *Hansenula polymorpha* (*3*, *4*).

In a previous study from our laboratory, site-directed mutagenesis was used to partially convert HPAO into a plant-like CAO. To accomplish this, a second sphere ligand to the active site copper, D630 in HPAO, was mutated to a neutral side chain to generate D630N (*5*). This residue hydrogen bonds with the imidazole group of H624 (**Scheme 4-1**, **Figure 4-1**). Other second sphere ligands include Y407, which hydrogen bonds with the imidazole group of H458, and H454, which hydrogen bonds with the imidazole group of H456 through the former's carboxyl oxygen (**Scheme 4-1**, **Figure 4-1**). The D630N mutant protein had a significantly altered redox potential and pK_a (for bound water) at the active site copper (*5*). While previous work was mostly done with respect to this mutant protein's catalytic properties, the ability to tune the redox potential and pK_a of the active site copper has interesting applications for studying cofactor biogenesis. As was discussed in Chapter 2, unnatural amino acid incorporation into the TPQ precursor position can help test the importance of redox potential and pK_a in forming a charge transfer complex that is proposed to form during biogenesis. By incorporating a pAF residue into position 407, replacing the phenol functionality of Tyr, we can make a nearly isosteric mutation that is much less perturbing than mutation to Phe or Asn. Mutation of Tyr at position 407 to pAF would also be much less perturbing than replacing Asp630 with a pAF residue.

Looking at the active site (**Scheme 4-1, Figure 4-1**), we can see that the ε-nitrogen of H458 is positioned to interact with the Cu, whereas the δ-nitrogen is positioned to hydrogen bond with the O-4 of Y407. The phenol of Y407 should be a poor hydrogen bond acceptor, given that neutral phenol is a much better Brønsted acid than base i.e. pK_a(Ph-OH) = 10 versus pK_a(Ph-OH_2^+) = -6.5-7.0) (*6*). By replacing the phenol group of tyrosine with the aniline group of pAF, we will be inserting a much better hydrogen bond acceptor because neutral aniline is a better Brønsted base than acid i.e. pK_a(Ph-NH_3^+) = 4.6 versus pK_a(Ph-NH_2) = 31 (*7*). By inserting a better hydrogen bond acceptor as a second sphere ligand, this will increase the electron-donating ability of H458, which will result in less positive charge on the Cu. This might result in easier formation of a LMCT that supports oxygen insertion in the normal TPQ biogenesis pathway (see Introduction, Chapter 2). It will be particularly interesting to see whether or not HPAO with pAF inserted at position Y407 will form TPQ, the same 450-nm species seen in Y405pAF and Y305pAF, or something different altogether.

4.2   Materials and Methods

HPAO-Y407pAF Mutagenesis

Mutations were made to the pET3a-HPAO plasmid (*8*) in order to substitute an amber stop codon for the sequence that encodes for Tyr at position 407. The pET expression system relies on the bacteriophage T7 RNA polymerase to drive expression, which is induced with Isopropyl β-D-1-thiogalactopyranoside (IPTG). Site-directed mutagenesis was performed using the Stratagene QuikChange II XL kit. HPLC-purified primers were purchased from Eurofins MWG Operon. The forward primer is listed in the 5' to 3' direction, and the reverse primer is listed in the 3' to 5' direction. The mutated codon is in bold, and the changed bases are in italics. DNA mutation was confirmed by automated sequencing at the UC Berkeley Sequencing Facility.

HPAO Y407pAF:
```
5'-GCTGCCAATTACGAGTAGTGTCTGTACTGGGTG-3'
3'-CGACGGTTAATGCTCATCACAGACATGACCCAC-5'
```

HPAO-Y407pAF Expression

Expression of HPAO-Y407pAF was carried out identically to Y405pAF (see Chapter 2).

HPAO-Y407pAF Purification

Protein purification of HPAO-Y407pAF was carried out identically to Y405pAF, using ion-exchange and size-exclusion chromatography (see Chapter 2).

HPAO Y407pAF Characterization

Protein quantitation

Protein concentration was measured by the Bradford assay (Bio-Rad) (*9*). Typical protein yields were ~2-4 mg/9 L cell culture (in comparison to ~10-20 mg/9 L for WT apo-protein).

Aerobic Cu^{2+} reconstitution

HPAO-Y407pAF was diluted with 50 mM CHES, pH 9 to 110 μl at 40 μM (3 mg/mL) Spectral changes to this sample after addition of 4.4 μl $CuSO_4$ (1 equivalent) were monitored over 2 h in a Varian Cary 50 Bio UV-Vis spectrophotometer.

Phenylhydrazine reaction

To test for the presence of TPQ, reaction with an excess of phenylhydrazine HCl was used. 1 μl 5 mg/ml phenylhydrazine was added to 40 μM enzyme reconstituted with Cu(II) (see protocol above), and the reaction was monitored at 448 nm on a Varian Cary 50 Bio UV-Vis spectrophotometer. An extinction coefficient of 40500 $M^{-1}cm^{-1}$ was used to quantitate phenylhydrazone formation (*10*).

HPAO-Y407pAF Kinetic Measurements

To test for activity toward benzylamine, benzaldehyde formation was monitored at 250 nm (ε = 12800 $M^{-1}cm^{-1}$) on a Varian Cary 50 Bio UV-Vis spectrophotometer (*11*). Standard conditions were as follows: 50 mM HEPES, pH 7.0 at 25ºC, with a total volume of 1 mL and initiation of the reaction by addition of 40-90 μl Cu(II)-reconstituted enzyme.

HPAO-Y407pAF Proteolytic Digestions

Y407pAF was digested with chymotrypsin similarly to Y405pAF (see Chapter 2). To isolate a phenylhydrazone-containing peptide, the following procedure was used. 40-50 nmol protein was reconstituted with 0.75-1 equivalent of $CuSO_4$, and let to incubate at room temperature. Spectral changes during this incubation were monitored in a Varian Cary 50 Bio UV-Vis spectrophotometer. Then, 1 equivalent of phenylhydrazine was added, and spectral changes were monitored over 20 min. Following derivitization with phenylhydrazine, this protein was subjected to proteolytic digestion by chymotrypsin, thermolysin, or trypsin similarly to Y405pAF (see Chapter 2).

Mass Spectrometry

Y407pAF samples were processed similarly to Y405pAF (see Chapter 2).

Peptide Separation by High-Performance Liquid Chromatography (HPLC)

HPLC was conducted on a Beckman system equipped with a diode array detector and operated by 32 Karat version 8.0 software. The software was also used for data collection. Reversed-phase HPLC was performed on a Phenomenex Luna 5μm, 100 Å, 250 mm x 4.60 mm C18 column. Peptides were eluted under the following conditions: flow rate of 1 mL/min, 0.1% TFA in 5% acetonitrile for 5 min, followed by a linear gradient from 5 to 80% acetonitrile over 25 min, then a wash with 5% acetonitrile for 25 minutes (55 min total). Spectra were recorded at 280 nm and 450 nm.

4.3   Results

Expression and Purification of Y407pAF

The same expression and purification conditions used for Y405pAF and Y305pAF were used for the Y407pAF variant. Following purification by ion-exchange and size-exclusion chromatography, HPAO-Y407pAF runs as a single band on SDS-PAGE and similarly to HPAO Y405pAF and Y305pAF (data not shown). No issues were seen with truncation due to incorporation of an amber stop codon at residue 407.

Chymotrypsin Digestion and Mass Spectrometry

In collaboration with Dr. Tony Iavarone (Chemistry/QB3 Mass Spectrometry Facility, UC Berkeley), we used mass spectrometry to provide direct evidence that pAF had been incorporated at position 407. Given our previous success with using chymotrypsin on the Y405pAF protein (see Chapter 2) and Y305pAF protein (see Chapter 3), we used the same protease to digest Y407pAF. Among the peptides measured by tandem mass spectrometry (MS/MS) was a $[M+H]^+$ ion with m/z = 743.3 corresponding to E(pAF)(CMC)LY, where CMC = carboxymethylcysteine (cysteines were capped with iodoacetate) (**Figure 4-2**). No peptides containing Tyr instead of pAF at position 407 were measured from the sample by MS/MS.

Aerobic Reconstitution and Quinone Cofactor Detection

Aerobic reconstitution of HPAO-Y407pAF at pH 9.0 generated a species with a λ_{max} ~450 nm (WT HPAO λ_{max}TPQ = 480 nm) that grew in over two hours (**Figure 4-3**). In contrast to Cu^{2+}-reconstituted Y405pAF and Y305pAF proteins, this new 450-nm species did react with phenylhydrazine to form a hydrazone (**Figure 4-4**). Based on an extinction coefficient of 40500 $M^{-1}cm^{-1}$, the amount of hydrazone (and thus TPQ) formed is ~5% of total protein, in contrast to 15-25% seen for reconstitution of apo-WT protein (*10*).

Reactivity Toward Benzylamine

Cu(II)-reconstituted protein was also tested for activity toward benzylamine. When Cu(II)-reconstituted HPAO-Y407pAF was added to a solution of 5 mM benzylamine in 50 mM HEPES, pH 7, an increase in absorbance at 250 nm (where benzaldehyde product absorbs) was observed (**Figure 4.5**). Based on the calculation that 5% of total protein contained TPQ (see previous section on quinone cofactor detection with phenylhydrazine), we can estimate a k_{obs} for this enzyme of 1.61×10^{-2} s^{-1}, compared with k_{cat} = 6.6×10^{-2} s^{-1} for WT holo-protein (*12*). k_{cat} for WT holo-protein was calculated using the concentration of TPQ as the concentration of active protein (as determined by phenylhydrazine reaction) (*12*). It should also be noted that WT holo-HPAO (HPAO-1) turns benzylamine over much slower than it does methylamine, for which k_{cat} = 6.2 s^{-1} (*13*). Without enough data points for an entire Michaelis-Menten curve, k_{obs} for Y407pAF was calculated under the assumption that 5 mM benzylamine is saturating (K_m for benzylamine in WT protein is <1 mM (*12*)) and thus under the assumption that the observed velocity approximates V_{max}.

Efforts Toward Isolation of Phenylhydrazone-Containing Peptide

To isolate a phenylhydrazone-containing peptide, 40-50 nmol protein was first reconstituted with CuSO$_4$, then derivatized with phenylhydrazine (**Figure 4.3**, **Figure 4.4**). This derivatized protein was then subject to proteolytic digestion using chymotrypsin. To isolate a phenylhydrazone-

containing peptide from this mixture, we first sought to separate the peptides by HPLC, using an analytical C18 column and an acetonitrile gradient. We monitored the separated peptides at both 280 nm and 450 nm, with the former monitoring all Trp-containing and Tyr-containing peptides and the latter monitoring phenylhydrazone-containing peptides (**Figure 4.6**). Under these conditions, however, no peptides were observed in the LC-MS/MS that contained residue 407. This is most likely the result of losing much of our sample during the HPLC separation step, as indicated by observing only a very small peak that absorbed at 450 nm (**B**, **Figure 4.6**). Thus, we also tried the same procedure for Cu^{2+}-reconstitution and phenylhydrazine dervitization, followed by digestion by chymotrypsin, thermolysin, or trypsin, but then subjected the digested peptides directly to LC-MS/MS. This resulted in much better sequence coverage than was observed with the HPLC-purified peptides, but again no identification of peptides that contained residues 405 and/or 407.

4.4   Discussion

We have successfully inserted pAF into position 407 of HPAO, with no apparent issues due to truncation of protein or misincorporation of Tyr into that position. This brings the total number of positions of insertion to three, along with 305 and 405. Our initial characterization of Y407pAF indicates that this protein forms ~5% TPQ upon Cu(II)-reconstitution and is active toward benzylamine as a substrate. This behavior is in marked contrast to both Y405pAF and Y305pAF variants. It is quite interesting that perturbing a second sphere ligand to the copper, replacing the native phenol of Tyr with the aniline of pAF, would still support TPQ formation and generate an active enzyme. In previous studies, the Y407N mutant was also seen to form TPQ and turn over substrate similarly to WT (*5*). In the case of Y407pAF, activity appears to be lower than that of WT, though the exact magnitude of reduction in activity has not been established definitively.

Another interesting result is that Y407pAF appears to form a 450-nm species upon Cu(II) reconstitution, similar to both Y305pAF and Y405pAF. There is no evidence for a separate peak at 480 nm indicative of TPQ. Given the low extinction coefficient of TPQ ($\varepsilon = 2400\,\mathrm{M}^{-1}\mathrm{cm}^{-1}$) and how broad the 450-nm species is, however, it would be hard to distinguish whether a small 480-nm peak was forming over the same time period as a 450-nm species. Derivitization with phenylhydrazine to generate strongly absorbing hydrazone is a more sensitive test for TPQ formation, and this test clearly showed formation of a hydrazone (**Figure 4.4**).

Given that Y407pAF appears to form TPQ, we sought to distinguish between two possibilities. The first is that the purified protein contains only pAF at position 407 and Tyr at position 405 (that leads to TPQ). The second is that there is a small population of protein with Tyr at position 405 (that leads to TPQ) and Tyr at 407, which would be wild type protein. In the second case, we would still detect a small amount of TPQ by phenylhydrazine derivitization or activity by turning over benzylamine, results that could be mistaken for Y407pAF being capable of forming TPQ and activity. In the same LC-MS/MS run that identified pAF at position 407 (**Figure 4-2**), a peptide was also identified that contained Tyr at position 405 (TAANY). This second peptide, however, could be derived from protein that contains either a pAF at position 407 or a Tyr at position 407. It is worth noting that there was no detection of a peptide containing Tyr at position 407 i.e. no peptide analogous to what was seen in **Figure 4.2** except with a Y at position 407 rather than pAF (no EY(CMC)LY was seen).

To further clarify this point, we sought to isolate a single peptide that contained both Tyr at position 405 and pAF at position 407. Chymotrypsin normally cleaves on the carboxyl side of aromatic residues, including Tyr, making the isolation of a peptide containing residues 405 and 407 difficult because chymotrypsin would preferably cleave after Y405. Therefore, we also digested HPAO-Y407pAF with trypsin, which cleaves on the carboxyl side of Lys and Arg, as well as thermolysin, which primarily cleaves after bulky hydrophobic residues. Unfortunately, LC-MS/MS analysis of peptides generated by these enzymes was also unable to identify any peptides that contained both resides 405 and 407. Our attempts to derivatize Y407pAF with phenylhydrazine, and then isolate a peptide containing a hydrazone at position 405 and pAF at 407, were also unsuccessful, regardless of whether peptides were first separated by HPLC and 450-nm absorbing fractions collected, or whether they were subjected directly to analysis by LC-

MS/MS. It is possible that a secondary reaction occured with the hydrazone product, complicating the MS/MS ion selection and data analysis. While the data seem to confirm Y407pAF protein containing a Tyr at position 405 that leads to TPQ, and pAF at 407, we cannot totally exclude the possibility that there is a small amount of WT contamination. It should be noted that the tRNA/synthetase pair for pAF is known to incorporate pAF with high fidelity and does not suffer from misincorporation of the native amino acid, a phenomenon seen with some of the other systems.

4.5   Conclusions and Future Work

Overall, our work on incorporating unnatural amino acids into HPAO has been very provocative, both for elucidating the mechanism of the CAOs and for introducing a new tool to prove the behavior of the active site metal in copper-dependent enzyme reactions. We have successfully incorporated pAF into three positions within HPAO, one of the largest proteins used for unnatural amino acid studies. We have firmly established that Y405pAF does not form TPQ or a modified quinone, and does not turn over amine substrates. We believe that Y405pAF instead forms a species that absorbs at 450 nm, which we have assigned to a Cu(II)-aniline LMCT or outer sphere electron transfer from aniline to Cu(II), forming aniline radical and Cu(I). The formation of this species appears to be independent of O_2. Our efforts to characterize this species by spectroscopic methods such as resonance Raman, EPR, and EXAFS have not been able to definitively identify this species. What has been insightful is the x-ray crystal structure of HPAO-Y405pAF, which shows aniline unmodified by O_2 insertion into the ring and liganded to the Cu, properly positioned for electron transfer or LMCT formation.

Interestingly, Y305pAF also forms a 450-nm species that appears to be independent of oxygen, and does not form a quinone cofactor capable of enzymatic turnover. In this case, the aniline at position 305 is too far to form a LMCT with the Cu center or undergo inner sphere electron transfer, but could transfer an electron to the Cu(II) through outer sphere electron transfer, possibly mediated by water molecules in the active site. We have not subjected the Y305pAF variant to a full battery of spectroscopic techniques as we did Y405pAF, but these experiments would be of great interest to pursue in the future in order to compare the features of Y305pAF to those of Y405pAF.

We have also probed the role of second sphere ligands using pAF incorporation by studying Y407pAF. This protein, unlike both Y305pAF and Y405pAF, does form TPQ and turns over substrate, albeit at an apparently reduced rate compared to WT-HPAO. In order to make more definitive conclusions about the kinetic behavior of Y407pAF, we would need to do a full kinetic characterization, including determining k_{cat} and K_m for methylamine and benzylamine, K_m for oxygen, and the effect of pH on these parameters. We would also like to study the oxidative half-reaction by stopped flow and examining ^{18}O kinetic isotope effects, as this is the half-reaction in which the Cu(II) could undergo electron transfer with cofactor to form Cu(I). The ability to tune the redox potential of the metal by incorporating unnatural amino acids into second sphere ligands could be a very useful technique for probing the mechanism of a wide array of metalloproteins in the future.

The field of unnatural amino acid incorporation continues to make gains, including constructing improved tRNA/tRNA synthetase pairs that result in higher protein yields (*14*), and efforts toward multiple site incorporation (*15*) and scanning unnatural amino acid mutagenesis (*16*). With apo-HPAO, yields are already low (10-20 mg/ 9L media) due to the restrictive requirements of the metal-free media. Expression of an unnatural amino acid incorporated HPAO reduced these already low protein yields to the point where more protein-intense spectroscopic work became rather challenging. In addition, it appears that whatever process is happening in these proteins upon Cu(II) reconstitution is happening in only a small population of the total protein, further reducing signal. We attempted to improve expression by moving to an

arabinose-autoinducible system (pBAD vector), which has previously been used with success in unnatural amino acid protein generation (*17-19*), as well as a Strep-Tag plasmid system, but were unable to get very far with these efforts. We also undertook a collaboration with Chris Murray and Nathan Uter of Sutro Biopharma, who are developing a scalable cell-free expression system capable of incorporating unnatural amino acids. Unlike previous efforts toward *in vitro* incorporation, which resulted in μg quantities of protein, Sutro is able to generate several mg of protein in a 10 mL cell-free reaction, and up to 5 g in a 5-L reactor, with no apparent misincorporation. Unfortunately, we ran into several problems during purification of HPAO from the cell-free extract, and were unable to fully utilize this technology to generate high quantities of protein for detailed spectroscopic work. Future work on unnatural amino acid-incorporated HPAO will greatly benefit from efforts toward increasing yield, facilitating the pursuit of protein-intense spectroscopic investigations.
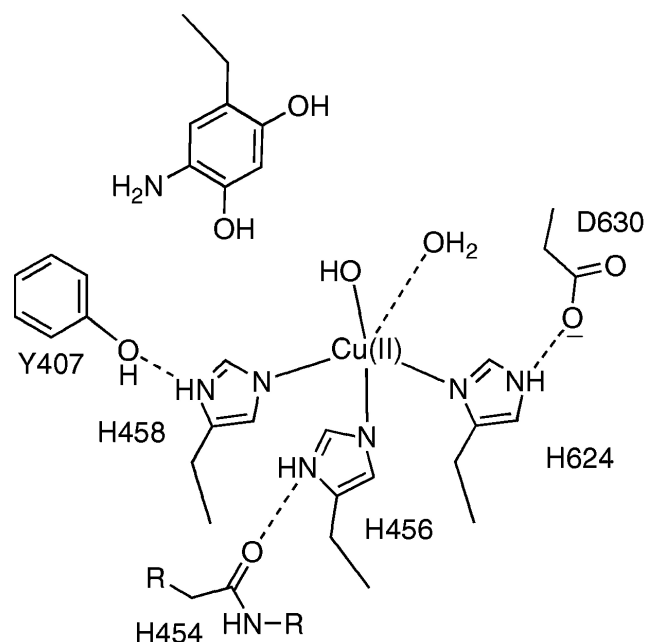
Scheme 4-1. Active Site Schematic based on the X-ray structure for HPAO (*20*). TPQ cofactor is in the reduced aminoquinol form observed after the reductive half-reaction. Reprinted (adapted) with permission from (*5*). Copyright 2007 American Chemical Society.
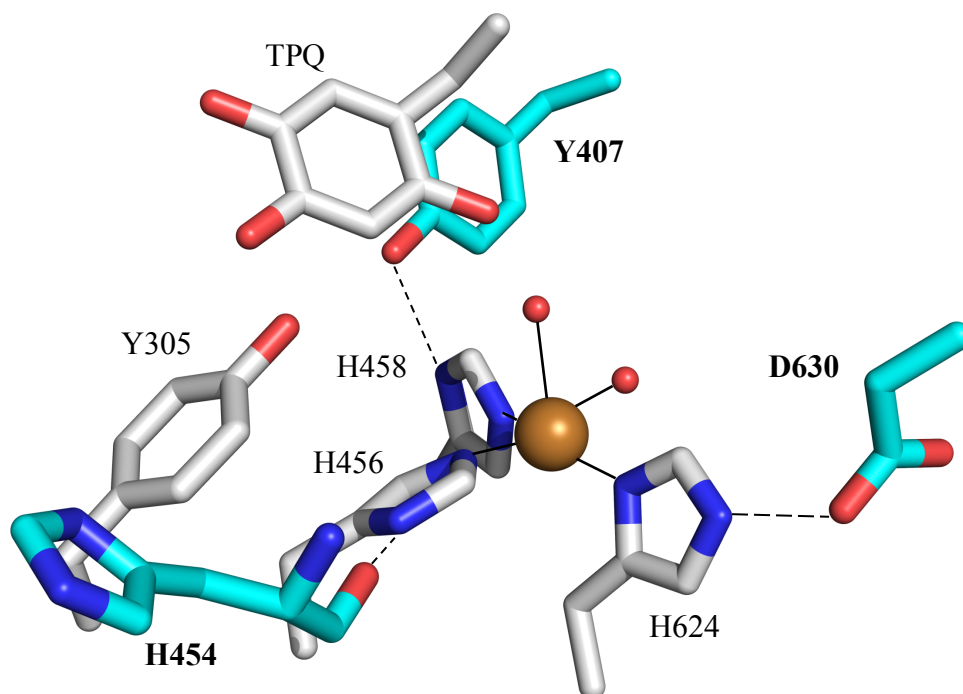

Figure 4-1. Active Site Structure of HPAO (PDB entry; 2OOV). Second sphere ligands are shown in cyan, their labels in bold. Copper ion shown as orange sphere, water ligands as red spheres.
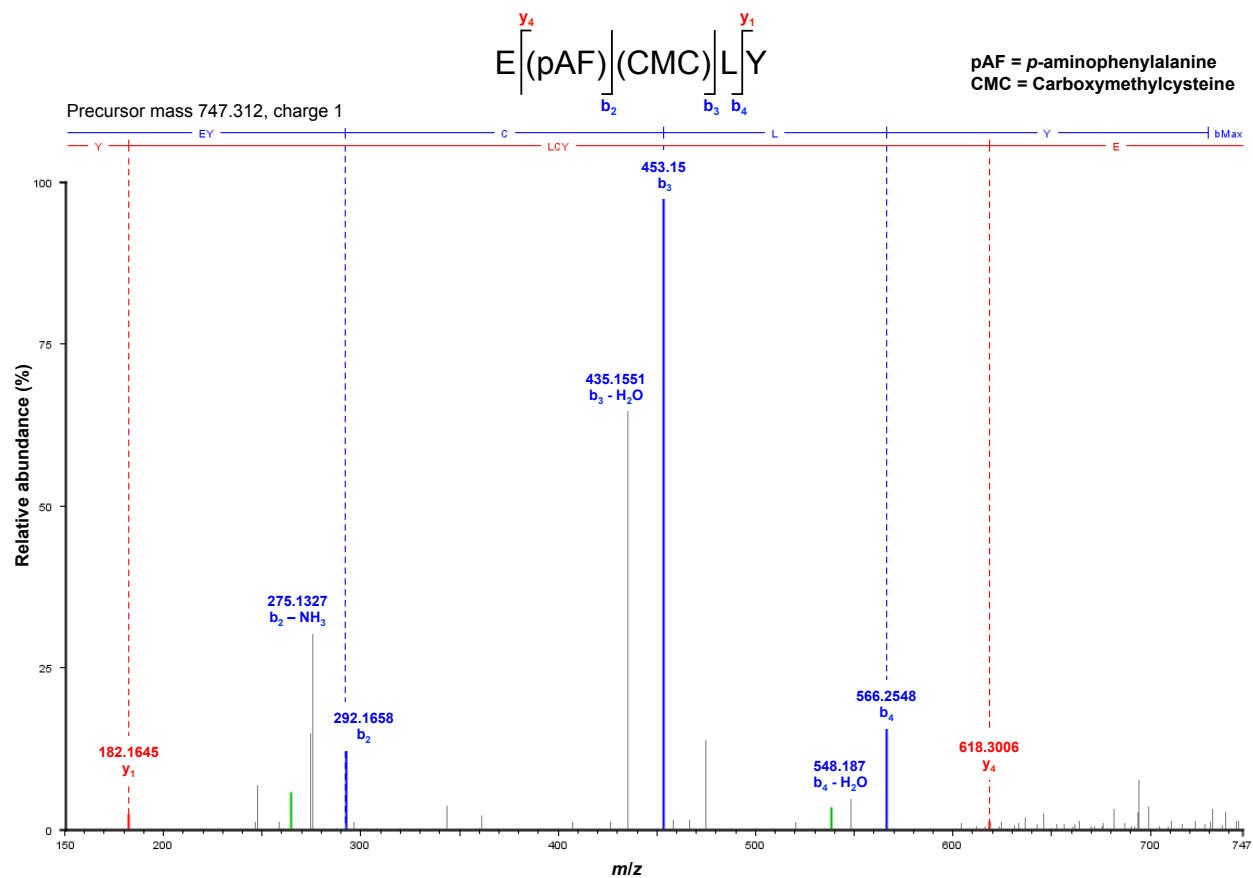
Figure 4-2. MS/MS spectrum of pAF-containing precursor ion derived from Y407pAF protein. Labels indicate b and y fragment ions generated as a result of collisionally activated dissociation (CAD). Figure generated by Tony Iavarone (QB3/Chemistry Mass Spectrometry Facility).
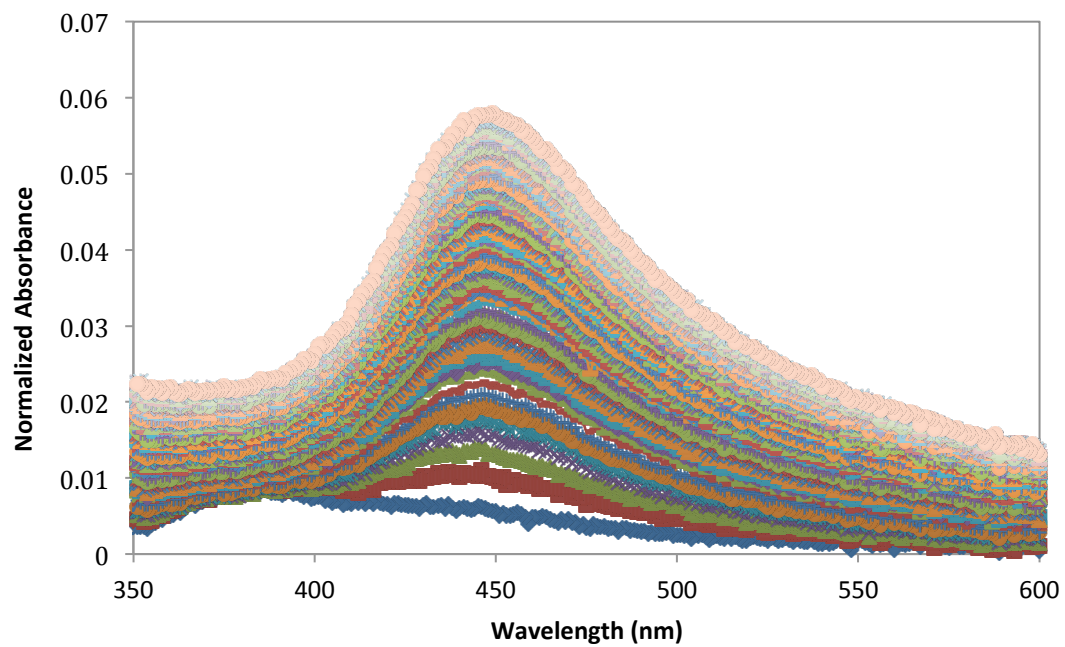
Figure 4-3. Spectral changes after addition of Cu(II) to apo-HPAO-Y407PAF at pH 9.0. The initial spectrum has been subtracted from each subsequent spectrum to emphasize the spectral changes. Spectra were measured every 2 min for 120 min.
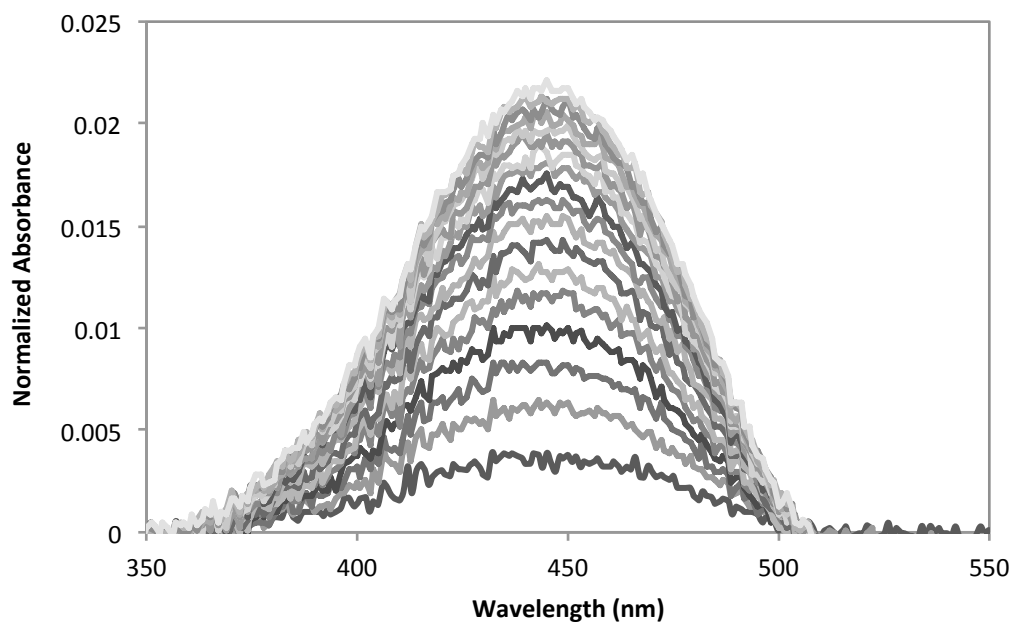
Figure 4-4. Spectral changes after addition of phenylhydrazine to Cu(II)-reconstituted HPAO-Y407PA. The initial spectrum has been subtracted from each subsequent spectrum to emphasize the spectral changes. Spectra were measured every 0.1 min for the first 2 min, then every min for a total of 20 min.
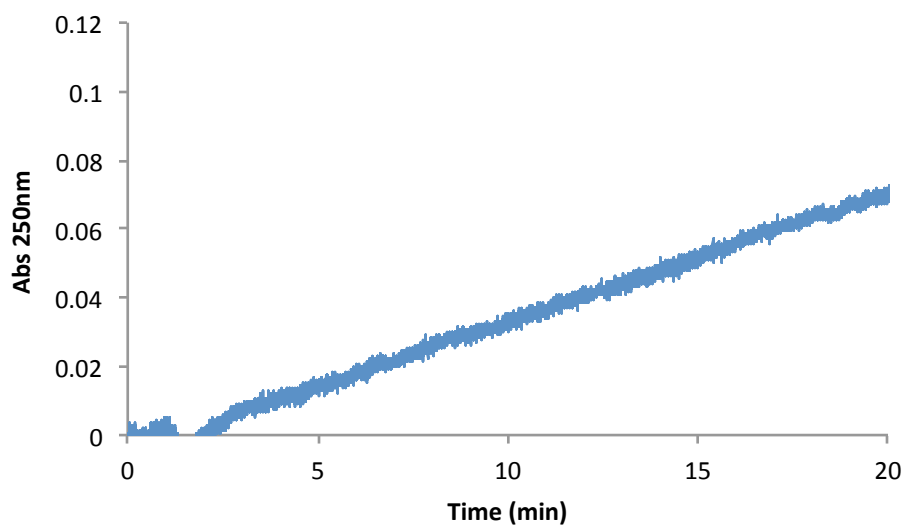
Figure 4-5. Representative trace of HPAO-Y407pAF activity toward benzylamine. Absorbance at 250 nm (ε_{250} benzaldehyde = 12800 $M^{-1}cm^{-1}$ (*11*)) was measured over 20 min using a Varian Cary 50 Bio UV-Vis spectrophotometer. Conditions: 50 mM HEPES pH 7, 5 mM benzylamine, 68 µM Cu^2-reconstituted HPAO-Y407pAF.
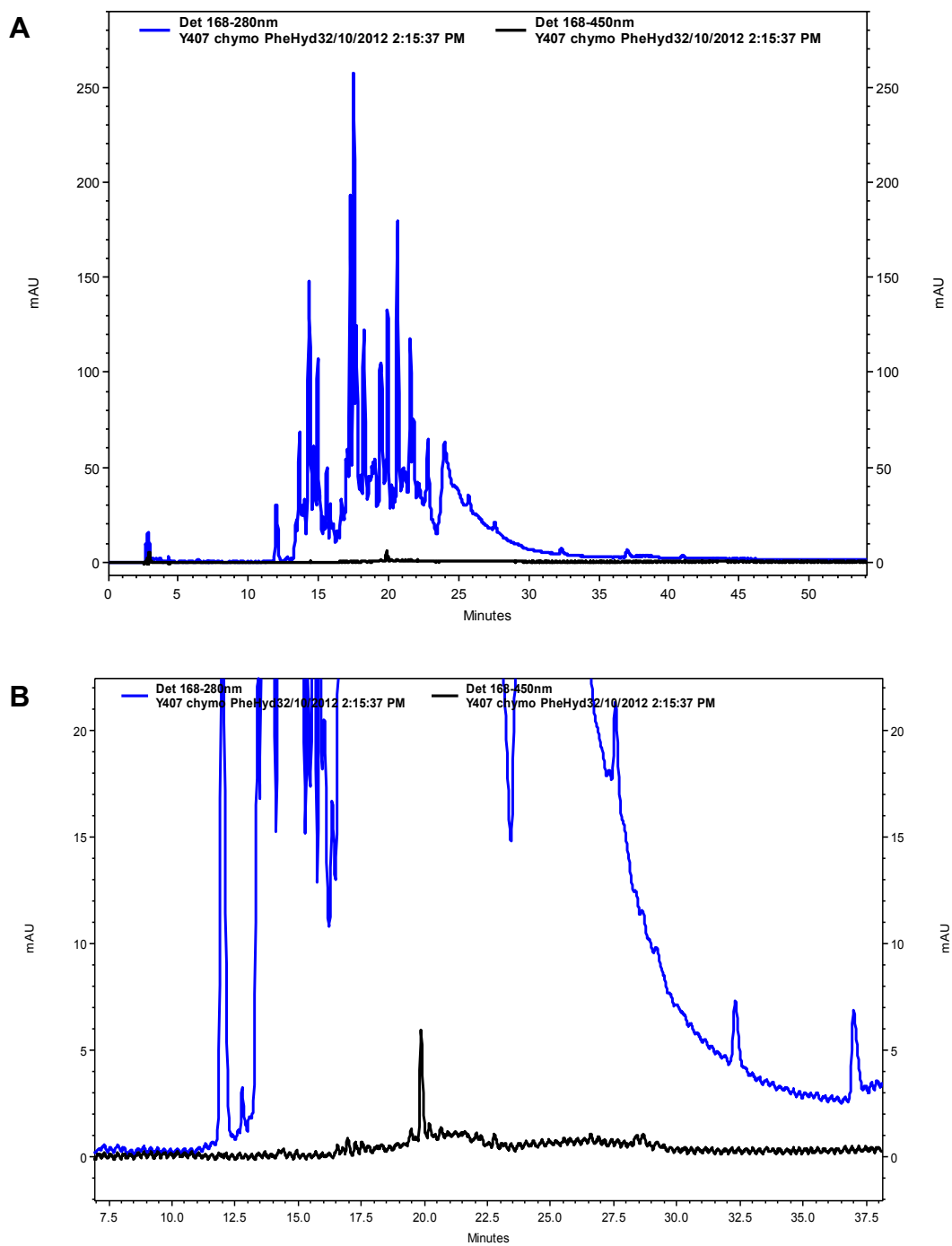
Figure 4.6. Trace of Y407pAF chymotryptic peptides separated by HPLC. Absorbance was monitored at 450 nm (black) and 280 nm (blue). **B** is a zoomed in version of the same trace in **A**.

References

1.   Mure, M., Mills, S. A., and Klinman, J. P. (2002) Catalytic Mechanism of the Topa Quinone Containing Copper Amine Oxidases, *Biochemistry 41*, 9269–9278.
2.   Dooley, D. M., McGuirl, M. A., Brown, D. E., Turowski, P. N., McIntire, W. S., and Knowles, P. F. (1991) A Cu(I)-semiquinone state in substrate-reduced amine oxidases, *Nature 349*, 262–264.
3.   Mills, S. A. S., Goto, Y. Y., Su, Q. Q., Plastino, J. J., and Klinman, J. P. J. (2002) Mechanistic comparison of the cobalt-substituted and wild-type copper amine oxidase from *Hansenula polymorpha*, *Biochemistry 41*, 10577–10584.
4.   Mills, S., and Klinman, J. (2000) Evidence against reduction of Cu^{2+} to Cu^+ during dioxygen activation in a copper amine oxidase from yeast, *J. Am. Chem. Soc. 122*, 9897–9904.
5.   Welford, R. W. D., Lam, A., Mirica, L. M., and Klinman, J. P. (2007) Partial Conversion of *Hansenula polymorpha* Amine Oxidase into a "Plant" Amine Oxidase: Implications for Copper Chemistry and Mechanism, *Biochemistry 46*, 10817–10827.
6.   Dalton, D. R. (2011) Foundations of Organic Chemistry, John Wiley & Sons.
7.   Smith, M., and March, J. (2007) March's Advanced Organic Chemistry, John Wiley & Sons.
8.   Samuels, N. M., and Klinman, J. P. (2005) 2,4,5-Trihydroxyphenylalanine Quinone Biogenesis in the Copper Amine Oxidase from *Hansenula polymorpha* with the Alternate Metal Nickel, *Biochemistry 44*, 14308–14317.
9.   Bradford, M. M. (1976) A rapid and sensitive method for the quantitation of microgram quantities of protein utilizing the principle of protein-dye binding, *Anal. Biochem. 72*, 248–254.
10.   DuBois, J. L., and Klinman, J. P. (2004) Methods for characterizing TPQ-containing proteins, *Meth. Enzymol. 378*, 17–31.
11.   Hartmann, C., and Klinman, J. P. (1991) Structure-function studies of substrate oxidation by bovine serum amine oxidase: relationship to cofactor structure and mechanism, *Biochemistry 30*, 4605–4611.
12.   Chang, C. M., Klema, V. J., Johnson, B. J., Mure, M., Klinman, J. P., and Wilmot, C. M. (2010) Kinetic and structural analysis of substrate specificity in two copper amine oxidases from *Hansenula polymorpha*, *Biochemistry 49*, 2540–2550.
13.   Takahashi, K., and Klinman, J. P. (2006) Relationship of Stopped Flow to Steady State Parameters in the Dimeric Copper Amine Oxidase from *Hansenula polymorpha* and the Role of Zinc in Inhibiting Activity at Alternate Copper-Containing Subunits, *Biochemistry 45*, 4683–4694.
14.   Young, T. S., Ahmad, I., Yin, J. A., and Schultz, P. G. (2010) An enhanced system for unnatural amino acid mutagenesis in *E. coli*, *Journal of Molecular Biology 395*, 361–374.
15.   Loscha, K. V., Herlt, A. J., Qi, R., Huber, T., Ozawa, K., and Otting, G. (2012) Multiple-site labeling of proteins with unnatural amino acids, *Angew. Chem. Int. Ed. 51*, 2243–2246.
16.   Liu, J., and Cropp, T. A. (2012) Experimental methods for scanning unnatural amino acid mutagenesis, *Methods Mol. Biol. 794*, 187–197.
17.   Farrell, I. S., Toroney, R., Hazen, J. L., Mehl, R. A., and Chin, J. W. (2005) Photo-cross-linking interacting proteins with a genetically encoded benzophenone, *Nat Meth 2*, 377–

384.

18.   Hammill, J. T., Miyake-Stoner, S., Hazen, J. L., Jackson, J. C., and Mehl, R. A. (2007) Preparation of site-specifically labeled fluorinated proteins for ^{19}F-NMR structural characterization, *Nat Protoc 2*, 2601–2607.

19.   Carrico, Z. M., Romanini, D. W., Mehl, R. A., and Francis, M. B. (2008) Oxidative coupling of peptides to a virus capsid containing unnatural amino acids, *Chem. Commun. (Camb.)* 1205–1207.

20.   Li, R., Klinman, J. P., and Mathews, F. S. (1998) Copper amine oxidase from *Hansenula polymorpha*: the crystal structure determined at 2.4 Å resolution reveals the active conformation, *Structure 6*, 293–307.